INDUCTIVE COUPLING BETWEEN IDEALIZED CONDUCTORS AND ITS SIGNIFICANCE FOR THE GEOMAGNETIC COAST EFFECT

by

Detlef Wolf
Department of Physics
University of Toronto

A thesis submitted in conformity with the requirements for the degree of Master of Science in the University of Toronto

CONTENTS

ACKNOWLEDGEMENTS

This work was funded by an NSERC research grant and a University of Toronto Open Fellowship. Scott Holladay and Jim Mcnae kindly provided plotting routines for the graphical display of the numerical results. Khader Khan assisted in the drafting of the illustrations. Richard Bailey, Colin Thomson, and Michael Weber carefully read preliminary versions of the manuscript and made useful suggestions for improvements. Thanks are due to all of them for their kind assistance.

ABSTRACT

A problem of current interest is the inductive coupling between an ocean, a solid earth conductor and a conductosphere. The anomaly of this configuration is modelled by (i) the inductive response of a two-dimensional system consisting of two thin half sheets and an underlying thin whole sheet or (ii) the superposition of the responses of two related systems, each consisiting of only one of the two half sheets and the whole sheet. The conductivity of these conducting planes is assumed to be perfect, and rigorous solutions for the induced magnetic fields are derived by conformal mapping. A comparison between the anomalies (i) and (ii) permits us to ascertain the degree of inductive coupling between the idealized conductors. This establishes a reference for estimating the inductive coupling between more realistic conductors and may therefore assist in the interpretation of complicated magnetic variation anomalies in coastal regions. Our substitute configurations can also be used directly for the rapid modelling of the inductive response of the earth in the vicinity of coastlines. This is demonstrated by analyzing some field data from the recent literature.

NOTATION

All electromagnetic quantities are measured in M.K.S.A. units. Underlined quantities are to be understood as vectors. An asterisk denotes the complex conjugate of the respective number. Whenever electromagnetic field quantities are considered, their transient part is implied. In the following list, numbers in brackets refer to the primary or first occurrences of the symbols being explained.

A - complex scaling factor of Schwarz-Christoffel transformation (sec. 5.3)

a - anomalous variation in Schmucker's sense (eqs. 6.1)

$\underline{B}$ - magnetic induction (sec. 4.1)

B - analytic magnetic field (eq. 4.13)

C - complex inductive scale length of layered half space (sec. 5.2); also contour in complex plane (sec. 5.5)

d - depth of homogeneous substitute half space (sec. 5.2)

$\underline{E}$ - electric field (sec. 4.1)

$\hat{\underline{e}}$ - arbitrary unit vector

$\underline{H}$ - magnetic field (sec. 4.1)

h_1 - separation between half plane 1 and whole plane (sec. 5.3)

h_2 - separation between half plane 2 and whole plane (sec. 5.3)

h_3 - separation between measuring profile and whole plane (chap. 6)

$\underline{J}$ - electric volume current density (chap. 1, sec. 5.2)

$\underline{K}$ - electric surface current density (chap. 1, secs. 4.1, 5.2)

L - horizontal separation between edges of half planes 1 and 2 (sec. 5.3)

l - characteristic length (eq. 3.2)

m - number of vertices of polygon (sec. 5.3)

n - direction normal to conductivity discontinuity (fig. 4.2); also normal magnetic variation in Schmucker's sense (eqs. 6.1); also number of Newton-Raphson iterations (sec. 5.4)

P - Parkinson transfer function (eq. 3.1)

p - inductive scaling parameter (eq. 3.2)

r - modulus of complex number (sec. 5.5)

S - Schmucker transfer functions (eqs. 6.2)

s - strike direction (fig. 4.1)

T - period (sec. 5.2)

t - direction tangential to conductivity discontinuity (fig. 4.2); also time

u - horizontal direction of w plane

v - vertical direction of w plane

w - complex auxiliary plane perpendicular to s (fig. 4.3)

x - horizontal direction of z plane

y - vertical direction of z plane

y_m - depth of perfect substitute conductor (fig. 5.1, eq. 5.4)

y_s - skin depth of homogeneous half space (eq. 5.3)

z - complex physical plane perpendicular to s (fig. 4.3)

α - polygon angle (fig. 5.2)

δ - thickness of conductive layer (chap. 1); also Dirac delta function (eq. 5.39)

θ - phase of complex number (sec. 5.5)

κ - electric surface conductivity (eq. 1.1)

λ - source current parameter (sec. 5.6)

μ - magnetic permeability

μ_0 - magnetic permeability of free space (sec. 4.1)

ρ - resistivity (sec. 5.2)

σ - electric volume conductivity (eqs. 1.3, 3.2, 5.3)

τ - decay time (eq. 3.2)

ϕ - magnetic scalar potential (eq. 4.6)

$\underline{\Psi}$ - magnetic vector potential (eq. 4.5)

Ψ - magnetic stream function (eq. 4.8)

Ω - analytic magnetic potential (eq. 4.11)

ω - angular frequency (eqs. 3.2, 5.3)

CHAPTER 1

INTRODUCTION

Time variations of the earth's magnetic field of the order of minutes to days are ultimately due to fluctuating ionospheric and magnetospheric current systems. Their associated transient magnetic fields penetrate through the earth's crust and mantle, thereby inducing telluric current systems and a corresponding internal field, which is superimposed on the external part. Both parts constitute the total magnetic variation, which may be observed at the surface of the earth.

Obviously, the distribution of these internal currents must be governed by both the behaviour of the inducing field in space and time as well as the conductivity distribution in the earth. Thus, the measurement of fluctuating magnetic fields contains information related to the subsurface conductivity structure, which can be recovered by suitable analysis of the observed variations.

Here this induction process is considered on a regional scale, i.e. lateral conductivity anomalies of wavelengths of the order of several hundred kilometres in the crust or upper mantle are investigated. This depth range necessitates the selection of an appropriate time scale, which is normally closely met by magnetic bay disturbances (T = 1 h, approximately).

The transitional region between continental and oceanic lithosphere will be of particular interest to us. This transition is usually dominated by the sharp conductivity contrast between sea-water and adjacent rocks. However, there are indications of other conductivity anomalies in coastal regions. These have sometimes been correlated with temperature anomalies in the upper mantle along recent subduction zones (cold, descending lithospheric slabs, partial melting). In other cases they are believed to be signatures of mineralogical or petrological changes in the lower crust (hydrous minerals, ancient plate boundaries).

The exact determination of the inductive response of a real (three-dimensional) ocean alone is a formidable task, and reliable solutions can only be obtained from scale model experiments (see chap. 3). If we assume that such solutions are available, the problem arises as to how to "deduct" the response of the ocean from the actually

observed coastal anomaly in a realistic manner. Such a reduction is desirable in order to interpret the residual in terms of the conductivity structure in the lower crust or upper mantle alone. An obvious way to allow for the influence of an ocean is to subtract its anomaly. However, this simple procedure neglects any inductive coupling existing even between insulated conductors, which may be significant. The existence of this effect has already been emphasized by Price (1964) and Rikitake (1966).

In order to shed some light on this problem, deliberately simple but nevertheless characteristic models of conductivity structures near coastlines will be developed. They only involve perfectly conducting half planes or whole planes of two-dimensional configuration. These ideal models can, however, serve as useful standards, as they establish an upper limit on the inductive coupling to be expected for more realistic configurations.

At this point it is necessary to define the meaning of the phrase "finitely (or perfectly) conducting thin sheet or plane". We thus stipulate that, whenever the term "conductivity" is referred to in association with the term "thin sheet", it is the surface conductivity κ of the latter that is implied. If the thin sheet replaces a layer of finite thickness, we are allowed to equate κ with the

integrated conductivity of the layer and write

$$(1.1) \qquad K = \int_0^{\delta} \sigma(y)dy$$

Here σ and δ denote the (volume) conductivity and thickness, respectively, of the actual layer being replaced. If, furthermore, $\underline{J}$ is the volume current density within this layer, we may also write

$$(1.2) \qquad \underline{K} = \int_0^{\delta} \underline{J}(y)dy = \int_0^{\delta} \sigma(y)\underline{E}(y)dy$$

with $\underline{K}$ as the surface current density within the thin sheet and $\underline{E}$ as the (horizontal) electric field vector in the layer being replaced. In eq. 1.2 the generalized form of Ohm's law, i.e.

$$(1.3) \qquad \underline{J} = \sigma \underline{E}$$

is implied. The conditions that permit this replacement will be formulated in sec. 5.1.

CHAPTER 2

REGIONAL INDUCTION ANOMALIES

Before we consider the problem of estimating the inductive coupling between an ocean and an earth conductor, a short survey of some work on other aspects of electromagnetic induction in the earth is helpful. This serves to set our particular problem into proper perspective. Here and in the following the term regional indicates that both the curvature of the earth and any topography will be neglected. In other words, neither global nor local phenomena are considered, and the earth is represented by a half space.

2.1. OBSERVATIONS

The method of probing the regional conductivity structure of the earth by natural fluctuations of the magnetic field is approximately thirty years old and developed along two different lines (see also Price, 1964).

Cagniard's (1953) magnetotelluric method allows the sounding of a one-dimensional conductivity distribution below a single station, if both the electric and magnetic fields are measured simultaneously (for details see also Wiese, 1965). The technique has been generalized to allow the investigation of more general conductivity structures.

The second method probes the earth by magnetic variations alone. It had originally been confined to studies of the global conductivity distribution. The application of this technique to regional problems was first implemented in Japan (Rikitake & Yokoyama, 1953; Rikitake, 1964) and Germany (Bartels, 1954, 1957; Schmucker, 1959). Work on the Central Japan and North German conductivity anomalies has continued until now (Honkura, 1978; Weidelt, 1978), but electromagnetic induction studies have become common elsewhere and revealed numerous lateral variations of conductivity in the crust and upper mantle. This is manifested by many publications on individual induction studies. Even the number of reviews has become large, and only some references are given here.

Rikitake's (1966) standard monograph was one of the first attempts to present a comprehensive review of all aspects of electromagnetic induction in the solid earth and also features a very complete list of references. Later

work includes Untiedt's (1970) summary of conductivity anomalies in central and southern Europe, which emphasizes work done in that area after 1964. During that time the question of the geophysical significance of regional conductivity anomalies became more prominent. On the one hand, the depth of some of the anomalies that were once believed to be in the upper mantle (see Bullard, 1967) decreased (Kertz, 1964; Hyndman & Hyndman, 1968; Garland, 1971). On the other hand, the new theory of plate tectonics was challenging enough to require an explanation of conductivity anomalies in terms of global dynamics (Uyeda & Rikitake, 1970; Law & Riddihough, 1971; Hutton, 1976a). The general upward shift of many conductors, once believed to be temperature-related upper mantle anomalies, was accompanied by the recognition of a new class of conductors in the lower crust (Garland, 1975, 1981), which have usually been correlated with old zones of weakness (paleorifts?) or hydrous minerals.

A very comprehensive review on the conductivity distribution of the earth and planets was written by Hutton (1976b). It includes virtually all aspects of the subject (except for theoretical modelling techniques) and provides a very extensive list of references.

2.2. THEORETICAL ASPECTS

All modelling techniques may be subdivided into (i) exact (but special) analytical and (ii) approximate (but general) numerical methods, even though a combination of both may sometimes be useful.

Analytical solutions usually consider the forward modelling problem and are limited to simple source field and conductor configurations, e.g. the one-dimensional half space (Cagniard, 1953) or two homogeneous quarter spaces (Weaver, 1963), both being subject to a homogeneous inducing field. But even an extremely simple conductivity distribution like the latter requires some approximations to be soluble for both polarizations of the magnetic field. Parker (1968) considered the induction by a magnetic field normal to a thin conducting strip. Using a series expansion, he derived a formal solution for the magnetic field, which also demonstrated that the field had a logarithmic singularity at the edges, whereas the current remained finite there.

Some exact solutions of inverse problems will also be mentioned. Schmucker (1971) derived the (one-dimensional) surface conductivity distribution of a thin sheet from its anomalous response for both polarizations. However, the

conductivity distribution of the layered half space below the sheet must be known. Siebert (1974) considered an arbitrarily deformed surface of perfect conductivity and demonstrated how its geometry could be derived from the distribution of the magnetic variations in a plane above the conductor.

Very useful references for the general theory of electromagnetic induction in the earth are Price (1967) and Schmucker & Weidelt (1975).

There exist several purely numerical methods for more general classes of conductors and source fields. As an example we refer to Madden & Swift's (1969) two-dimensional transmission line analogy. A similar technique is the finite difference method. The latter has been improved during the last decade and can now model three-dimensional conductivity distributions subject to non-uniform inducing fields. The foundations of this method are well-documented in Jones & Price (1970), Jones & Pascoe (1971), Pascoe & Jones (1972) and Haak (1978).

CHAPTER 3

GEOMAGNETIC COAST EFFECT

The first reference to the effect of coastlines on geomagnetic variations dates back at least to 1927/1928 (see Gregori & Lanzerotti, 1978/79). The basic observation is that, at a particular point on the earth's surface, the magnetic variation vector $\underline{B}$ tends to be closely confined to a plane, which strikes approximately parallel to the ocean-continent conductivity contrast.

To explain this observation, we consider a magnetic disturbance that is plane polarized. If x is the horizontal direction perpendicular to the strike direction of the variation plane, y the vertical direction and t the time, we always have

(3.1) $$B_y(t) = P\, B_x(t)$$

P is usually called the Parkinson transfer function. So far nothing is implied about the physical significance of the

direction of x and the constant P. However, for uniform inducing fields and the inductive limit, P and the direction of the x co-ordinate are independent of the frequency and polarization characteristics of the source field and solely determined by the subsurface conductivity structure. This means that, at a particular point, all variations proceed in the same plane. If the subsurface is even two-dimensional, this variation plane extends along the strike of the conductivity distribution, i.e. x designates the direction normal to it (Untiedt, 1964). This is the case that will be of interest to us.

More general concepts that allow for finite conductivities have also been introduced. However, then all phenomena are frequency-dependent, and the polarization characteristics of the inducing field also become important. Linear relations similar to eq. 3.1 may still be shown to be valid, but their significance in terms of the subsurface conductivity structure becomes more difficult to assess, particularly for inhomogeneous source fields.

3.1. OBSERVATIONS

It was not until the publication of Parkinson's classic papers that the geomagnetic coast effect became well-known

to the geophysical community. Parkinson (1959, 1962, 1964) presented evidence for a behaviour of rapid variations corresponding to eq. 3.1 for coastal stations in Australia and on other continents. But he also pointed out that the body of sea-water constituting an ocean might not suffice to explain the observed effects. In particular, the Central Japan anomaly was difficult to understand in terms of the ocean alone. Today this anomaly is believed to be largely the signature of a cold, descending lithospheric slab.

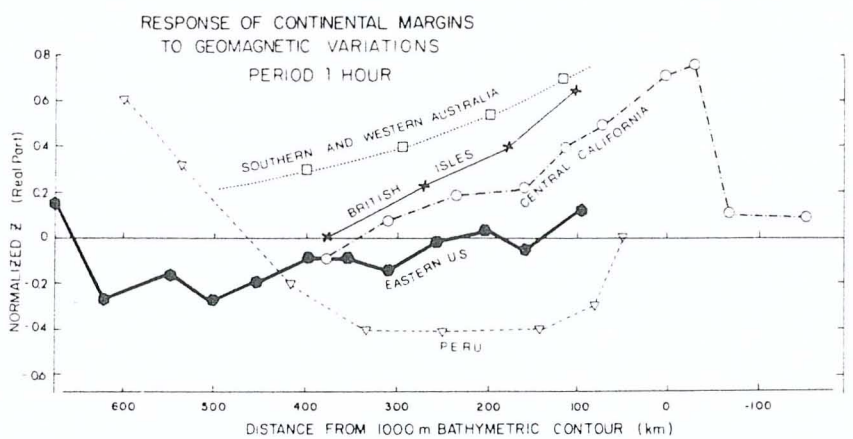

Fig. 3.1. Real part of normalized vertical variation $Z \equiv B_y$ at a period of 1 h as a function of the distance from the continental margin for several coasts: Central California (Schmucker, 1964, 1970a; Greenhouse, 1972); Peru (Schmucker et al., 1966); south-western Australia (Everett & Hyndman, 1967); British Isles (Edwards et al., 1971); eastern U.S.A. (Edwards & Greenhouse, 1975)

As more data on the geomagnetic coast effect became available, various interpretations in terms of conducting sea-water, with or without underlying lateral conductivity structure, were proposed. Most workers now agree that electric currents in the oceans alone are insufficient for

an explanation of the observed anomalies, simply because the latter are too different for comparable coasts (Bullard & Parker, 1970). However, no general agreement on the basic features of the underlying differences in conductivity structure has been reached so far. Clearly, any anomaly in the horizontal variations on the land surface requires at least images of the induced ocean currents in a conducting half space below. This is Schmucker's (1964, 1970a) and Jones' (1981) interpretation of the Californian and Scandinavian coastal anomalies, respectively. Others have related the varying rate of decrease of P in the inland direction for different coasts (fig. 3.1) to the depth or conductivity of this half space, i.e. to differences in the geologic history of the continental areas involved. Regions of recent tectonic activity ought to cause a more sudden decrease than ancient shields (Everett & Hyndman, 1967, Bailey et al., 1974; Edwards & Greenhouse, 1975; Greenhouse & Bailey, 1981).

On the basis of seismic and geothermal evidence, it was speculated that the temperature, composition and structure of the oceanic lithosphere be consistently different from that of the continental lithosphere (Jacobs, 1960; Coode & Tozer, 1965). This has also been concluded from the results of some very deep induction studies (see e.g. Haak, 1980). If such a difference is reflected in any of the observed

geomagnetic coast effects remains to be decided. Gough (1973) doubted whether the ambiguity could be resolved by variation field observations on the land only. This is in line with numerical results by Lines et al. (1973), who demonstrated the poor detectability of underlying lateral conductivity variations close to the coast.

On the other hand, the central Japan and Peruvian Andes anomalies appear to be subduction zone anomalies, with a complicated interaction between ocean effect and temperature-related local mantle anomalies. Some preliminary modelling on that basis for Peru (Schmucker, 1969a; Greenhouse et al., 1973) and Japan (Honkura, 1978) proved to be successful. Jones et al. (1981) attempted to model the general characteristics of the coast effect above a subduction zone numerically. But the number of assumptions and parameters involved is large, and the calculated response strongly depends on their specific choice. Thus no general conclusion is possible.

Recently, two reviews on induction effects along coastlines have been published by Gregori & Lanzerotti (1978/79) and Parkinson & Jones (1979). The latter also discussed the interpretational aspects of the problem exhaustively.

3.2. LABORATORY SCALE MODELS

It may be shown (Grant & West, 1965) that geometrically similar conductor configurations have inductive responses that are identical in space and time, if the involved change in length scale is accompanied by corresponding changes in the time or conductivity scales. More quantitatively, we define a scaling parameter by

$$p = \sigma l^2 / \tau \qquad (3.2)$$

which must be conserved during the transformation. Here l and τ denote the length and time, respectively, that are characteristic for the configuration and its inductive response. (Displacement currents have been neglected as usual.) This means that the modelling of any conductivity structure of the real earth may conveniently be performed on a corresponding laboratory configuration, as long as eq. 3.2 is satisfied. This technique is known as analogue or scale modelling and has been widely applied to interpretational problems of electromagnetic prospecting. The scale modelling of regional anomalies, on the other hand, is not so common, but was advanced by Dosso's group in Victoria (for a review of earlier work see Dosso, 1973).

More recently, substantially improved experimental

facilities in Victoria have permitted the scale modelling of complicated three-dimensional coastal regions. The results for several coasts have been published in a series of papers (for the east coast of Canada see Dosso et al., 1980). The common feature of the experiments is that they determine the anomaly caused by the body of sea-water and an underlying homogeneous half space. A comparison with field observations will therefore help discriminate between the effects of oceans or seas and the effects due to a laterally inhomogeneous subsurface conductivity structure.

3.3. THEORETICAL ASPECTS

The problem of electromagnetic induction in coastal regions has stimulated much theoretical work. For convenience, we subdivide the pertinent models into (i) isolated thin sheet conductors, (ii) non-uniform conducting half spaces and (iii) combinations of (i) and (ii).

The first class was reviewed by Ashour (1973) and encompasses, e.g., Parker's (1968) thin strip model (see chap. 2). Greenhouse et al. (1973) considered a thin sheet of finite conductivity, which is underlain by a perfectly conducting undulating surface, the whole system being two-dimensional. Perfectly conducting sheets were

introduced by Schmucker (1964, 1970a) and will later be considered in some detail.

But Bullard & Parker (1970) have already pointed out that, for thin conductive layers, induction by horizontal magnetic fields is negligibly small, because such layers are incompatible with vertical current loops. To induce such loops, induction in conductors of considerable vertical extent, such as those of the second or third classes, is necessary.

The second class includes models consisting of two adjacent quarter spaces with a vertical, sloping or shelving interface (Weaver, 1963; Jones & Price, 1970, 1971). Three-dimensional numerical models of complicated coastlines have also been presented (Jones & Lokken, 1975). But the application of configurations of this class to problems of electromagnetic induction near a coastline necessitates that the skin depth of the magnetic perturbation be small relative to the depth of the ocean (for further details see chap. 5). This holds for geomagnetic micropulsations (T = 1 min, characteristically).

For lower frequencies, configurations of the third class can be considered. Very instructive are two-dimensional models consisting of a uniform half space

that is overlain by a half plane of perfect conductivity. In some cases, a parallel and perfectly conducting whole plane has been added at some depth. Analytical and numerical results have been obtained for these configurations (for an analytical solution for H polarization see Bailey, 1977).

During the last few years, theoretical work has concentrated on generalizations of Schmucker's (1971) thin sheet approach, and several solutions have been found for three-dimensional induction in a thin layer of finite conductivity, overlying a homogeneous or layered half space (e.g. Vasseur & Weidelt, 1977; Dawson & Weaver, 1979). This should allow the abruptness inherent in any model involving perfectly conducting sheets to be avoided and permit the theoretical modelling of complicated coastal areas in a realistic manner.

A useful summary of theoretical work related to the geomagnetic coast effect has recently been prepared by Fischer (1979).

CHAPTER 4

APPLICATION OF CONFORMAL MAPPING TO ELECTROMAGNETIC INDUCTION

The application of conformal mapping techniques (Morse & Feshbach, 1953; Koppenfels & Stallmann, 1959) to problems of electromagnetic induction is based on certain assumptions. The most stringent requirement is that of either perfect or vanishing conductivity. Notwithstanding these limitations, various aspects of the induction process in the real earth can be explained by this method, as will be shown in the following chapters.

4.1. ASSUMPTIONS

To apply conformal mapping techniques to problems of electromagnetic induction, three fundamental assumptions have to be satisfied.

(4.1.1) The geometry of the problem must be two-dimensional, i.e., for an arbitrary function f of the space co-ordinates, we require f = f(x,y) (fig. 4.1).

(4.1.2) We only consider field components corresponding to E polarization or TM mode, i.e. we have $\underline{B} = B_x\hat{\underline{e}}_x + B_y\hat{\underline{e}}_y$ and $\underline{E} = E_s\hat{\underline{e}}_s$ for the magnetic induction and electric field, respectively (fig. 4.1).

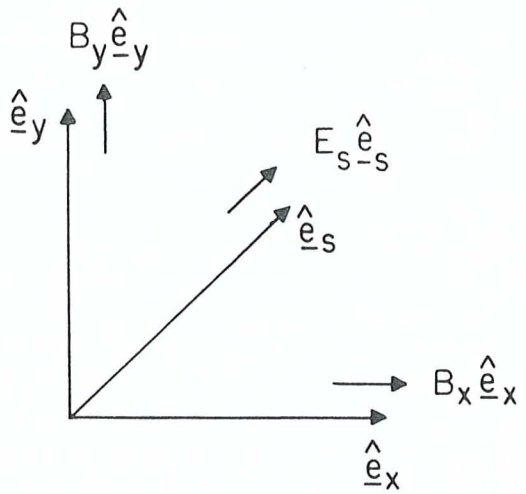

Fig. 4.1. Co-ordinate system used: s designates the direction tangential to strike, whereas x and y designate the horizontal and vertical directions, respectively, in a plane normal to strike (see also text)

The splitting of the field quantities into two independent modes (the other one being B polarization or TE mode) is inherent in any two-dimensional induction problem. It was proved by Untiedt (1964) and Jones & Price (1970).

(4.1.3) The physical space is subdivided into regions that are either perfectly conducting or non-conducting.

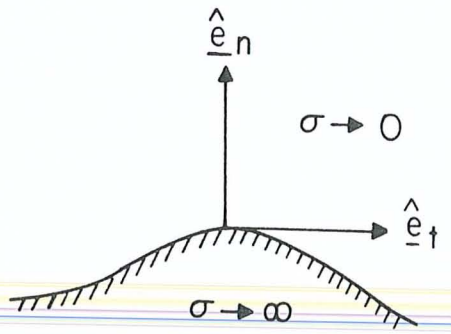

Fig. 4.2. Interface between perfectly conducting and non-conducting material. Indices n and t designate the directions normal and tangential to the interface (see also text)

This requirement immediately leads to the following boundary conditions at any interface between perfectly conducting and non-conducting regions (fig. 4.2).

(4.2.1) $$\hat{e}_n \cdot \underline{B} = 0$$

(4.2.2) $$\hat{e}_n \times \underline{H} = \underline{K}$$

where $\underline{K}$ is the surface current density and $\underline{H}$ the magnetic field, with $\underline{B} = \mu \underline{H}$. Here μ is always taken to be the permeability of free space, i.e. $\mu = \mu_0$. Neglecting displacement currents, we can then write the magnetic

induction

(4.3) $\underline{\nabla} \cdot \underline{B} = 0$

(4.4) $\underline{\nabla} \times \underline{B} = 0$

Thus, in terms of a vector and scalar potential, respectively

(4.5) $\underline{B} = \underline{\nabla} \times \underline{\Psi}$

(4.6) $\underline{B} = \underline{\nabla}\phi$

4.2. COMPLEX MAGNETIC QUANTITIES

Here we demonstrate that the magnetic field components as well as the magnetic potentials may, after suitable combination, be represented by (complex) analytic functions.

Considering eq. 4.6, we have in terms of components

(4.7.1) $B_x = \frac{\partial \phi}{\partial x}$

(4.7.2) $B_y = \frac{\partial \phi}{\partial y}$

But because of assumptions 4.1.1 and 4.1.2, the vector potential $\underline{\Psi}$ is directed along strike, i.e.

$$\underline{\Psi} = \Psi \hat{\underline{e}}_s \tag{4.8}$$

with $\Psi = |\underline{\Psi}|$ as the magnetic stream function. From eq. 4.5 it follows then that

$$B_x = \frac{\partial \Psi}{\partial y} \tag{4.9.1}$$

$$B_y = -\frac{\partial \Psi}{\partial x} \tag{4.9.2}$$

Inserting eq. 4.5 into 4.4 and eq. 4.6 into 4.3 therefore leads to

$$\frac{\partial^2 \phi}{\partial x^2} + \frac{\partial^2 \phi}{\partial y^2} = 0 \tag{4.10.1}$$

$$\frac{\partial^2 \Psi}{\partial x^2} + \frac{\partial^2 \Psi}{\partial y^2} = 0 \tag{4.10.2}$$

From eqs. 4.7, 4.9 and 4.10 it is apparent that $\phi(x,y)$ and $\Psi(x,y)$ are harmonic functions and satisfy the Cauchy-Riemann conditions. We thus combine Φ and Ψ and define the analytic magnetic potential by

$$\Omega(z) = \Omega(x+iy) = \phi(x,y)+i\Psi(x,y) \tag{4.11}$$

The corresponding field quantity may be derived as follows. We have

$$(4.12) \qquad \frac{d\Omega}{dz} = \frac{\partial \Phi}{\partial x} + i \frac{\partial \Psi}{\partial x}$$

and so, using eqs. 4.7.1 and 4.9.2, we can write for the magnetic induction

$$(4.13) \qquad B(z) = B(x+iy) = B_x(x,y) - iB_y(x,y)$$

4.3. TRANSFORMATION OF SOLUTIONS FOR MAGNETIC POTENTIAL

In this section, we outline the method of solving boundary-value problems of potential theory by conformal mapping.

We start with the formulation of a trivial boundary-value problem in a complex auxiliary plane, here denoted as w plane. This auxiliary plane is then "deformed" as necessary, such that the solution of the actual boundary-value problem in the complex z plane is obtained. Mathematically, this transformation is represented by a conformal mapping w(z), where w = u+iv and z = x+iy (fig. 4.3). It has the following properties.

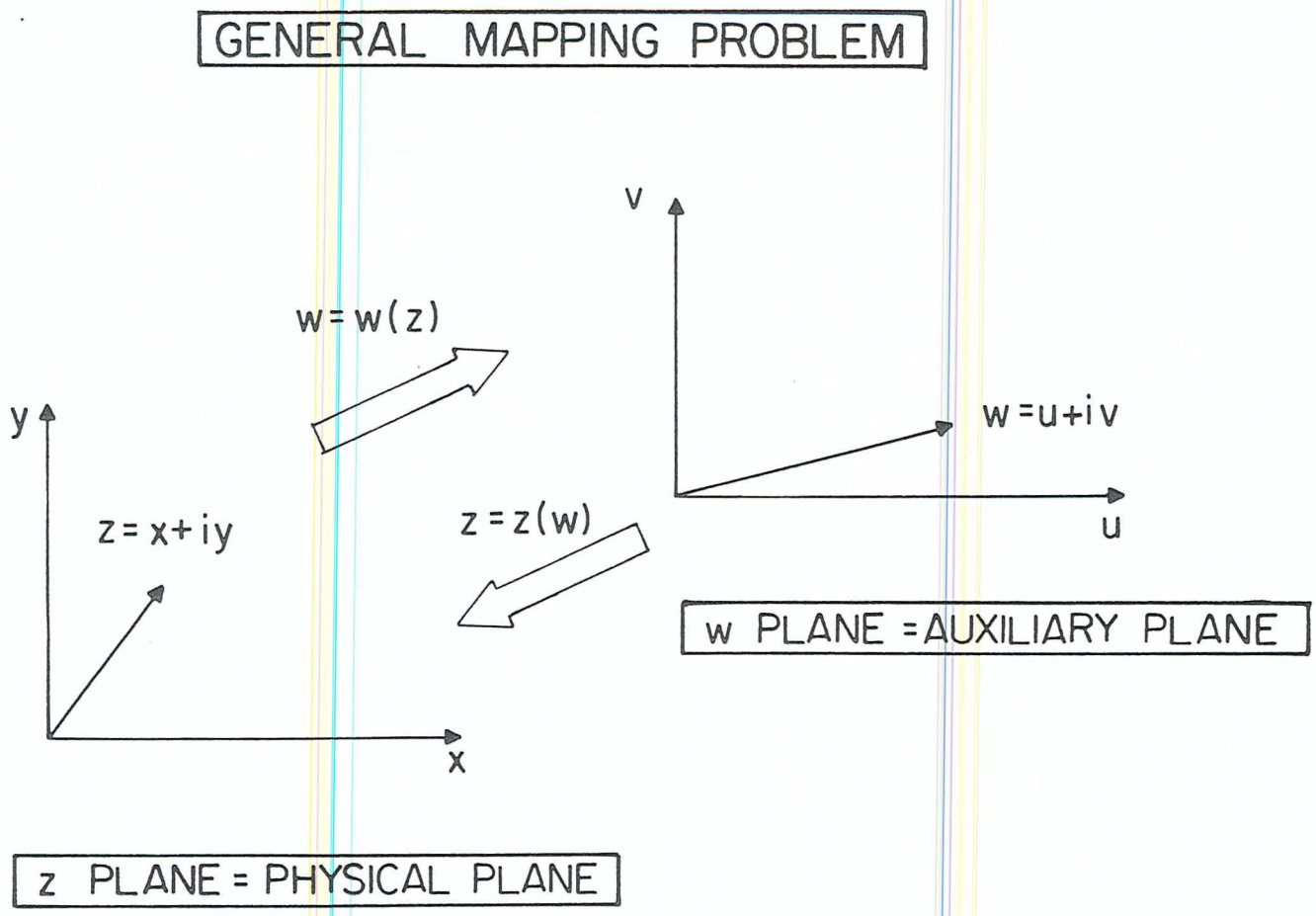

Fig. 4.3. Conformal mappings between complex w and z planes

(4.14.1) Angles of intersection of arbitrary curves in the w plane are conserved under the mapping of the curves into the z plane.

(4.12.2) Length ratios are conserved under the transformation, if the linear dimensions are infinitesimally small.

From these properties it is clear that a conformal transformation is a similarity transformation on an infinitesimally small scale.

We now assume that an auxiliary solution for the potential Ω in the w plane has been found, which necessarily satisfies the prescribed boundary conditions in that plane. This means that we know

(4.15.1) $$\Omega(w) = \Omega(u+iv) = \phi(u,v)+i\Psi(u,v)$$

But we wish to obtain the solution of the potential in the z plane, i.e.

(4.15.2) $$\Omega(z) = \Omega(x+iy) = \phi(x,y)+i\Psi(x,y)$$

This makes necessary the solution of the appropriate conformal mapping problem, i.e. w(z) must be derived. Then

we can write

(4.16) $\Omega(z) = \Omega(w(z))$

which constitutes the final solution in the z plane.

However, to be sure that $\Omega(z)$ is in fact this solution, we consider the following.

(4.17.1) With $\Omega(w)$ and $w(z)$ being single-valued analytic functions, $\Omega(z)$ is also single-valued and analytic, i.e. $\phi(x,y)$ and $\Psi(x,y)$ are harmonic and satisfy the Laplace equation.

(4.17.2) Considering boundary condition 4.1.1 with eqs. 4.7 and 4.9 for the w plane, we may reformulate eq. 4.2.1 as $\partial\phi/\partial n = \partial\Psi/\partial t = 0$ (see fig. 4.2). This demonstrates that the lines $\phi(u,v) = \text{const}$ are normal to the interface, which itself is one of the streamlines (field lines) $\Psi(u,v) = \text{const}$. Due to property 4.14.1 (conservation of angles), this also applies for the z plane, i.e. the boundary conditions are conserved.

This heuristic approach demonstrates that $\Omega(z)$ is the sought solution for the potential, provided this holds true

for $\Omega(w)$ and as long as $w(z)$ represents a conformal mapping. Thus, the whole problem obviously reduces to (i) finding $\Omega(w)$ (which is often trivial) and (ii) constructing $w(z)$ (which may be very challenging).

CHAPTER 5

SOLUTIONS FOR SOME PERFECTLY CONDUCTING THIN SHEET CONFIGURATIONS

In this section, some induction problems are formulated in terms of combinations of perfectly conducting half and whole planes in a non-conducting environment. In view of the conductivity distribution of the real earth, this is obviously a highly idealized model. However, there are some important facts that justify this choice.

For electromagnetic induction phenomena, a distribution of perfectly conducting or non-conducting regions constitutes the inductive limit, i.e. inductive effects completely dominate resistive effects. Since we will attempt to estimate the degree of electromagnetic interaction between galvanically insulated real earth conductors, a distribution of perfect conductors is a useful limit to consider.

On the other hand, a particular geophysical interpretation will be attached to our induction problem.

It is the situation in which a laterally discontinuous earth conductor is adjacent to an ocean and both conductors are underlain by a highly conducting region at some depth. Even though there is evidence for such situations in several areas of the earth (for the east coast of North America see e.g. Bailey et al., 1974; Edwards & Greenhouse, 1975), no systematic investigation of the electromagnetic interaction between such conductors has been attempted so far. The numerical approach of Lines et al. (1973) appears to be the only work related to that problem. But these authors emphasized the detectability of an anomalous upper mantle beneath an ocean. Their formulation of the coupling problem was not rigorous, and only a special and complicated model was examined. For investigating inductive coupling, simple but versatile combinations of finitely conducting thin sheets are more promising, as the number of free parameters remains limited. If only the inductive limit is to be investigated (see preceding paragraph), we thus have combinations of perfectly conducting half and whole planes, and analytical solutions for the potential are possible for certain configurations.

5.1. THIN SHEETS

The representation of laterally discontinuous conductors by thin sheets was introduced by Price (1949) and later used by many others (e.g. Schmucker, 1970a, 1971; Greenhouse et al., 1973). According to these authors, a layer of finite thickness can be replaced by a thin sheet, if the thickness δ of the former is small relative to its skin depth y_s (see eq. 5.3 below). This skin depth in turn must be smaller than that of any surrounding conductivity structure. Then the normal magnetic and tangential electric field components can be taken to be the same on both sides of the layer, which is the boundary condition for a thin sheet.

If part of this sheet is perfectly conducting, the conditions become different, because this part is no longer transparent for electromagnetic fields. As an example we consider a perfectly conducting half plane. Then the half layer it replaces must be thick relative to its own skin depth, but also thin relative to the skin depth of its host. According to Bailey (1977), for a real ocean (and thus for all real earth conductors of a regional scale), there exists no frequency such that this condition applies. However, we may only wish to model the in-phase part of the observed response. This leads us to the concept of perfect

substitute conductors, which will be investigated in the next section.

5.2. PERFECT SUBSTITUTE CONDUCTORS

The following arguments are intended to illustrate the significance of perfect substitute conductors (which must be chosen to satisfy the in-phase part of the observed response) for the imperfect conductivity distribution of the real earth. Since any distribution of perfect substitute conductors is completely characterized by a set of geometrical parameters, we wish to relate these parameters to characteristic features of the real conductivity distribution of the earth. For the sake of simplicity, we assume that this distribution be one-dimensional and essentially follow the arguments of Schmucker (1970a, b) and Haak (1978).

The inductive response of any layered half space to a homogeneous inducing field may be expressed by a frequency-dependent complex-valued response function C(y), which is usually called the inductive scale length. C(0) can be calculated directly from (i) magnetotelluric measurements (Cagniard, 1953) or (ii) measurements according to the gradient method (Schmucker, 1970a, b; Kuckes, 1973a,

b), both taken at the surface of the earth, i.e. at y = 0 (fig. 5.1).

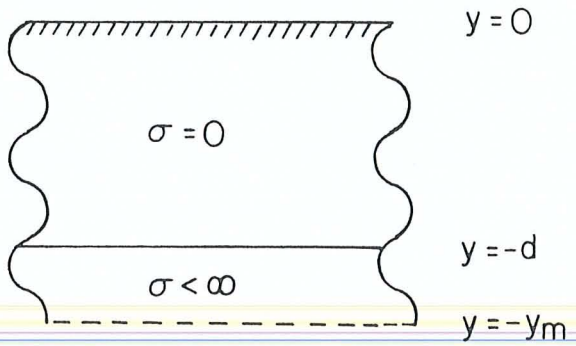

Fig. 5.1. Two-layer substitute half space (seealso text)

To obtain some insight into the properties of this response function, we now assume that the conductivity of the ground increases with depth. At a particular frequency, the subsurface can then be replaced by a two-layer substitute half space, where the conductivity of the upper layer vanishes. Therefore we effectively consider a homogeneous half space of finite conductivity σ, which extends down to infinity from some frequency-dependent depth d below the surface (fig. 5.1).

If y_s is the skin depth of this homogeneous half space, it can then be shown that

(5.1) $C(-d) = y_s/(1+i) = y_s(1-i)/2$

and also

(5.2) $C(0) = d+y_s/(1+i) = d+y_s(1-i)/2$

where y_s is given by

(5.3) $y_s = \sqrt{2/(\mu\omega\sigma)}$

Here $\omega = 2\pi/T$, which is the angular frequency in terms of the period of the harmonic oscillation. It can also be demonstrated (Weidelt, 1972) that the mean depth y_m of the in-phase part of the volume current distribution $\underline{J}(y)$ in any layered half space is given by

(5.4) $y_m = \mathrm{Re}\ C(0)$

In analogy with mechanics, where the whole mass of a body may be taken to be concentrated at the centre of gravity, we postulate an equivalent in-phase surface current $\underline{K}$ at the depth $y = y_m$. This is identical to considering a perfect substitute conductor at the same depth. For our simple model of fig. 5.1 we get

(5.5) $y_m = d+y_s/2$

which also demonstrates that, for a subsurface consisting of a homogeneous half space alone (d = 0), the skin depth is twice the mean depth of the induced currents. We thus conclude that, for the one-dimensional situation depicted in fig. 5.1, the depth of the top of the perfect substitute half space is equal to the real part of the inductive scale length of the subsurface, i.e. the mean depth of the in-phase eddy currents.

But in general Im C(0) ≠ 0, which allows us to calculate σ (eq. 5.3) and d (eq. 5.5) as well. (If the frequency behaviour of C(0,ω) is considered, Schmucker's (1969b) "ϱ*(y*)-method" results, where ϱ* and y* denote the resistivity and depth of the substitute half space, respectively.)

5.3. SCHWARZ-CHRISTOFFEL APPROACH

Now we consider some elementary two-dimensional configurations, which involve only parallel and perfectly conducting half planes or whole planes. To derive the solutions for these configurations, conformal mapping theory is applied in a specific way, which will be developed in the following.

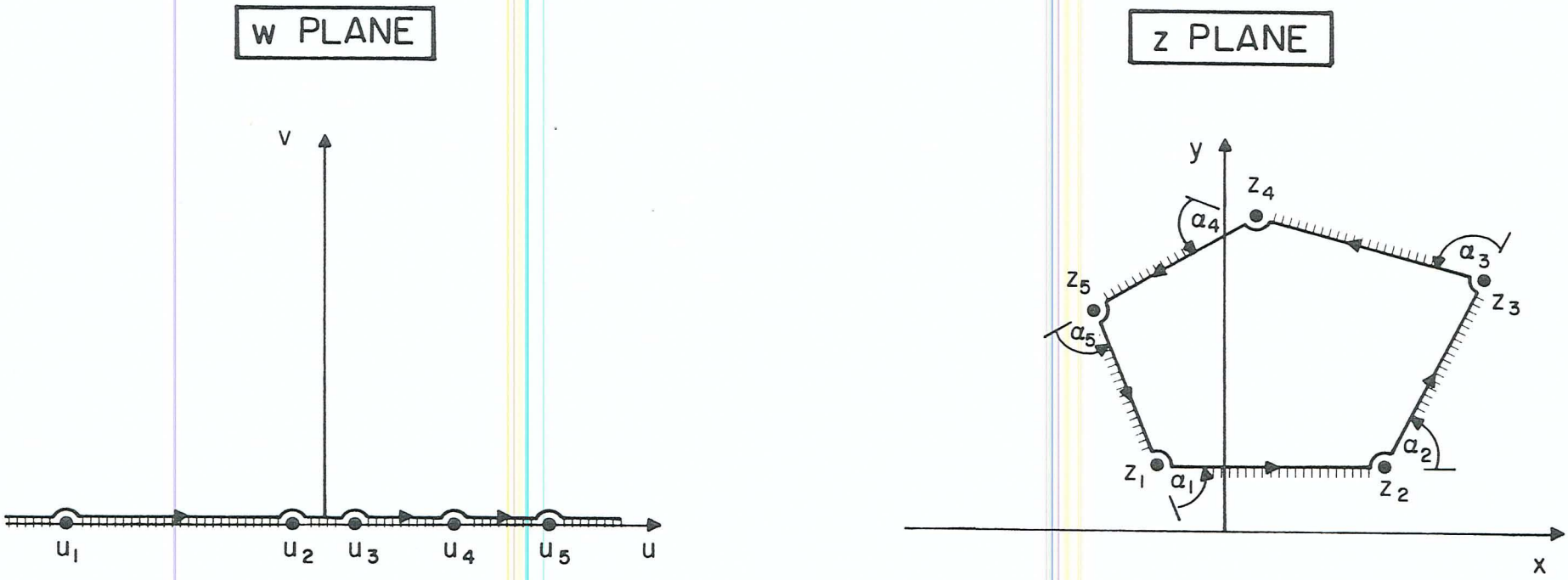

Fig. 5.2. Schwarz-Christoffel transformation (see also text)

The Schwarz-Christoffel transformation (Morse & Feshbach, 1953; Koppenfels & Stallmann, 1959) describes the mapping of the upper half of the w plane onto the interior of an arbitrary polygon of the z plane, i.e. allows us to construct the corresponding function z(w). Consider fig. 5.2. If we generalize to the case of m vertices, the differential form of the particular transformation depicted is

$$dz/dw = A\prod_{\mu=1}^{m}(w-u_\mu)^{-\alpha_\mu/\pi} \tag{5.6}$$

Integration of this equation yields the usual form of the Schwarz-Christoffel transformation, i.e.

$$z = z_\mu + A\int_{w_\mu}^{w}\prod_{\mu=1}^{m}(w'-u_\mu)^{-\alpha_\mu/\pi}\,dw' \tag{5.7}$$

Here z_μ is determined by the position of any of the polygon's vertices relative to the origin z = 0, whereas the magnitude and phase of A are related to the polygon's scale and orientation, respectively. The values of the real parameters u_μ are fixed by the requirement $z_\mu = z(u_\mu)$, for $\mu = 1,\ldots,m$ (see fig. 5.2). The meaning of the angles α_μ is obvious from the same figure. We thus have (m + 3) free parameters in total, and hence three of the u_μ's may be chosen arbitrarily. Often two of them are placed at infinity. Then the corresponding factors do not

appear in the integrand of eq. 5.7 any more (Morse & Feshbach, 1953).

In the following, the surfaces of the (two-dimensional) conductors will always be assumed to coincide with the contours of integration in the w or z planes (cf. the hatching in figs. 5.2 to 5.6, especially the cross-sections of perfectly conducting half or whole planes in figs. 5.3 and 5.5). In particular, we will consider two principal cases, which are designated as case A (fig. 5.4) and case B (fig. 5.6). Case A comprises three distinct polygons ("models"), certain parts of which are congruent. If the vertices approach infinity as indicated in fig. 5.4, three corresponding degenerate polygons (combinations of half and whole planes) result (fig. 5.3). More specifically, we have

Model A.L.1: The vertices are at z_1, z_2, z_3, z_4', z_7. Thus half plane 1 has its edge at $z_2 = -L/2+ih_1$ and extends towards $x = -\infty$ (L = "left"). The whole plane is at $y = 0$.

Model A.R.2: The vertices are at z_3', z_4, z_5, z_6, z_7. Thus half plane 2 has its edge at $z_5 = +L/2+ih_2$ and extends towards $x = +\infty$ (R = "right"). The whole plane is at $y = 0$.

Model A.L.1/R.2: The vertices are at

z_1, z_2, z_3, z_4, z_5, z_6, z_7. Half planes 1 and 2 and the whole plane are located as before.

We will later superimpose the responses of models A.L.1 and A.R.2 and compare this with the response of model A.L.1/R.2.

If we consider case B, we again have three distinct polygons, certain parts of which are congruent. Referring to figs. 5.5 and 5.6, we distinguish the following models.

Model B.L.1: The vertices are at z_1, z_2, z_5', z_6, z_7. Thus half plane 1 has its edge at $z_2 = -L/2+ih_1$ and extends towards $x = -\infty$ (L = "left"). The whole plane is at $y = 0$.

Model B.L.2: The vertices are at z_3', z_4, z_5, z_6, z_7. Thus half plane 2 has its edge at $z = +L/2+ih_2$ and extends towards $x = -\infty$ (L = "left"). The whole plane is at $y = 0$.

Model B.L.1/L.2: The vertices are at z_1, z_2, z_3, z_4, z_5, z_6, z_7. Half planes 1 and 2 and the whole plane are located as before.

This will allow us again to compare the sum of the responses of models B.L.1 and B.L.2 with the response of model B.L.1/L.2.

In secs. 5.3.1 to 5.3.6 we will summarize the relevant

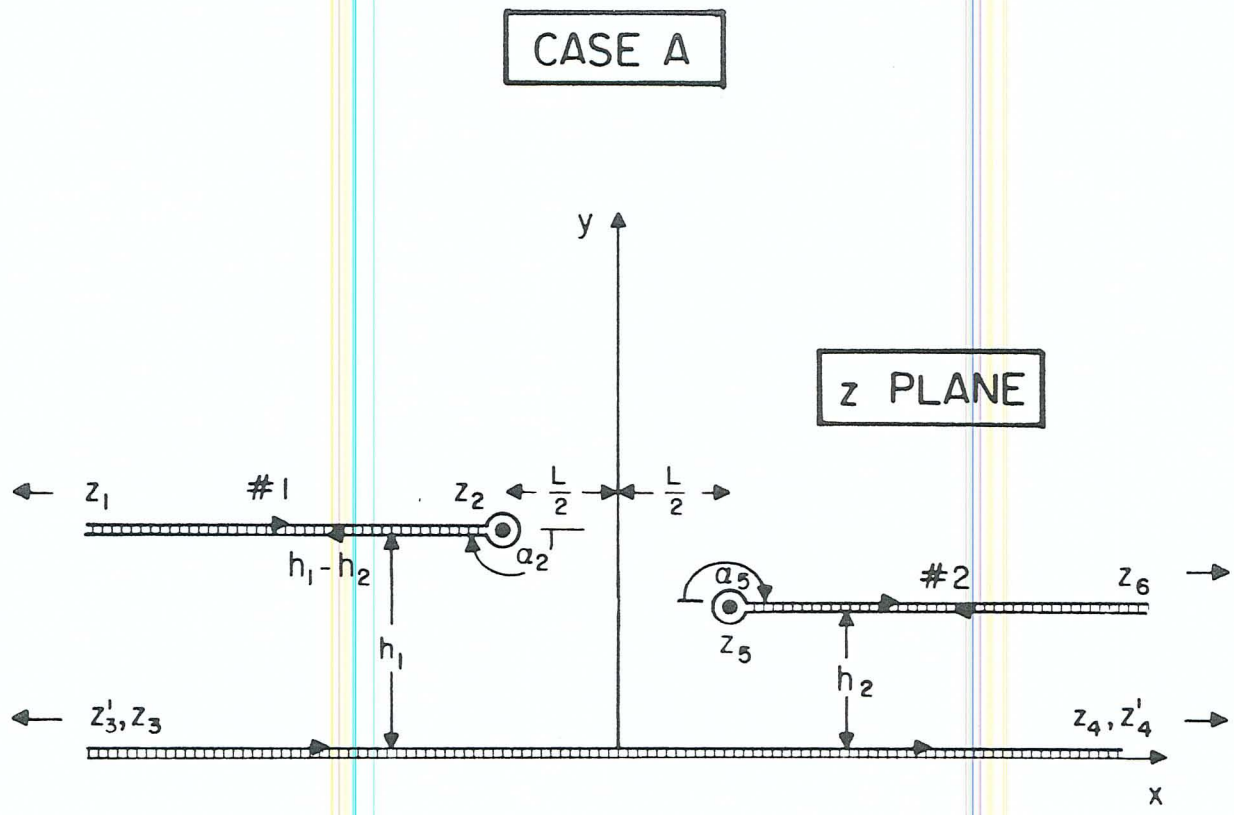

Fig. 5.3. Conductor configurations (degenerate polygons) of case A. Three distinct combinations of one or two conducting half planes and one conducting whole plane are possible (conductors are hatched): Model A.L.1: Half plane 1 ($x < -L/2$, $y = h_1$) and whole plane ($y = 0$). Model A.R.2: Half plane 2 ($x > +L/2$, $y = h_2$) and whole plane ($y = 0$). Model A.L.1/R.2: Half plane 1 ($x < -L/2$, $y = h_1$), half plane 2 ($x > +L/2$, $y = h_2$) and whole plane ($y = 0$)

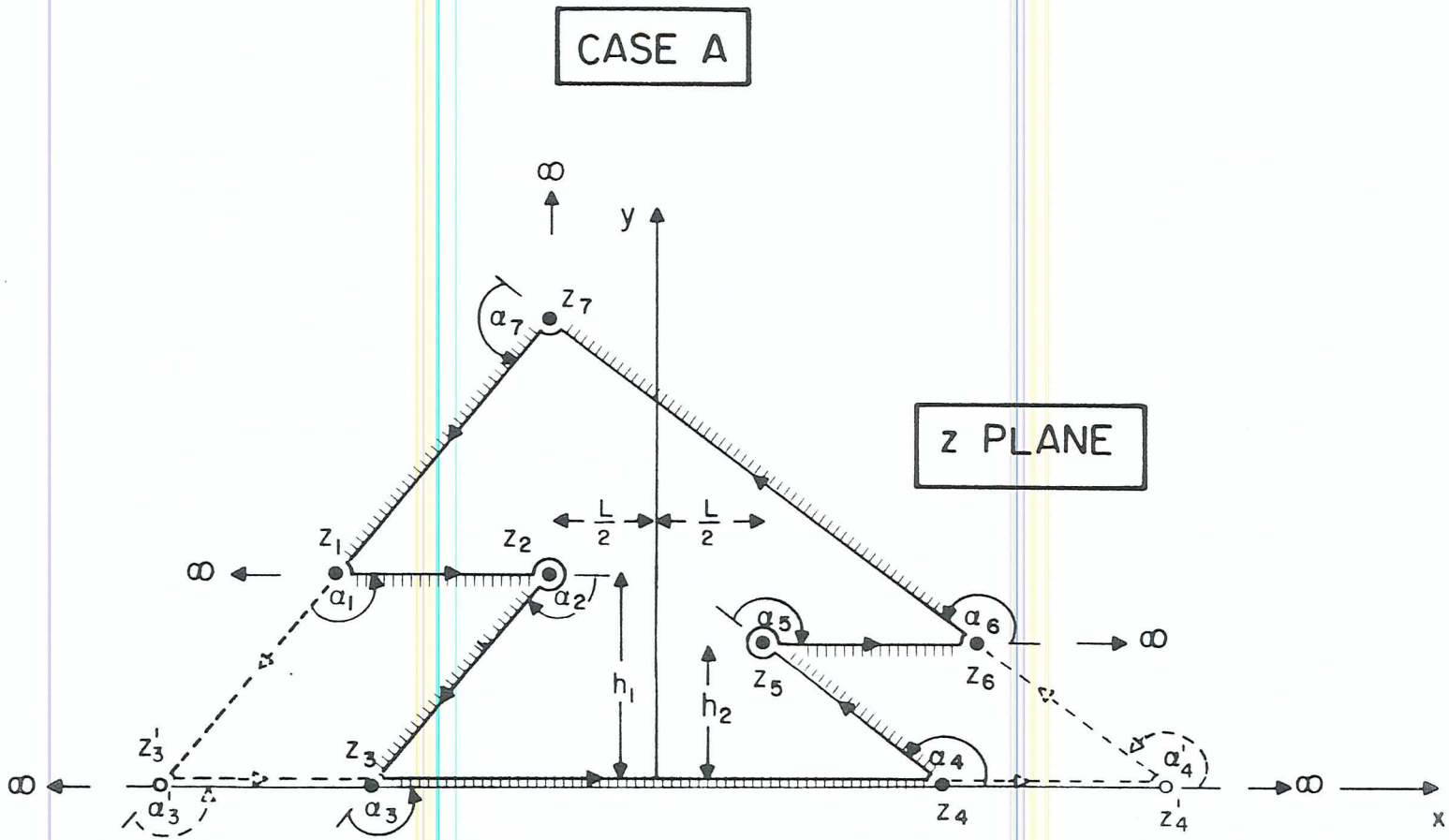

Fig. 5.4. Ordinary polygons corresponding to the three degenerate cases of fig. 5.3. Three distinct polygons are shown: Model A.L.1: Vertices at z_1, z_2, z_3, z_4', z_7. Model A.R.2: Vertices at z_3', z_4, z_5, z_6, z_7. Model A.L.1/R.2: Vertices at z_1, z_2, z_3, z_4, z_5, z_6, z_7

formulae for each of the six models.

5.3.1. MODEL A.L.1

Here we outline how the mapping corresponding to model A.L.1 is actually realized. Similar arguments apply to the remaining models (although for models A.L.1/R.2 and B.L.1/L.2 the calculations become considerably more complicated).

As was noted before, for a conformal transformation of the upper w plane onto a distinct polygon of the z plane, we may choose three of the u_μ's arbitrarily. Considering then u_2 as the parameter to be determined, we write

(5.8.1) $\quad u_1 = -\infty$

(5.8.2) $\quad u_2 = u_2(h_1, a, A)$

(5.8.3) $\quad u_3 = -a < 0$

(5.8.4) $\quad u_4' = +\infty$

If the geometry of the configuration is as shown in fig. 5.3, eq. 5.7 becomes

(5.9) $$z(w) = A\{w+a+\frac{h_1}{\pi A}[\ln(w+a)-\ln\frac{h_1}{\pi A}+1]-\frac{L}{2A}\}$$

In this equation, u_2 has been eliminated by integration of eq. 5.7 between $u_1 = -\infty$ and $u_4' = +\infty$, which yields

(5.10) $$u_2 = -(a+\frac{h_1}{\pi A}) < -a$$

Thus A is arbitrary as long as it is positive and determines the scale of the mapping.

Model A.L.1 is one of the basic models considered by Schmucker (1970a) in his attempt to explain the Californian coastal anomaly.

5.3.2. MODEL A.R.2

We choose

(5.11.1) $$u_3' = -\infty$$

(5.11.2) $$u_4 = a > 0$$

(5.11.3) $$u_5 = u_5(h_2, a, A)$$

(5.11.4) $$u_6 = +\infty$$

where u_5 is the parameter to be determined. The appropriate transformation is (see fig. 5.3)

$$(5.12) \qquad z(w) = A\{w-a-\frac{h_2}{\pi A}[\ln(w-a)-\ln\frac{h_2}{\pi A}+1-i\pi]+\frac{L}{2A}\}$$

where

$$(5.13) \qquad u_5 = a+\frac{h_2}{\pi A} > a$$

has been used. A may again be chosen arbitrarily, as long as it is positive.

5.3.3. MODEL A.L.1/R.2

Setting $u_3 = -u_4$, only two of the u_μ's, u_1 and u_6, can be chosen at will. We set

$$(5.14.1) \qquad u_1 = -\infty$$

$$(5.14.2) \qquad u_2 = u_2(h_1, h_2, a, A)$$

$$(5.14.3) \qquad u_3 = -a < 0$$

$$(5.14.4) \qquad u_4 = a(L, h_1, h_2, A)$$

(5.14.5) $u_5 = u_5(h_1, h_2, a, A)$

(5.14.6) $u_6 = +\infty$

The proper transformation is (see fig. 5.3)

(5.15) $$z(w) = A\left[w + \frac{h_1}{\pi A} \ln \frac{w+a}{\sqrt{2h_1 a/(\pi A)}} - \frac{h_2}{\pi A} \ln \frac{w-a}{\sqrt{2h_2 a/(\pi A)}} + \frac{h_1 - h_2}{2\pi A} + ih_2\right]$$

Here a is implicitly given by

(5.16.1) $$L = A\left\{2\sqrt{\ } + \frac{h_1}{\pi A} \ln \frac{\left[\sqrt{\ } + \left(a - \frac{h_1 - h_2}{2\pi A}\right)\right]^2}{2h_1 a/(\pi A)} + \frac{h_2}{\pi A} \ln \frac{\left[\sqrt{\ } + \left(a + \frac{h_1 - h_2}{2\pi A}\right)\right]^2}{2h_2 a/(\pi A)}\right\}$$

where

(5.16.2) $$\sqrt{\ } \equiv \sqrt{\frac{(h_1 - h_2)^2}{4\pi^2 A^2} + \frac{(h_1 + h_2)a}{\pi A} + a^2}$$

Eq. 5.16.1 is the inversion of eq. 5.14.4. In eq. 5.15 we have also used

(5.16.3) $$u_2 = -\frac{h_1-h_2}{2\pi A} - \sqrt{\ }$$

(5.16.4) $$u_5 = -\frac{h_1-h_2}{2\pi A} + \sqrt{\ }$$

with $\sqrt{\ }$ again given by eq. 5.16.2.

The special case $h_1 = h_2$ of this model has already been discussed by Schmucker (1964, 1970a) with reference to the anomaly caused by a (two-dimensional) island structure.

For simplicity, we set $A = h_1/\pi$. Numerical inversion of eq. 5.16.1 yields a. Then u_2 and u_5 of model A.L.1/R.2 are determined according to eqs. 5.16.3 and 5.16.4. These values of A and a are inserted into eqs. 5.10 and 5.13, which allows u_2 and u_5 to be redetermined for models A.R.1 and A.L.2. This choice of parameters is not the only one possible. However, it relates the three basic models in a convenient way.

Now we refer to figs. 5.5 and 5.6 and derive equivalent formulae for case B.

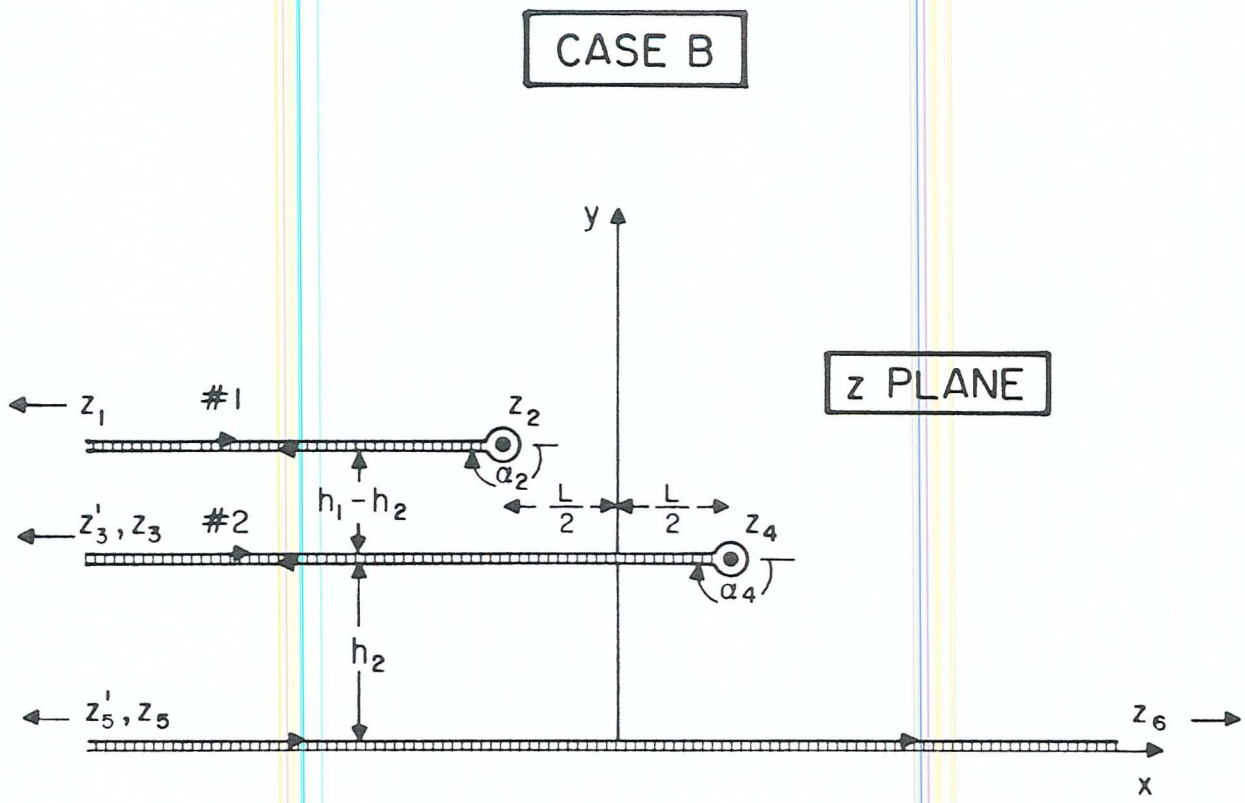

Fig. 5.5. Conductor configurations (degenerate polygons) of case B. Three distinct combinations of one or two conducting half planes and one conducting whole plane are possible (conductors are hatched): Model B.L.1: Half plane 1 ($x < -L/2$, $y = h_1$) and whole plane ($y = 0$). Model B.L.2: Half plane 2 ($x < +L/2$, $y = h_2$) and whole plane ($y = 0$). Model B.L.1/L.2: Half plane 1 ($x < -L/2$, $y = h_1$), half plane 2 ($x < +L/2$, $y = h_2$) and whole plane ($y = 0$)

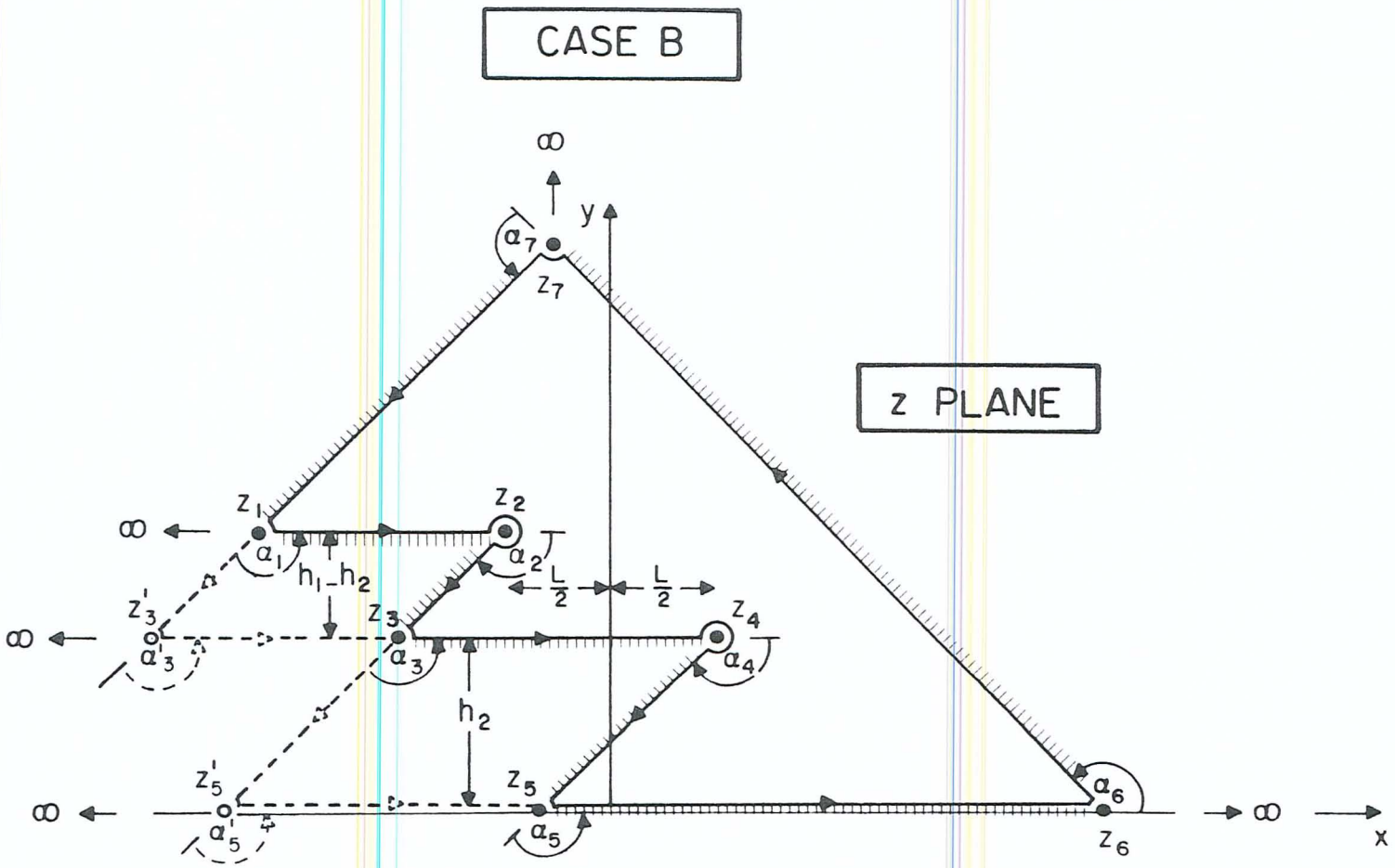

Fig. 5.6. Ordinary polygons corresponding to the three degenerate cases of fig. 5.5. Three distinct polygons are shown: Model B.L.1: Vertices at z_1, z_2, z'_5, z_6, z_7. Model B.L.2: Vertices at z'_3, z_4, z_5, z_6, z_7. Model B.L.1/L.2: Vertices at z_1, z_2, z_3, z_4, z_5, z_6, z_7

5.3.4. MODEL B.L.1

This model is identical with model A.L.1. For convenience it is listed here again according to the notation of fig. 5.5. We select

(5.17.1) $u_1 = -\infty$

(5.17.2) $u_2 = u_2(h_1, a, A)$

(5.17.3) $u_5' = -a < 0$

(5.17.4) $u_6 = +\infty$

where u_2 is to be determined. Thus

(5.18) $$z(w) = A\{w+a+\frac{h_1}{\pi A}[\ln(w+a)-\ln\frac{h_1}{\pi A}+1]-\frac{L}{2A}\}$$

as before, where

(5.19) $$u_2 = -(a+\frac{h_1}{\pi A}) < -a$$

with A as a positive quantity.

5.3.5. MODEL B.L.2

This model is closely related to models A.L.1 and B.L.1. However, this time the parameters are chosen to be

(5.20.1) $u_3' = -\infty$

(5.20.2) $u_4 = u_4(h_2, a, A)$

(5.20.3) $u_5 = a > 0$

(5.20.4) $u_6 = +\infty$

with u_4 to be determined. The transformation formula is (see fig. 5.5)

(5.21) $$z(w) = A\{w-a+\frac{h_2}{\pi A}[\ln(w-a)-\ln\frac{h_2}{\pi A}+1]+\frac{L}{2A}\}$$

This equation implies that

(5.22) $$u_4 = a-\frac{h_2}{\pi A} < a$$

and a positive scaling factor A is required.

5.3.6. MODEL B.L.1/L.2

As in section 5.3.3, a symmetrical choice of parameters ($u_3 = -u_5$) is employed. Thus, only two parameters, u_1 and u_6, can be chosen at will. Now we set

(5.23.1) $u_1 = -\infty$

(5.23.2) $u_2 = u_2(h_1, h_2, a, A)$

(5.23.3) $u_3 = -a < 0$

(5.23.4) $u_4 = u_4(h_1, h_2, a, A)$

(5.23.5) $u_5 = a(L, h_1, h_2, A)$

(5.23.6) $u_6 = +\infty$

This time we have the transformation (see fig. 5.5)

(5.24) $$z(w) = A\left[w + \frac{h_1 - h_2}{\pi A} \ln \frac{w+a}{\sqrt{2(h_1-h_2)a/(\pi A)}}\right.$$

$$\left. + \frac{h_2}{\pi A} \ln \frac{w-a}{\sqrt{2h_2 a/(\pi A)}} + \frac{h_1}{2\pi A}\right]$$

Parameter a is given by

$$(5.25.1) \qquad L = A\left\{2\sqrt{} + \frac{h_1-h_2}{\pi A}\ln\frac{\left[\sqrt{}+\left(a-\frac{h_1}{2\pi A}\right)\right]^2}{2(h_1-h_2)a/(\pi A)}\right.$$

$$\left. -\frac{h_2}{\pi A}\ln\frac{\left[\sqrt{}+\left(a+\frac{h_1}{2\pi A}\right)\right]^2}{2h_2 a/(\pi A)}\right\}$$

with

$$(5.25.2) \qquad \sqrt{} \equiv \sqrt{\frac{[h_2+(h_1-h_2)]^2}{4\pi^2A^2} - \frac{[h_2-(h_1-h_2)]\,a}{\pi A} + a^2}$$

Eq. 5.25.1 is the inversion of eq. 5.23.5. In eq. 5.24 it is also implied that

$$(5.25.3) \qquad u_2 = -\frac{h_1}{2\pi A} - \sqrt{}$$

$$(5.25.4) \qquad u_4 = -\frac{h_1}{2\pi A} + \sqrt{}$$

where $\sqrt{}$ has been defined in eq. 5.25.2.

To correlate the three models of case B, we again set $A = h_1/\pi$. Numerical inversion of eq. 5.25.1 yields a, and it then becomes possible to determine u_2 and u_4 for model B.L.1/L.2 according to eqs. 5.25.3 and 5.25.4. Since a and A are now known, we obtain u_2 and u_4 for models B.L.1 and B.L.2.

5.4. INVERSION OF MAPPINGS AND SOLUTIONS FOR MAGNETIC POTENTIAL

As was emphasized at the end of chap. 4, the problem of obtaining solutions for the models of cases A and B reduces to deriving the solutions $\Omega(w)$ for the potential in the w plane and obtaining the transformations w(z). In the preceding secs. 5.3.1 to 5.3.6, the equations of the corresponding inverse functions z(w) have been given for the various models. Thus, if $\Omega(w)$ is known, the task remains to invert the functions z(w) and obtain w(z).

In the w plane, we have assumed a perfectly conducting whole plane at $v = 0$ (see fig. 5.2). The simplest solution for this configuration is a potential that yields a homogeneous magnetic field in the u direction. Thus

(5.26.1) $\Omega(w) = B_u w$

(5.26.2) $B(w) = B_u$

where B_u is the horizontal component of the magnetic induction in the w plane. If we transform this to the z plane, we obtain

(5.27.1) $\Omega(z) = B_u w(z)$

(5.27.2) $$B(z) = B_u \frac{dw}{dz} = \frac{B_u}{dz/dw}$$

If we consider the different mappings z(w), we realize that, for $z \to \infty$, we again have a homogeneous and horizontal field, which, for $B_u = A$, is of unit strength. Our different conductor configurations in the z plane are therefore subject to a uniform inducing field. This is the magnetic source geometry most widely assumed. A discussion of the limitations of this assumptions has been given by several authors, see e.g. Price (1964) or Greenhouse et al. (1973).

To obtain solutions $\Omega(z)$ or B(z) at arbitrary points of the z plane, the inverse functions w(z) of z(w) must be derived. However, a short inspection of the different functions z(w) shows that the inversions have to be carried out numerically. Here we employ the Newton-Raphson iteration scheme.

This algorithm, which was originally derived by Raphson in 1690 (but has some points in common with an earlier method proposed by Newton), calculates the zeros of a function, which can also be complex-valued. We therefore rearrange z = z(w) and write

(5.28) $$g(w) = z - z(w) = 0$$

where w is a zero of the function g(w). However, for $w_0 = w+\varepsilon$, we have in general $z \neq z(w_0)$ and

(5.29) $$g(w_0) = z-z(w_0) \neq 0$$

The Newton-Raphson iteration scheme can now be formulated as

(5.30) $$w_\nu = w_{\nu-1}-g(w_{\nu-1})/g'(w_{\nu-1}) \qquad (\nu = 1,\ldots,n)$$

where g' denotes the first derivative of g with respect to w. With a suitable initialization w_0 the iterations rapidly converge towards the required zero, and after n steps we set

(5.31) $$w_n = w$$

If we wish to invert z(w) for a rectangular grid of i lines and j columns of values in the z plane, eq. 5.30 must be applied to an (i,j) matrix of z values. The initial values w_0 in general depend on the particular z value chosen, but some trial and error initialization ensures that the correct zeros w are obtained. The same iteration scheme has been applied to invert eqs. 5.16.1 and 5.25.1, i.e. to obtain $a = a(L,h_1,h_2,A)$, where a is real.

With w(z) determined (at least for a rectangular grid in the z plane), we can now calculate $\Omega(z)$ and B(z)

according to eqs. 5.27.1 and 5.27.2. But with eqs. 4.11 and 4.13, the real quantities ϕ, ψ, B_x, B_y are also determined, and we can derive various transfer functions as necessary.

A versatile FORTRAN program has been written in order to facilitate the numerical aspects of this investigation. It is capable of calculating all major magnetic quantities at arbitrarily spaced points in the vicinity of arbitrary conductor configurations of cases A or B. The program output is in form of profiles or grids of data and allows rapid comparisons between related configurations.

5.5. CAUCHY INTEGRAL APPOACH

A somewhat different approach of constructing conformal mappings will also be outlined. For an arbitrary closed contour in the w plane, the Cauchy integral formula states that

$$\tilde{z}(w) = (1/2\pi i)\oint_C \frac{\tilde{z}(w')}{w'-w}dw' \tag{5.32}$$

if w is an interior point of C, or

$$0 = (1/2\pi i)\oint_C \frac{\tilde{z}(w')}{w'-w}dw' \tag{5.33}$$

if w is an exterior point of C. Here $\tilde{z}(w)$ must be analytic within C and continuous on C. Consider a contour around the upper half w plane. If $\tilde{z}(w)$ vanishes for $w \to \infty$ sufficiently fast, the contour integrals reduce to integrations along the u axis, and we can show (see Morse & Feshbach, 1953) that

$$\tilde{z}(w) = (1/\pi i)\int_{-\infty}^{+\infty} \frac{\tilde{x}(u')}{u'-w}\,du' \qquad (5.34.1)$$

$$\tilde{z}(w) = (1/\pi)\int_{-\infty}^{+\infty} \frac{\tilde{y}(u')}{u'-w}\,du' \qquad (5.34.2)$$

where $\tilde{y}(u') \equiv \tilde{y}(u',0)$ and $v > 0$. Thus, either the real or the imaginary part of $\tilde{z}(w)$ along the real u axis alone suffice to determine the function everywhere in the upper half w plane.

More generally, for a function z(w) that does not necessarily vanish for $w \to \infty$, we write instead of eq. 5.34.2

$$z(w) = w - \frac{y^+ - y^-}{\pi} \ln\, w + iy^+ + (1/\pi)\int_{-\infty}^{+\infty} \frac{\tilde{y}(u')}{u'-w}\,du' \qquad (5.35)$$

and for the imaginary part of z along the u axis

$$y(u) = \begin{cases} \tilde{y}(u) + y^-, & u < 0 \\ \tilde{y}(u) + y^+, & u > 0 \end{cases} \qquad (5.36)$$

Here we have implied the definition

$$y^{\pm} \equiv \lim_{u \to \pm\infty} y(u) \tag{5.37}$$

Eq. 5.35 was used by Weidelt (1981) for the solution of a related inverse problem (see chap. 8). It can be proved by showing that

$$\lim_{v \to +0} \mathrm{Im}\, z(w) = y(u) \tag{5.38}$$

However, eq. 5.38 is readily established if we make use of the identity

$$\delta(u'-u) \equiv \lim_{v \to +0} \frac{1}{\pi} \frac{v}{(u'-u)^2 + v^2} \tag{5.39}$$

where δ denotes the Dirac delta function.

We may visualize eq. 5.35 as being a single-valued analytic function that maps the trace v = 0 of the w plane onto another trace x(u)+iy(u) of the z plane (contour C_1 in fig. 5.7). If it can even be shown that this function has a single-valued inverse, it constitutes a conformal mapping, and C_1 can be identified as the surface of a perfect conductor. In particular, it becomes possible to derive the various mapping functions inherent in cases A and B in an alternative way.

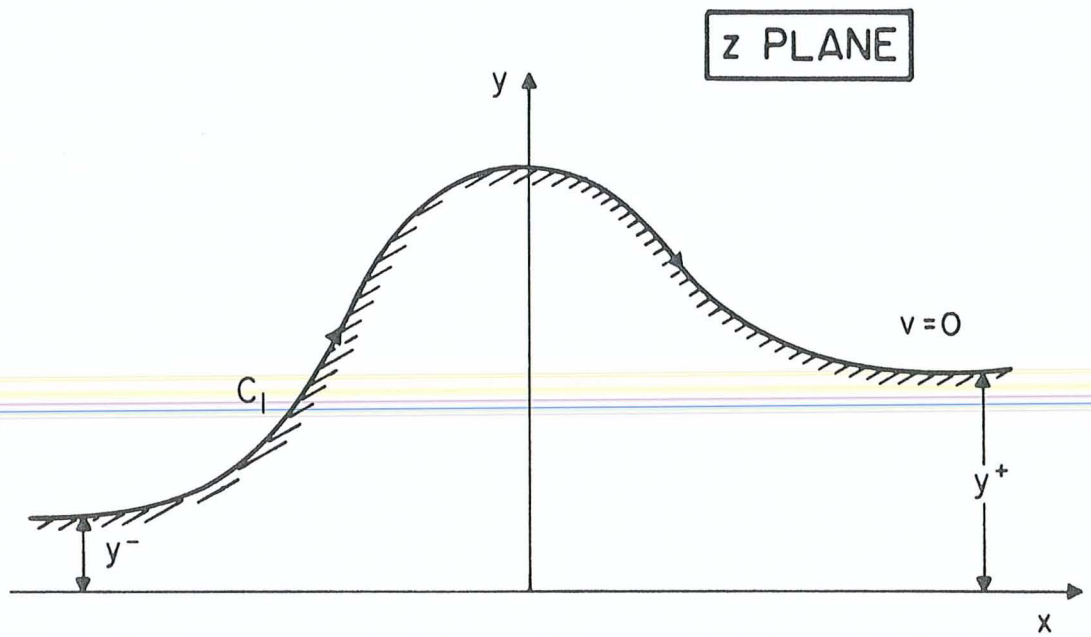

Fig. 5.7. Contour C_1 in the z plane (see also text)

As an example, let us consider model A.L.1. If we set $y^- = h_1$ and $y^+ = 0$, with $\tilde{z}(w) = 0$, we can write for eq. 5.35

(5.40) $$z(w) = w + (h_1/\pi) \ln w$$

Referring to eq. 5.9, we realize that, with A = 1, we simply have to apply the transformations

(5.41) $u_3 \rightarrow u_3 - a$

(5.42) $z \rightarrow z-(h_1/\pi)[\ln(h_1/\pi)-1]-L/2$

and eqs. 5.9 and 5.40 become identical.

In a similar fashion, all the other mappings that we have derived above using the Schwarz-Christoffel transformation may now be recovered by a consideration of eq. 5.35. But for the configurations involving two conducting half planes, $\tilde{y}(u)$ does not vanish in general, and eq. 5.34.2 has to be integrated to obtain $\tilde{z}(w)$.

Finally, a method for the direct calculation of inverse mappings $w(z)$ will be indicated. If $\tilde{w}(z)$ vanishes sufficiently fast for $z \rightarrow \infty$, we can give the Cauchy integral formula the form

(5.43) $$w(z) = z+\tilde{w}(z) = z+(1/2\pi i)\int_{C_1} \frac{\tilde{w}(z')}{z'-z}dz'$$

where C_1 coincides with the surface of a perfect conductor (see fig. 5.7) and $y^- = y^+ = 0$ (local distortion). Here, we have along contour C_1

(5.44) $\quad Im\ w(z') = v(x',y') = y'+\tilde{v}(x',y')$

But from fig. 5.7 we realize that $v(x',y') = 0$, and therefore

$$\tilde{v}(x',y') = -y' \tag{5.45}$$

Obviously, $\tilde{v}(x',y')$ is known for the problem, and it remains to calculate $\tilde{u}(x',y')$ and then evaluate eq. 5.43. Several different methods exists for determining Re $\tilde{w}(z')$ from Im $\tilde{w}(z')$, where z' is on C_1, e.g. Fourier transform methods (Bailey, personal communication). The following approach, however, is due to Gerschgorin and Lichtenstein (see Koppenfels & Stallmann, 1959).

For a point z on contour C_1, the Cauchy integral formula reads

$$w(z) = (1/\pi i)\oint_{C_1} \frac{\tilde{w}(z')}{z'-z}\,dz' \tag{5.46}$$

where $\oint$ denotes the principal value of the integral. Introducing

$$z'-z = r\exp(i\theta) \tag{5.47}$$

we get

$$dz'/(z'-z) = dr/r+id\theta \tag{5.48}$$

Eq. 5.46 then becomes

$$(5.49) \qquad \tilde{w}(z) = (1/\pi i) \oint_{C_1} [\tilde{u}(x',y')+i\tilde{v}(x',y')][dr/r+id\theta]$$

Taking the imaginary part, eq. 5.49 reduces to

$$(5.50) \qquad \tilde{u}(x,y) = (1/\pi)\Big[\oint_{C_1} \tilde{u}(x',y')d\theta + \oint_{C_1} \tilde{v}(x',y')(dr/r)\Big]$$

Because of eq. 5.45, the second integral can be evaluated and is set equal to $\gamma(x,y)$. Then we have

$$(5.51) \qquad \tilde{u}(x,y) = (1/\pi) \oint \tilde{u}(x',y')d\theta + \gamma(x,y)$$

This is an inhomogeneous Fredholm equation of the second kind, which can be solved by expansion into a Neumann series.

The advantage of this method is obviously that, although C_1 can be rather arbitrarily shaped, $\tilde{w}(z)$ is obtained directly by numerical integration without any inversion. On the other hand, $\tilde{v}(x',y')$ must vanish for large values of z', i.e. only a local distortion of an otherwise horizontal interface can be considered.

No numerical evaluation of eqs. 5.46 and 5.51 has been carried out, but a possible application of this method will

be referred to in chap. 8.

5.6. SINGULARITIES OF MAGNETIC FIELD AND ELECTRIC CURRENT

As has been stated in sec. 2.2, Parker (1968) demonstrated that at the edge of a finitely conducting half plane the (vertical) magnetic field had a logarithmic singularity, whereas the surface current density remained finite. In this section we consider the corresponding behaviour for a perfectly conducting half plane.

Referring to fig. 5.8, we can state the conformal transformation of the upper w plane onto the whole z plane as

$$z = x+iy = w^2 = u^2-v^2+2iuv \tag{5.52}$$

This mapping was used by Hermance (1968) in his investigation of the coast effect in Iceland. It transforms a perfectly conducting whole plane at $u = 0$ into a corresponding half plane at $y = 0$, $x \geq 0$. The complex magnetic potential of a line current at w_o (its image current being at w_o^*) is given by

$$\Omega(w) = i\lambda \ln \frac{W-W_o^*}{W-W_o} - \frac{\lambda\pi}{2} \tag{5.53}$$

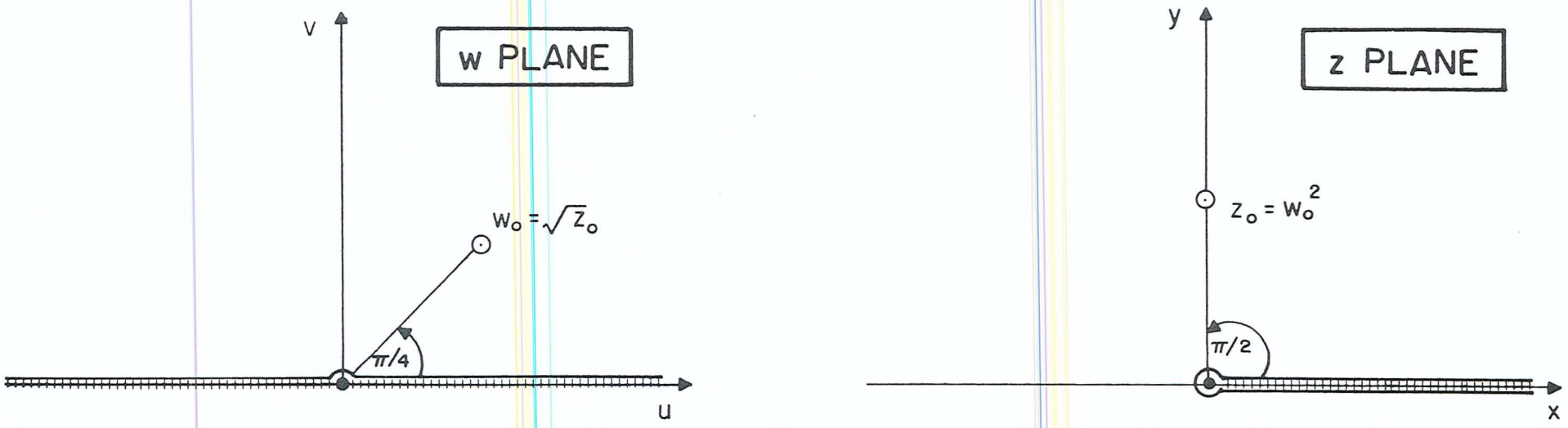

Fig. 5.8. Conformal mapping of the upper half w plane onto the whole z plane

where λ is a measure for the strength of the source current. Transformation onto the z plane yields

$$(5.54) \qquad \Omega(z) = \Omega(w(z)) = i\lambda \ln \frac{z^{1/2} - z_0^{*1/2}}{z^{1/2} - z_0^{1/2}} - \frac{\lambda\pi}{2}$$

where we have $\Omega(z=0) = 0$. We then find for the magnetic field

$$(5.55) \qquad B(z) = \frac{i\lambda}{2\sqrt{z}} \left(\frac{1}{\sqrt{z} - \sqrt{z_0^*}} - \frac{1}{\sqrt{z} - \sqrt{z_0}} \right)$$

But with $|z_0| \equiv y_0$ and arc $z_0 = \pi/2$, we can also write

$$(5.56) \qquad B(z) = \frac{i}{\sqrt{2z}} \left(\frac{1}{\sqrt{z/y_0} - \sqrt{-i}} - \frac{1}{\sqrt{z/y_0} - \sqrt{i}} \right)$$

where we have chosen $\lambda^2 = 2y_0$. If z/y_0 is a very small quantity, we effectively consider the region very close to the edge of the sheet, where the field is quasi-homogeneous, and get

$$(5.57) \qquad B(z) = B_x - iB_y = 1/\sqrt{z}$$

$$(5.58) \qquad \Omega(z) = \phi + i\Psi = 2\sqrt{z}$$

Eq. 5.57 is equivalent to a normalization of the magnetic field such that for $z = 1$ we have $B_x = 1$ and $B_y = 0$.

If we consider the situation in the plane of the perfectly conducting sheet, i.e. for y = 0, we get

(5.59.1) $$B_x^+(x) = x^{-1/2} \quad , \; x \geq 0$$

(5.59.2) $$B_x^-(x) = -x^{-1/2} \quad , \; x \geq 0$$

where we have used the definition

(5.60) $$B_x^{\pm}(x) \equiv \lim_{y \to \pm 0} B_x(x,y)$$

With $B_y(x) \equiv B_y(x,0)$, the vertical component becomes

(5.61) $$B_y(x) = (-x)^{-1/2} \quad , \; x < 0$$

Instead of boundary condition 4.2.2 we have for a thin sheet

(5.62) $$\hat{\underline{e}}_n \times (\underline{B}^+ - \underline{B}^-) = \mu_0 \underline{K}$$

where the unit vector points into the positive direction. This immediately leads to

(5.63) $$K(x) = 2x^{-1/2} / \mu_0$$

for the magnitude of the surface current density in the

vicinity of the edge.

Clearly, the problem of finding the magnetic field in the vicinity of an isolated and perfectly conducting half plane, subject to a uniform inducing field, is indeterminate or ill-posed, i.e. no unique solution exists. This was emphasized by Siebert (1965) and is due to the fact that no length scale is inherent in this model. The problem can be rendered unique, if it is considered as the limit of a more general case. In this section, a uniform source field structure has been obtained after the line current has approached infinity and become infinitely strong.

CHAPTER 6

INDUCTIVE COUPLING BETWEEN OCEAN, EARTH CONDUCTOR AND CONDUCTOSPHERE

6.1. GENERAL REMARKS

In this chapter some results for the models described in the previous chapter are presented. To facilitate our discussion, a common normalization of the magnetic field components is adopted. We define as normal the field at a point far away from the lateral discontinuity, where the conductivity structure is effectively one-dimensional.

The following decompositions of the total field components may now be performed (Schmucker, 1964, 1970a).

(6.1.1) $B_x = B_{xn} + B_{xa}$

(6.1.2) $B_y = B_{yn} + B_{ya}$

Here $B_{yn} = 0$, because the source fields are uniform, and we can therefore write instead of eq. 3.1

(6.2.1) $$B_{xa}(t) = S_{xx} B_{xn}(t)$$

(6.2.2) $$B_{ya}(t) = S_{yx} B_{xn}(t)$$

where S_{xx} and S_{yx} are the horizontal and vertical Schmucker transfer functions, respectively. It should be noted that no causal relation is implied by eqs. 6.2. This was emphasized by Bailey et al. (1977).

Since we deal with perfect conductors, the scaling parameter p (see eq. 3.2) is always infinite. In other words, all geometrically similar configurations are inductively equivalent, irrespective of the time scale chosen. If we confine ourselves to configurations that involve a single half plane parallel to a whole plane, only one geometrical parameter, viz. their separation, is involved, and all such configurations are geometrically similar and therefore inductively equivalent. This in turn suggests the normalization of all lengths relative to this geometrical parameter. In the more general case, however, we have two half planes parallel to the whole plane, i.e. three geometrical parameters h_1, h_2 and L (see figs. 5.3 and 5.5). This means that different configurations are not, in general, equivalent.

In the following, all lengths will be normalized relative the separation h_1 between half plane 1 and the whole plane, and the inductive response for several values of the ratios h_2/h_1 and L/h_1 will be investigated. To gain some insight into the basic features of the response, the normalized field distribution for two characteristic configurations of models A.L.1/R.2 and B.L.1/L.2 are shown in figs. 6.1 and 6.2, respectively. The forcing of the field vectors about the edges of the half planes is very conspicuous. This behaviour is related to the fact that the magnetic field must be tangential to the surfaces of the perfect conductors. The screening effect of the half planes is also displayed, but some magnetic flux "leaks" into the region between the half planes and the whole plane.

When interpreting our results in the following two sections, emphasis will be placed on the inductive coupling between the conductors. More specifically, we will compare the sum of the responses of two models, each one involving only one half plane parallel to a whole plane, with the response of the corresponding complete model consisting of both half planes and the whole plane. Theoretically, the latter response is not identical to the sum of the two individual responses, because of a redistribution of the current systems in all three conductors due to their interaction.

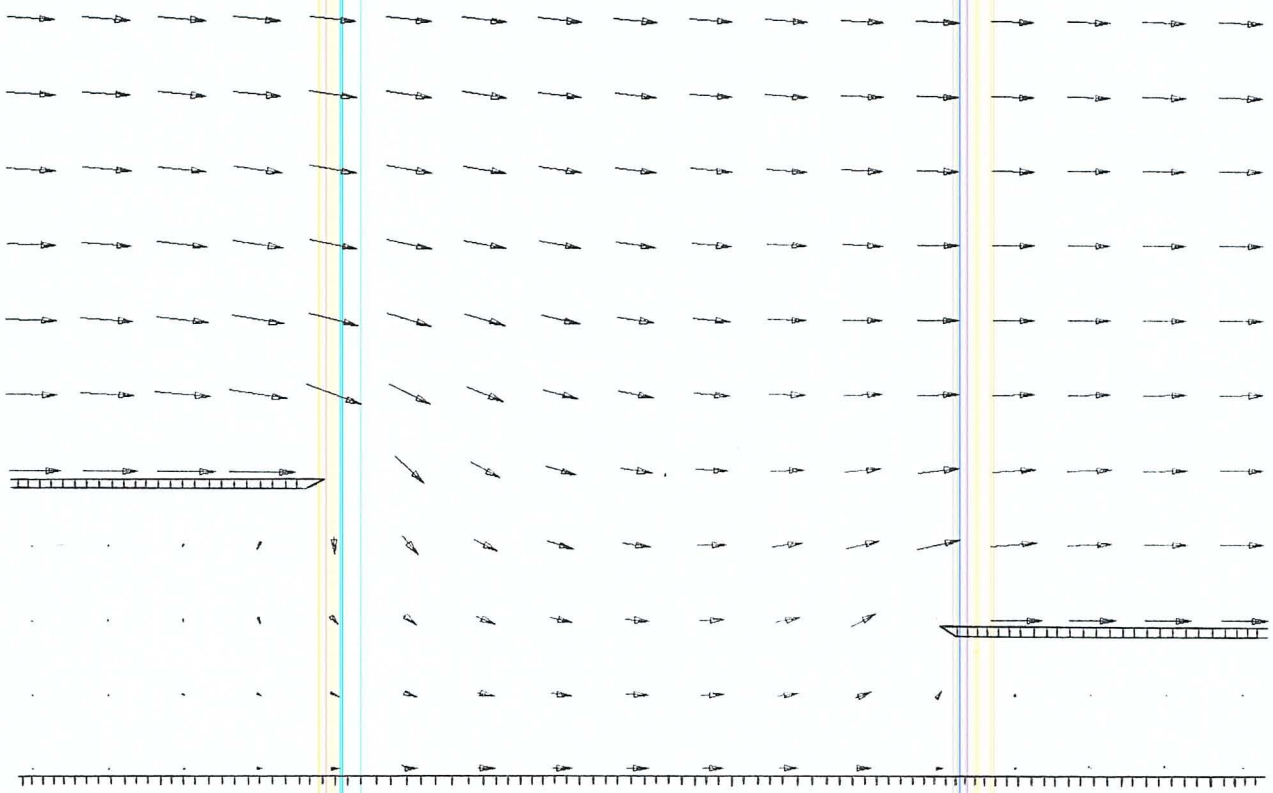

Fig. 6.1. Distribution of magnetic field vectors for model A.L.1/R.2 (L/h_1 = 2.0, h_2/h_1 = 0.5). No vector has been plotted at the edge of the sheet, where the field is singular

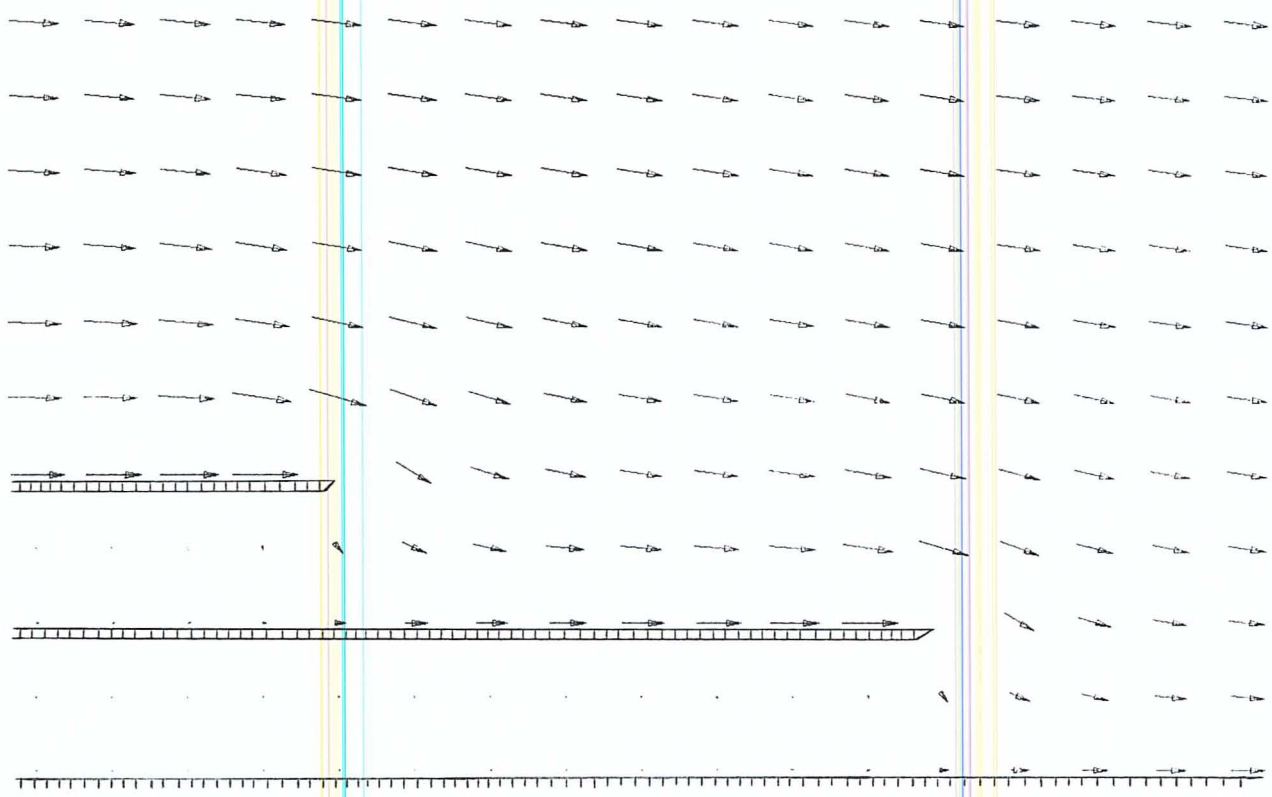

Fig. 6.2. Distribution of magnetic field vectors for model B.L.1/L.2 ($L/h_1 = 2.0$, $h_2/h_1 = 0.5$). No vector has been plotted at the edge of the sheet, where the field is singular

To give our results some geophysical relevance, we assume that half plane 1 represents an ocean and half plane 2 a laterally discontinuous earth conductor. The underlying whole plane is associated with the conductosphere, i.e. with the depth range of the sharp downward increase of conductivity, for the particular frequency being considered. We have calculated the Schmucker transfer functions along a horizontal profile close to the level of the ocean. The separation h_3 between this profile and the conductosphere has always been chosen to be 105 % of the separation h_1 between the ocean and the conductosphere ($h_3/h_1 = 1.05$). Although this choice seems arbitrary, it nevertheless takes into account the fact that the centre of the (in-phase) current distribution must be below the surface of a real ocean and no singularities are observed along ocean-continent boundaries.

6.2. CASE A: NUMERICAL RESULTS AND DISCUSSION

The configurations considered belong to models A.L.1, A.R.2 or A.L.1/R.2. As indicated before, it is the perturbation of the edge effect of a laterally discontinuous earth conductor (model A.R.2) by an adjacent ocean (model A.L.1) that is of most interest to us. A different interpretation would be to consider the perturbation of the "ordinary"

ocean effect (model A.L.1) by including a earth conductor (model A.R.2) at some distance from the coast. In either case, the resulting response (model A.L.1/R.2) is a combination of the effects of both the linear superposition of the individual current systems and their redistribution due to their mutual interaction.

The responses of many conductor configurations have been calculated in the course of these investigations, but a limited number of geometries suffices for a demonstration of the general behaviour, and only combinations of the following ratios are considered: L/h_1 = 0.5, 1.0, 2.0, 3.0 and h_2/h_1 = 0.25, 0.75, which gives a total of eight configurations.

Let us first discuss the characteristics of the Schmucker vertical transfer function, i.e. the normalized (anomalous) vertical field. Then the ocean effect is negative throughout, whereas the edge effect of the earth conductor is always positive (figs. 6.3). If linear superposition holds, the magnitude of the latter effect therefore decreases by the magnitude of the ocean effect. The top panels of figs. 6.3 allow us to compare the vertical transfer function of any complete configuration of model A.L.1/R.2 (solid line) with the same response of the corresponding configuration without an ocean (model A.R.2,

Figs. 6.3.1 to 6.3.8. Top and center: Transfer functions for model A.L.1 (dashed), model A.R.2 (dot-dashed) and model A.L.1/R.2 (solid). Bottom: Corresponding conductor configurations (solid) and position of measuring profile (dotted). For further explanations see text

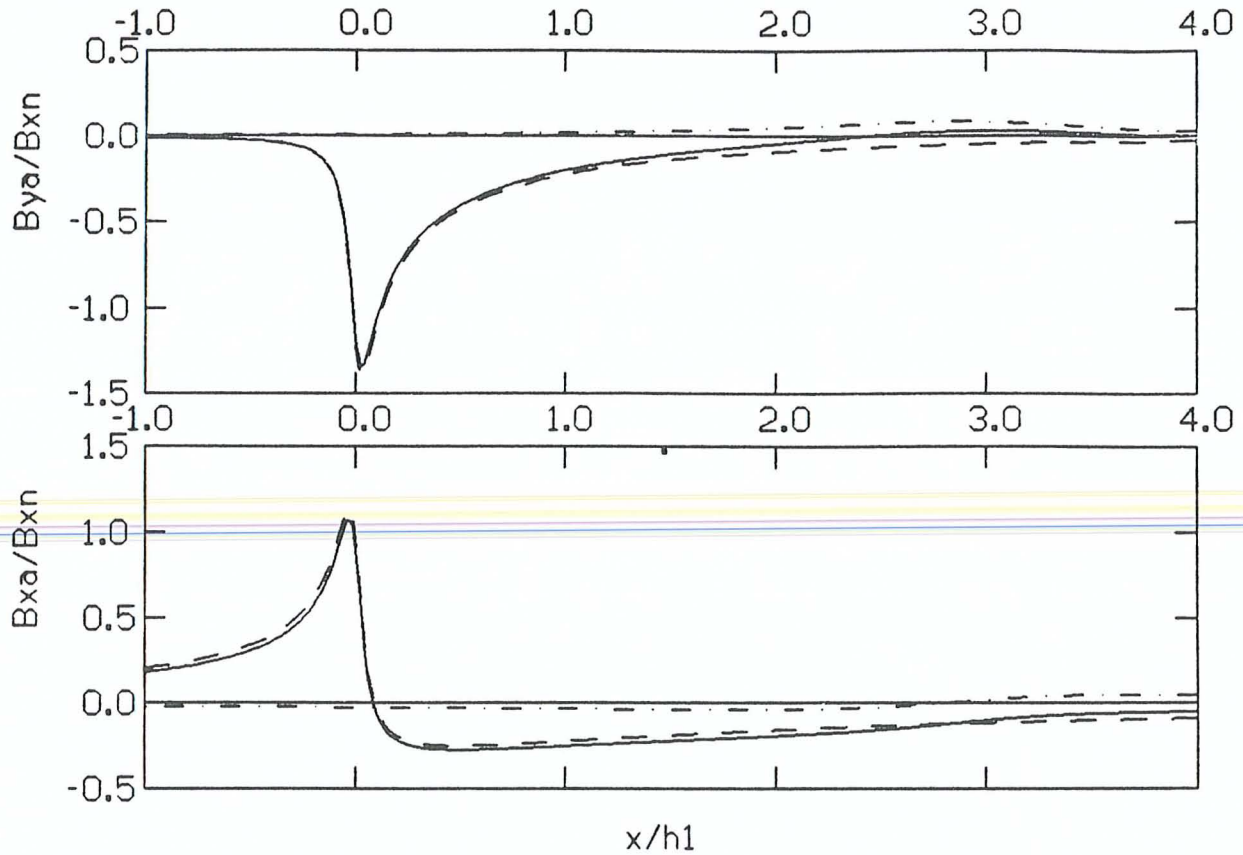

SCHMUCKER TRANSFER FUNCTIØNS

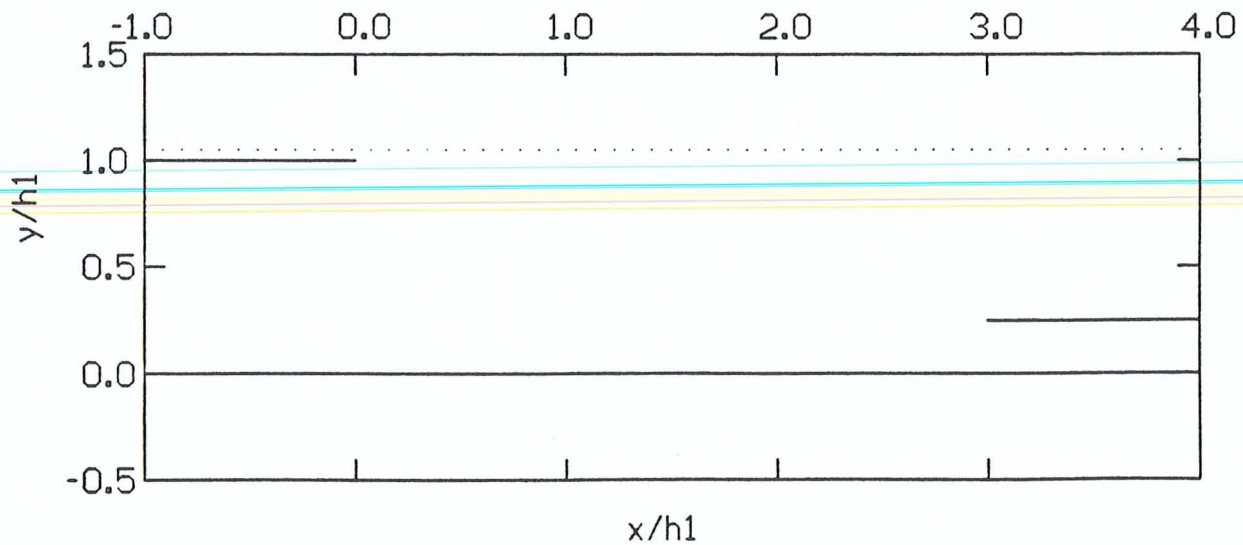

FIG. 6.3.1. L/h1 = 3.0 h2/h1 = 0.25

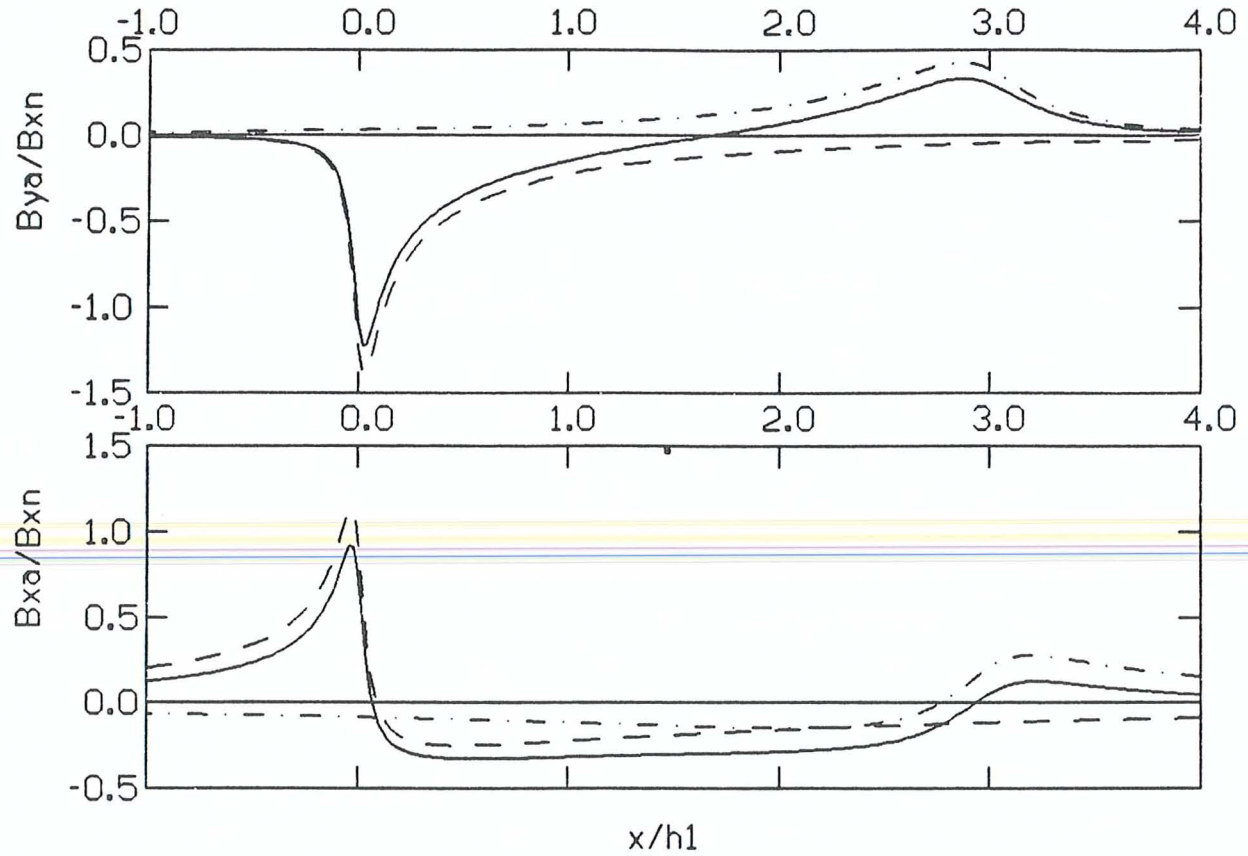

SCHMUCKER TRANSFER FUNCTIØNS

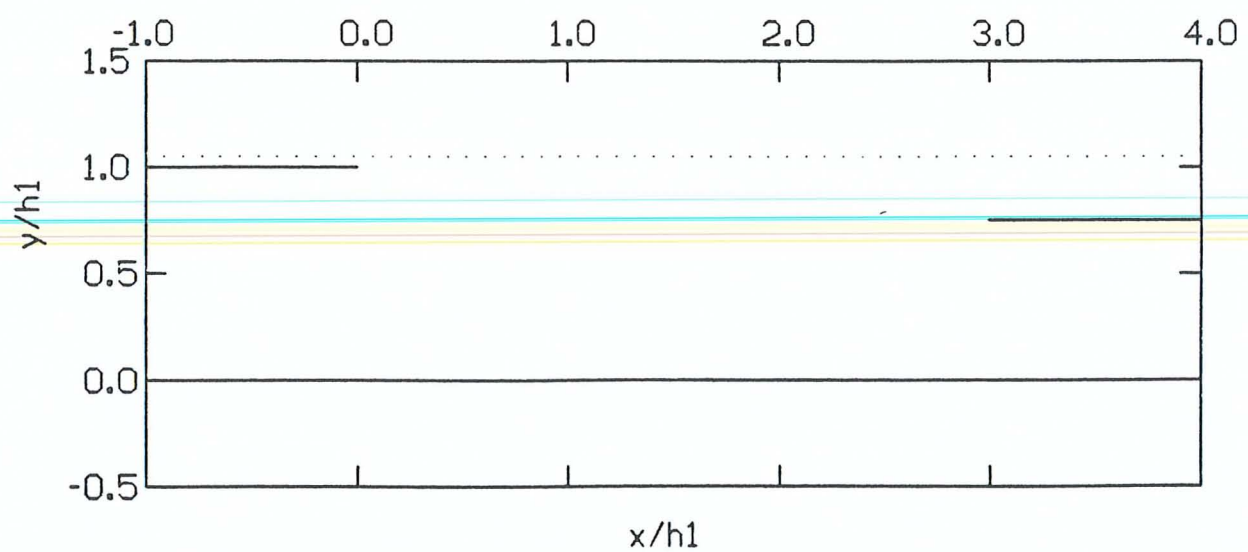

FIG. 6.3.2. L/h1 = 3.0 h2/h1 = 0.75

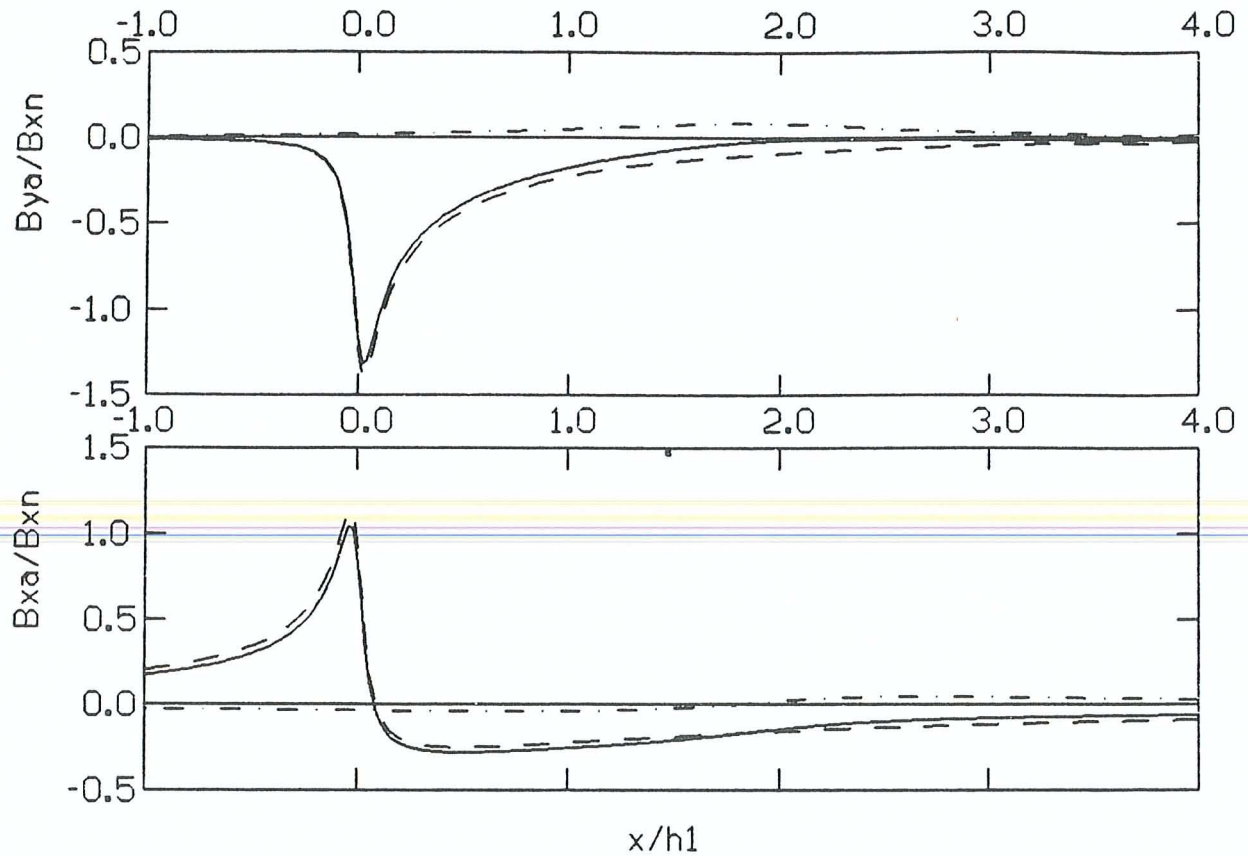

SCHMUCKER TRANSFER FUNCTIØNS

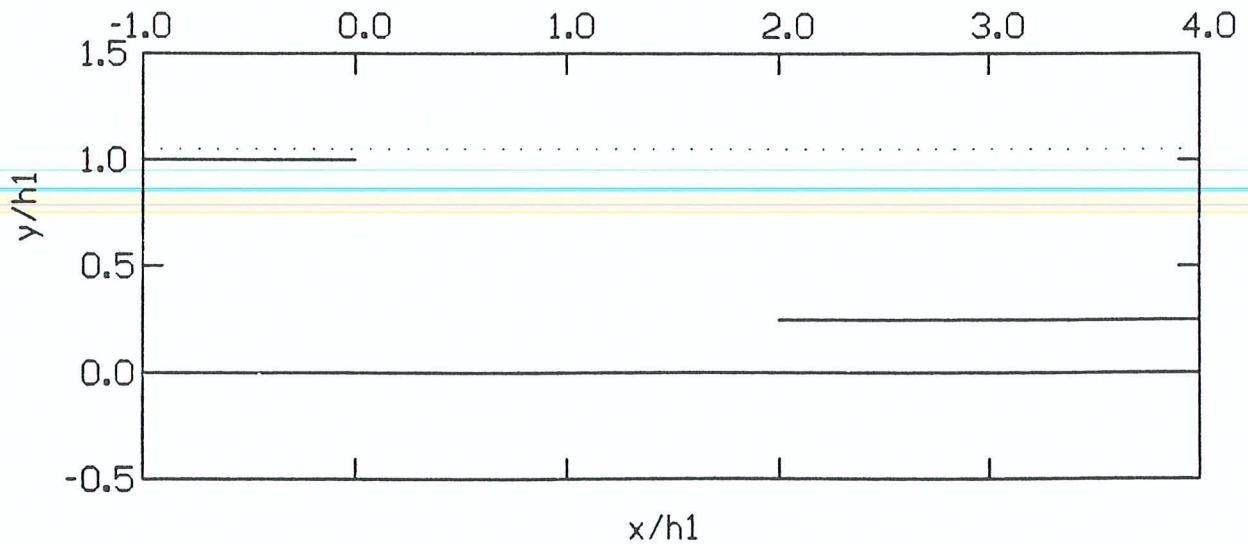

FIG. 6.3.3. L/h1 = 2.0 h2/h1 = 0.25

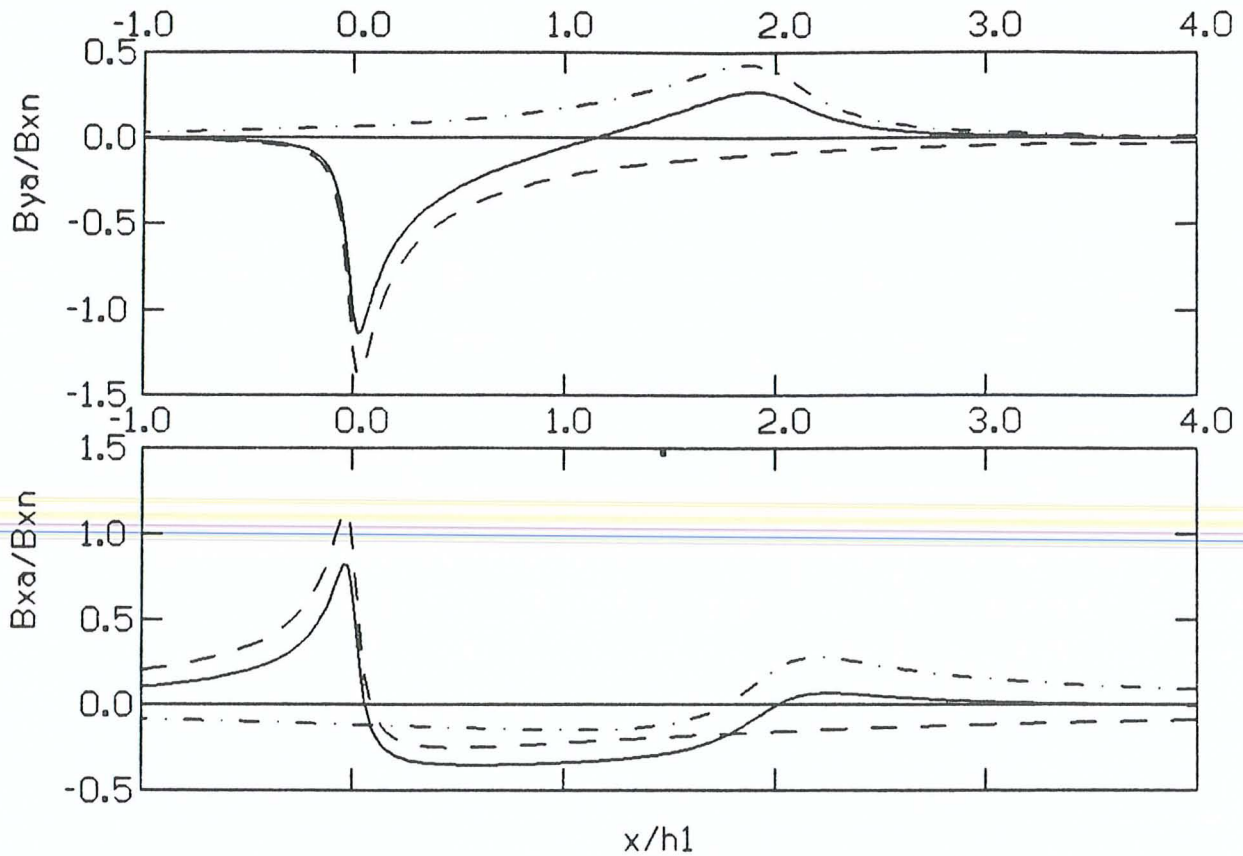

SCHMUCKER TRANSFER FUNCTIØNS

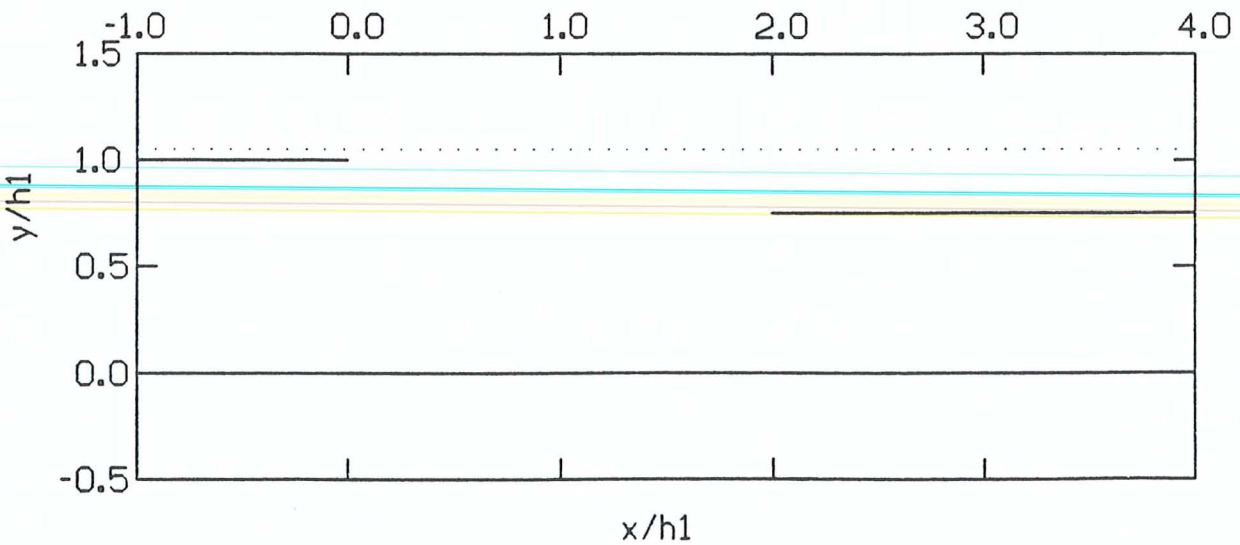

FIG. 6.3.4. L/h1 = 2.0 h2/h1 = 0.75

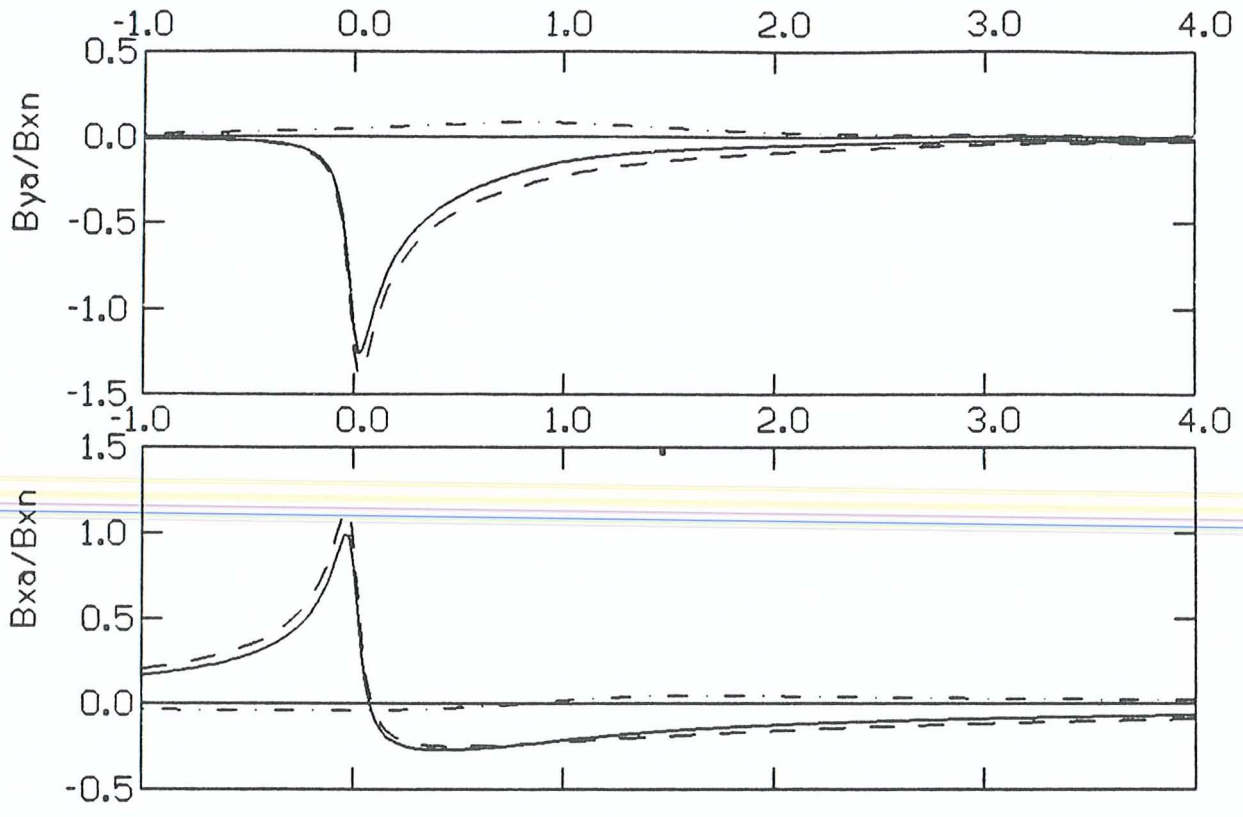

SCHMUCKER TRANSFER FUNCTIØNS

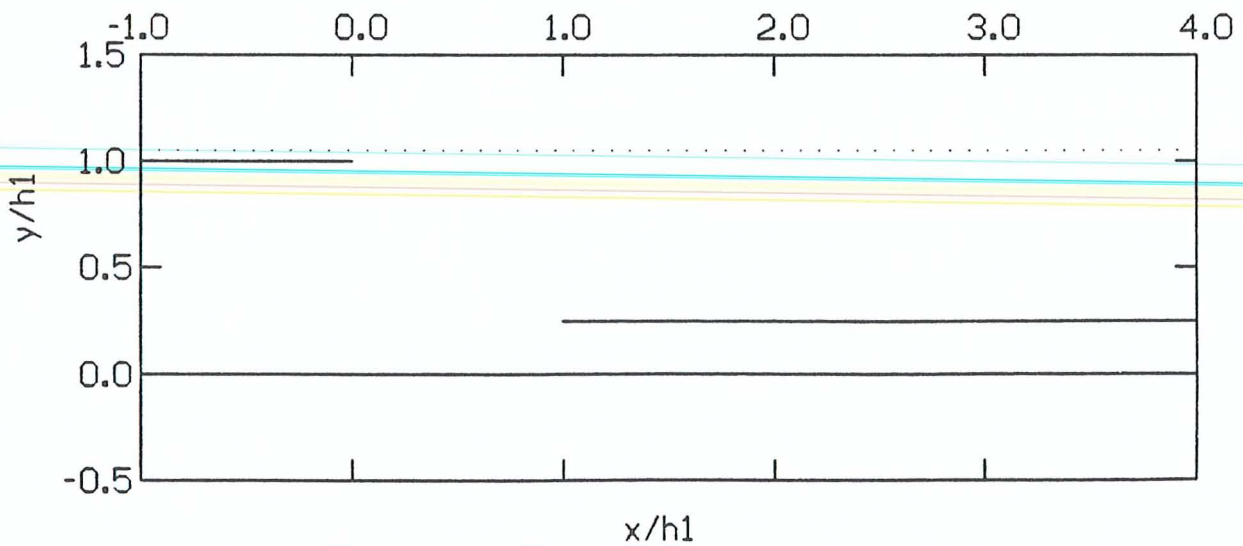

FIG. 6.3.5. L/h1 = 1.0 h2/h1 = 0.25

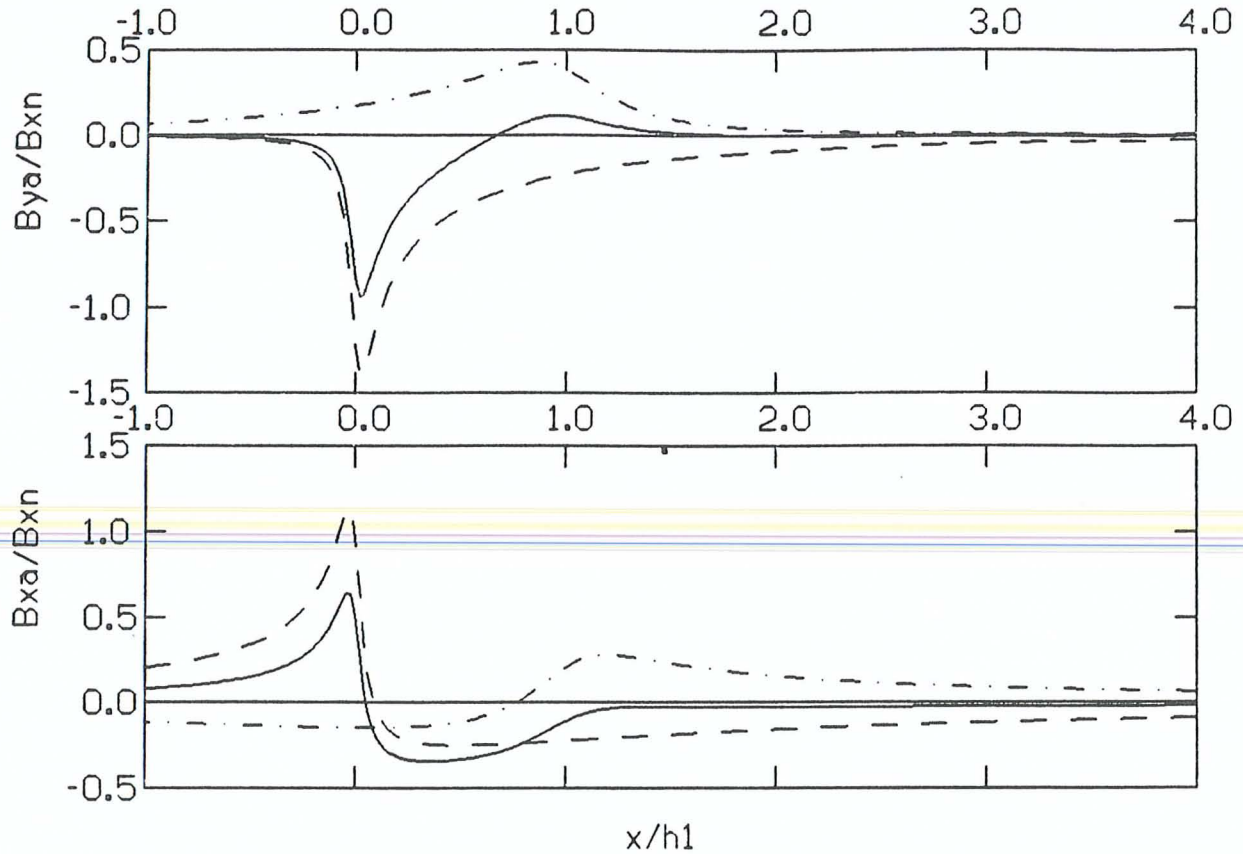

SCHMUCKER TRANSFER FUNCTIØNS

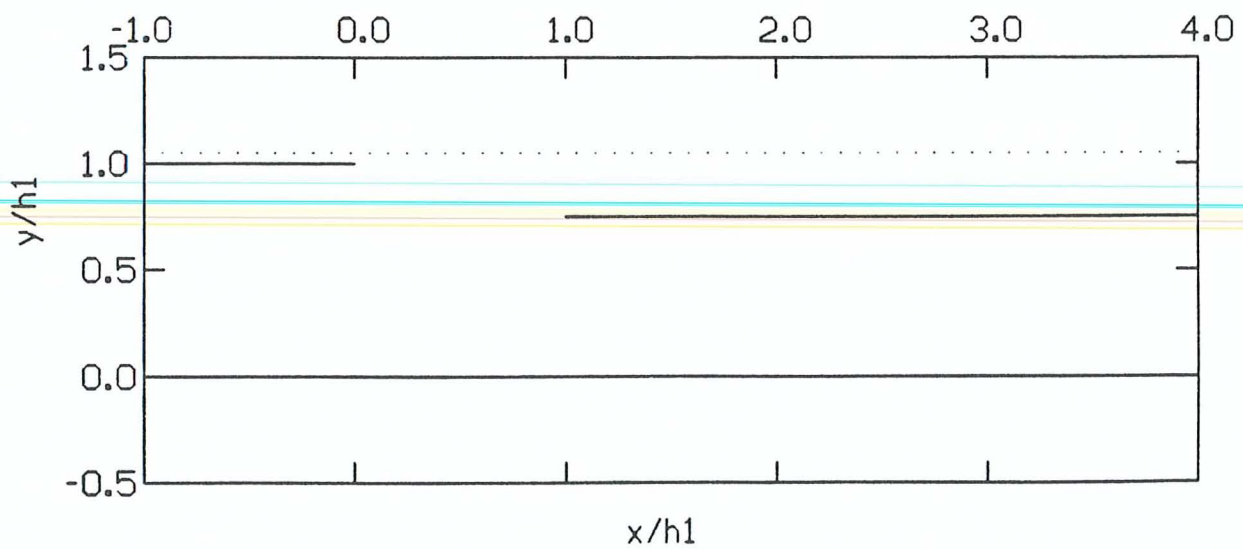

FIG. 6.3.6. L/h1 = 1.0 h2/h1 = 0.75

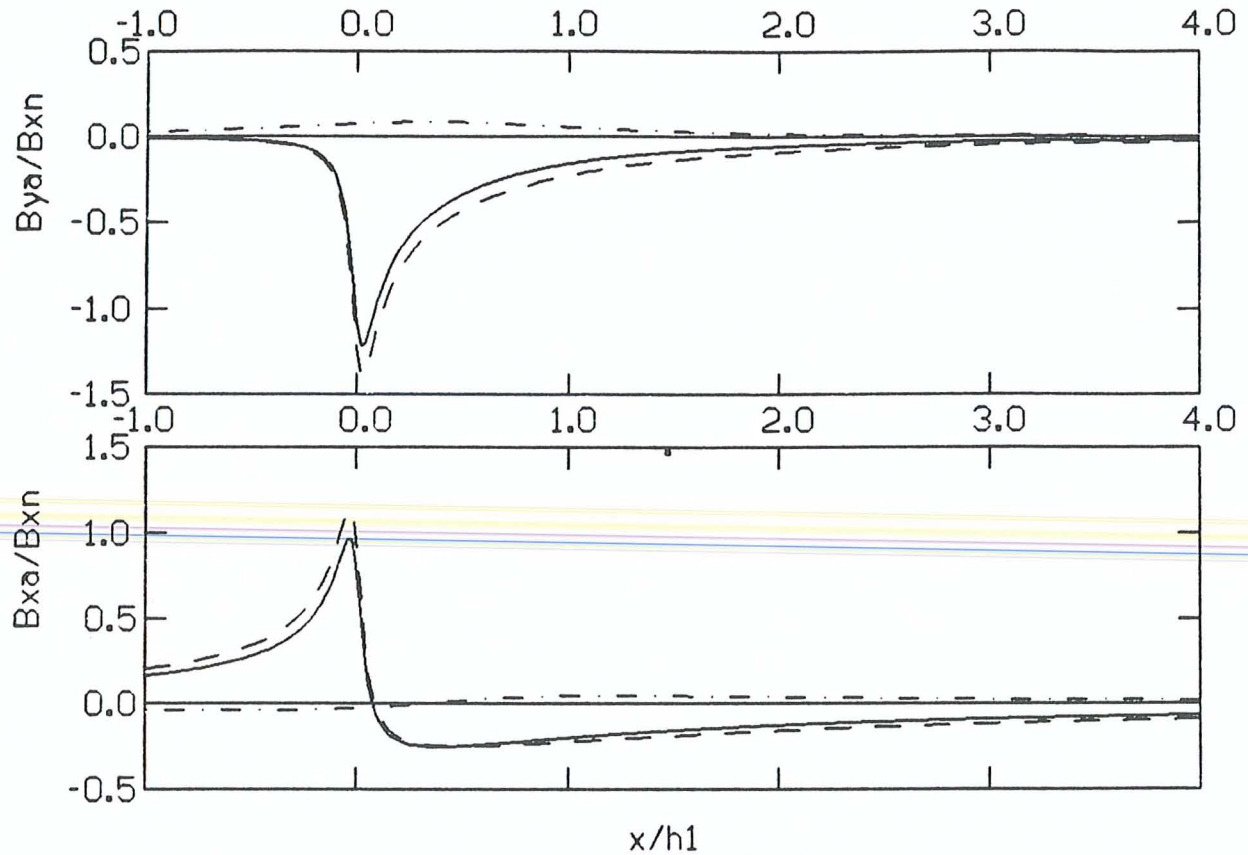

SCHMUCKER TRANSFER FUNCTIØNS

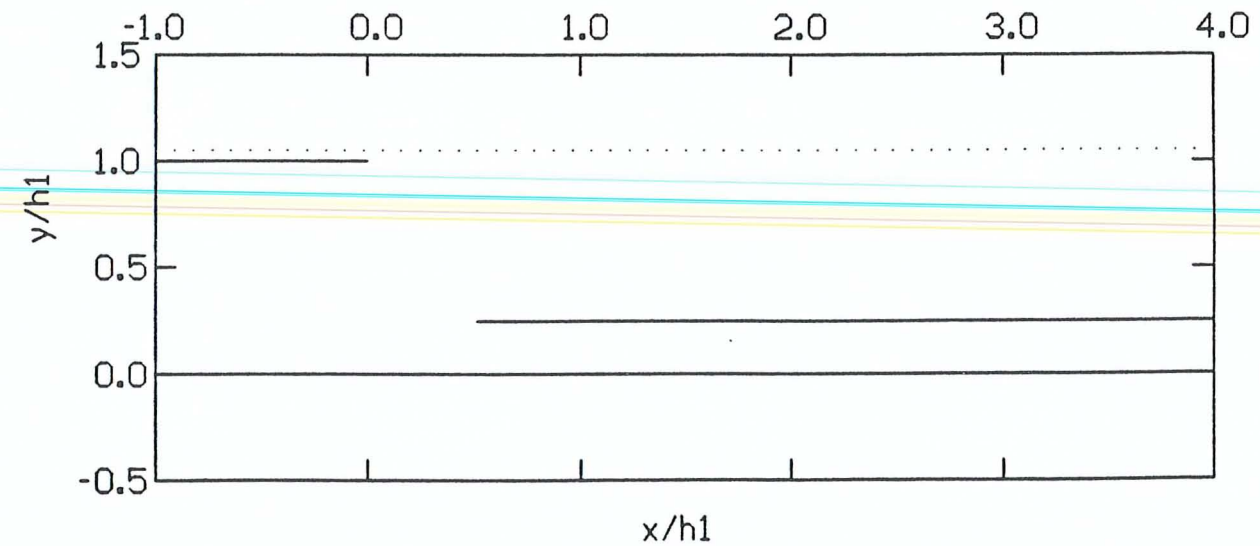

FIG. 6.3.7. L/h1 = 0.5 h2/h1 = 0.25

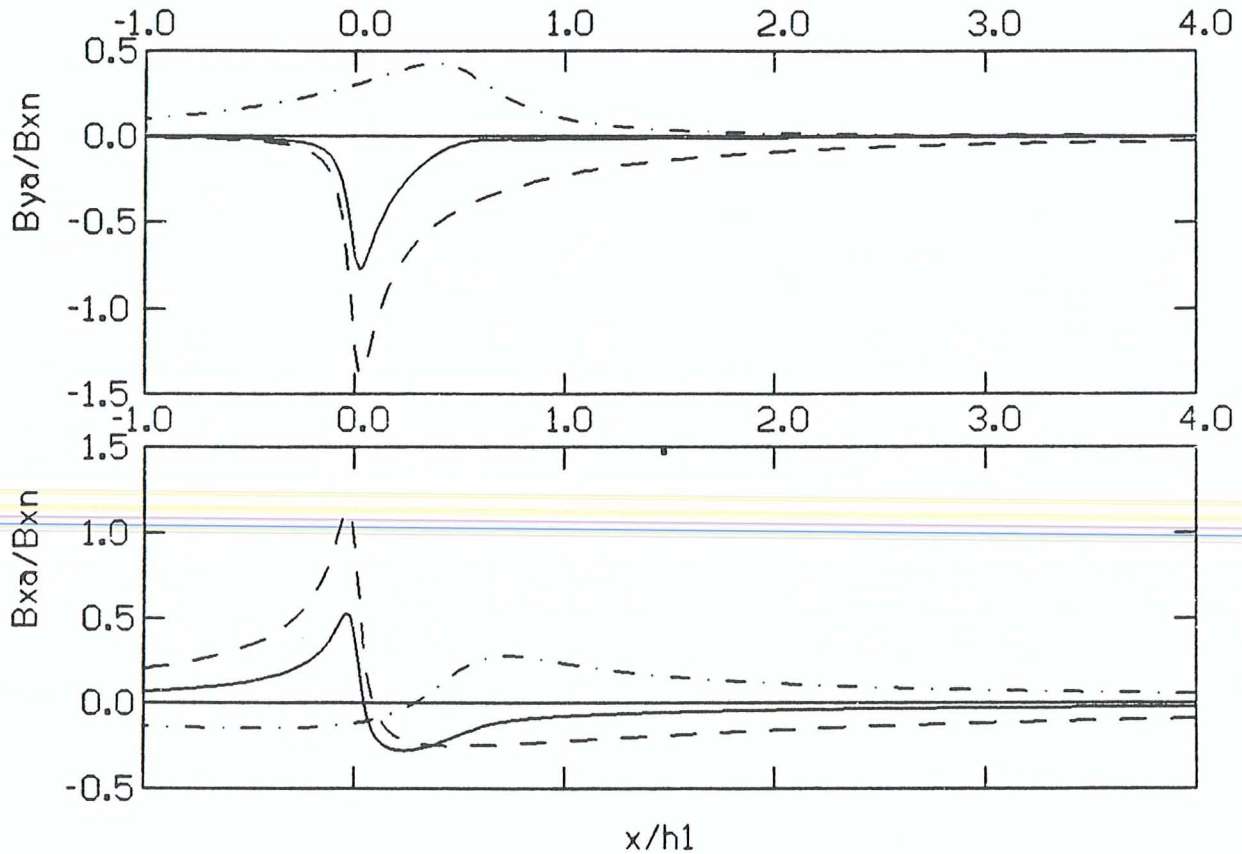

SCHMUCKER TRANSFER FUNCTIØNS

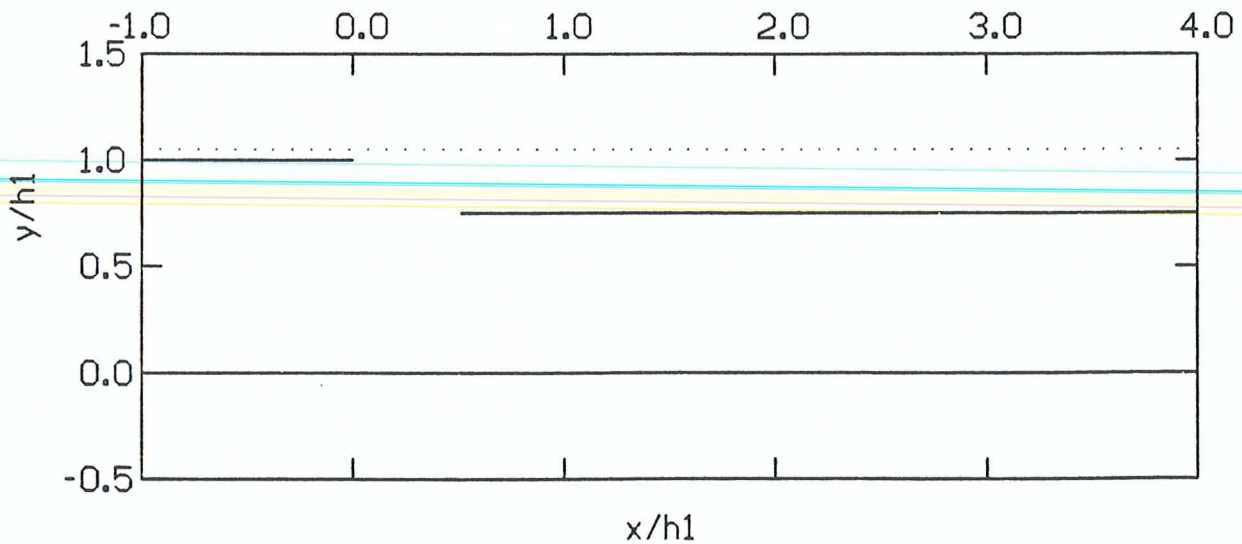

FIG. 6.3.8. L/h1 = 0.5 h2/h1 = 0.75

dot-dashed line). If we focus on the section of the profile above the edge of the earth conductor, we can make the following observations. Usually, the response of the complete configuration (solid) approximates the sum of the responses of the two individual configurations, i.e. the edge effect of the earth conductor (dot-dashed) is diminished by the magnitude of the response of the ocean (dashed). The anomaly of a deep earth conductor ($h_2/h_1 = 0.25$) close to the edge of the ocean ($L/h_1 < 1.0$) is therefore completely masked by the comparatively strong anomaly of the latter (figs. 6.3.5 and 6.3.7). On the other hand, for a shallow earth conductor ($h_2/h_1 = 0.75$) close to the edge of the ocean ($L/h_1 < 1.0$), some electromagnetic interaction can be identified (see figs. 6.3.6 and 6.3.8). This is not surprising, because the distance between the edges of half planes 1 and 2 is now comparable with or less than either half plane's separation from the conducting whole plane underneath.

We have also calculated the Schmucker horizontal transfer functions, which are equal to normalized anomalous horizontal fields, for the same configurations (figs. 6.3, centre panels). Since the ocean effect is negative in the region above the earth conductor, linear superposition causes a downward shift of the edge effect of the earth conductor by the magnitude of the ocean effect. From the

individual figures it is obvious that, for a deep earth conductor (h_2/h_1 = 0.25), additivity of the anomalies holds to a very good approximation. But its response is almost completely masked by the comparatively strong ocean anomaly. If the earth conductor is shallow (h_2/h_1 = 0.75), its edge effect becomes very conspicuous. The individual anomalies are roughly additive, except when the edges of half planes 1 and 2 are very close ($L/h_1 < 1.0$).

To distinguish the effect of interaction more clearly, the sum of the responses according to models A.L.1 and A.R.2 (dashed lines) has been calculated and compared with the response of model A.L.1/R.2 (solid lines). The results are shown in figs. 6.4.1 to 6.4.8 for the different configurations, for vertical (top panels) and horizontal transfer functions (centre panels), and may be summarized as follows. For a deep earth conductor (h_2/h_1 = 0.25), the anomalies are in fact completely additive. But, if we consider a shallow earth conductor (h_2/h_1 = 0.75), the effect of inductive coupling can be identified, although it remains small. It mainly causes an attenuation of the peak values of the anomalies, as compared with the corresponding peaks of the superimposed anomalies.

Figs. 6.4.1 to 6.4.8. Top and center: Sum of transfer functions for models A.L.1 and A.R.2 (dashed) and transfer function for model A.L.1/R.2 (solid). Bottom: Corresponding conductor configurations (solid) and position of measuring profile (dotted). For further explanations see text

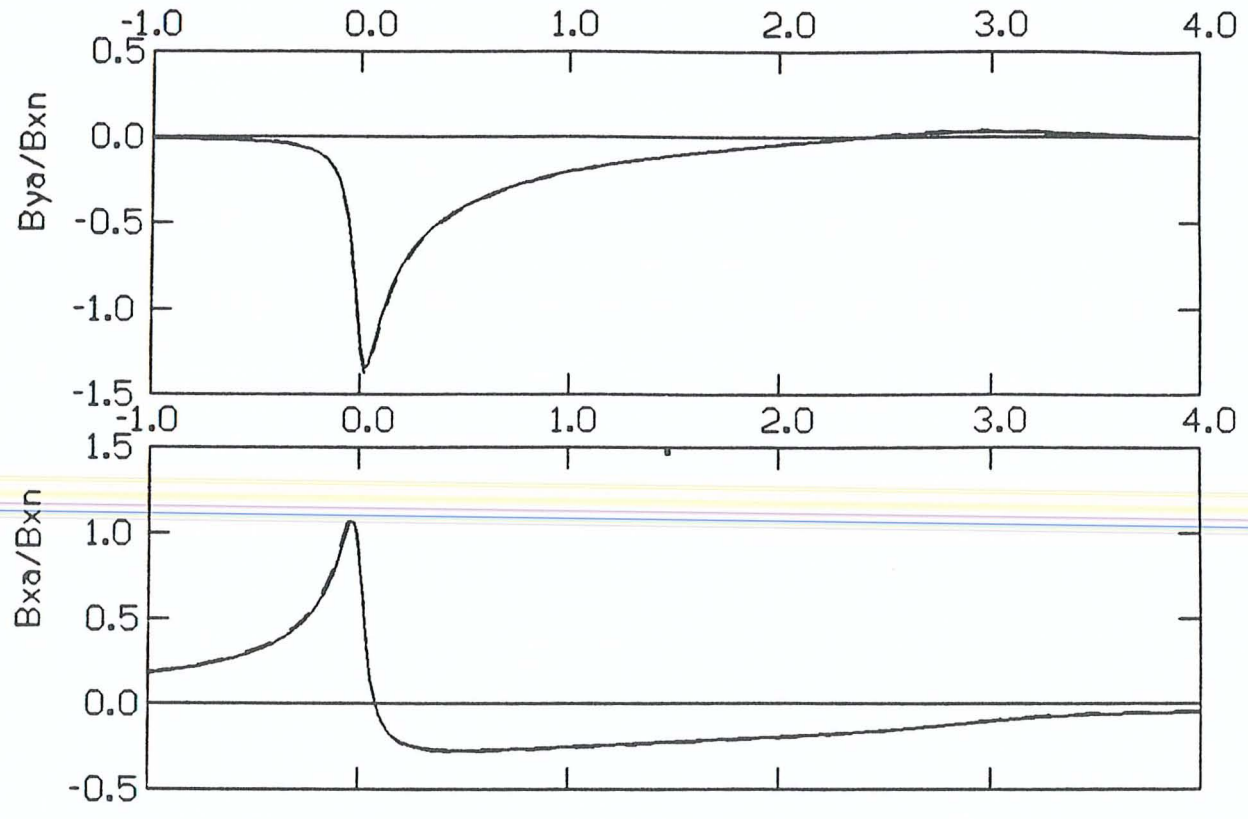

SCHMUCKER TRANSFER FUNCTIØNS

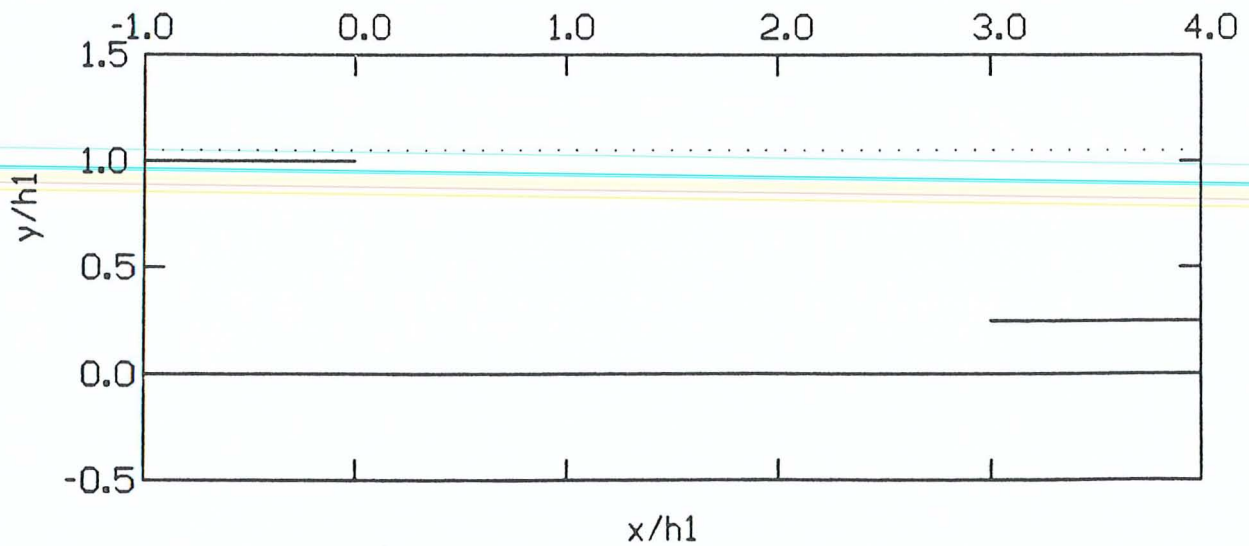

FIG. 6.4.1. L/h1 = 3.0 h2/h1 = 0.25

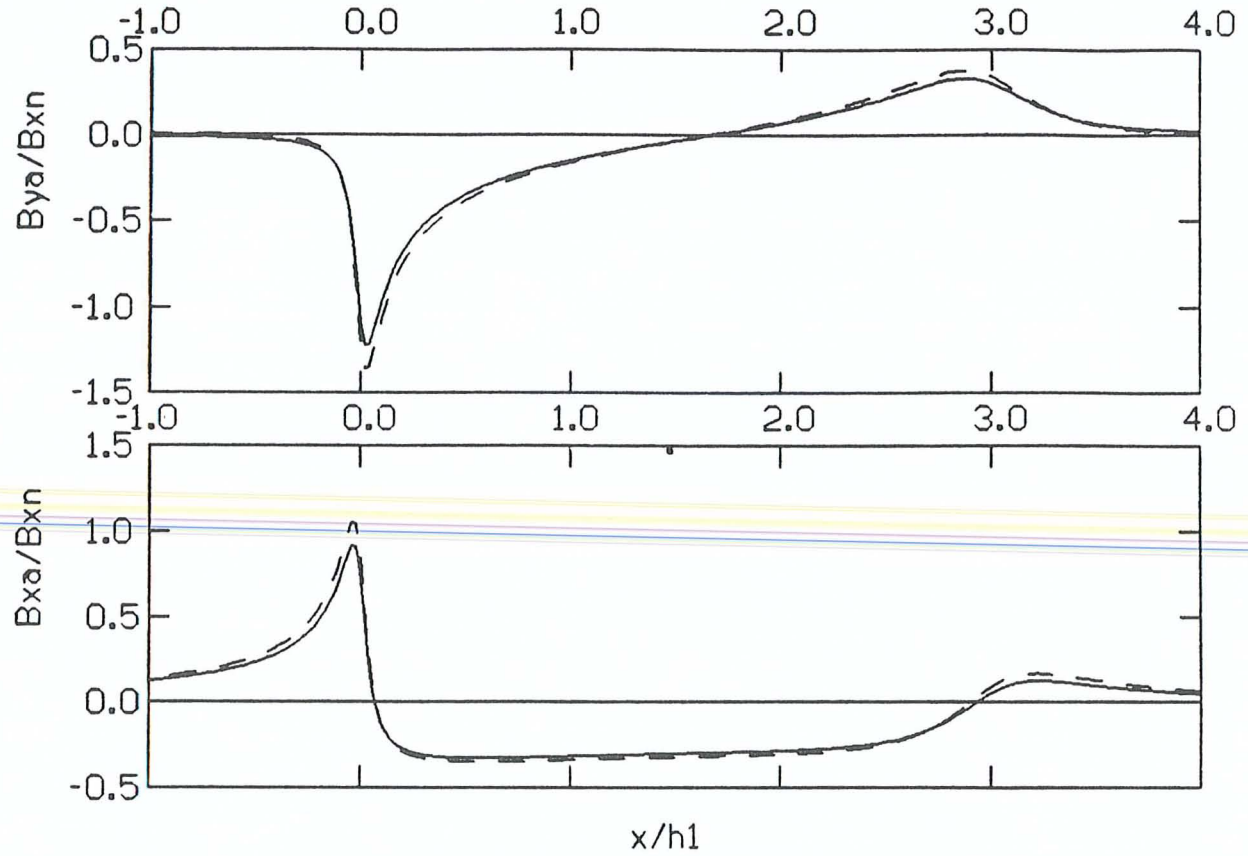

SCHMUCKER TRANSFER FUNCTIØNS

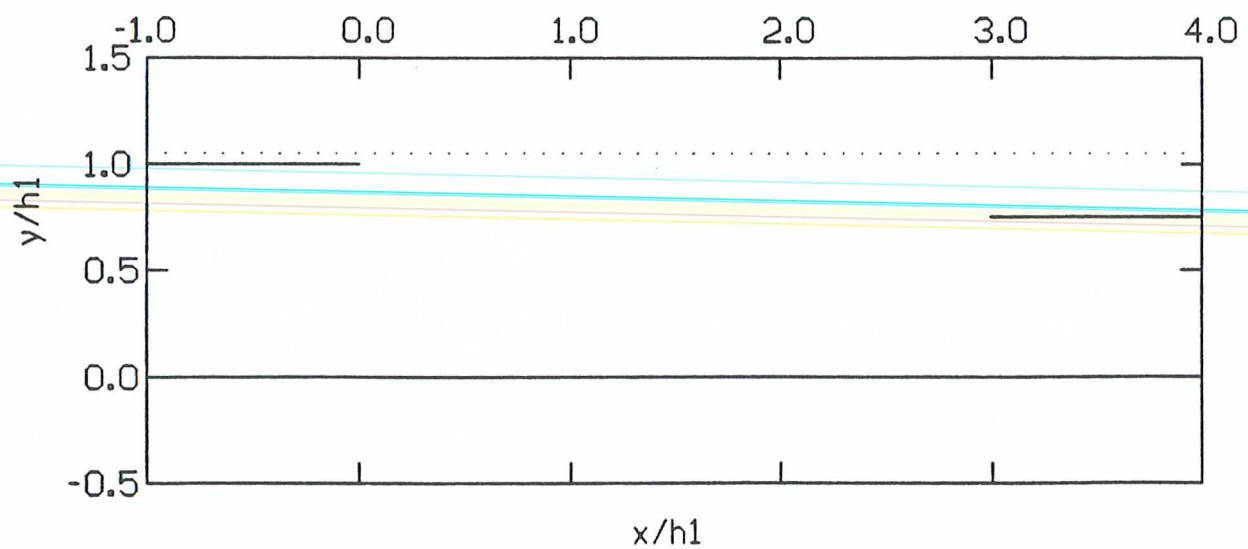

FIG. 6.4.2. L/h1 = 3.0 h2/h1 = 0.75

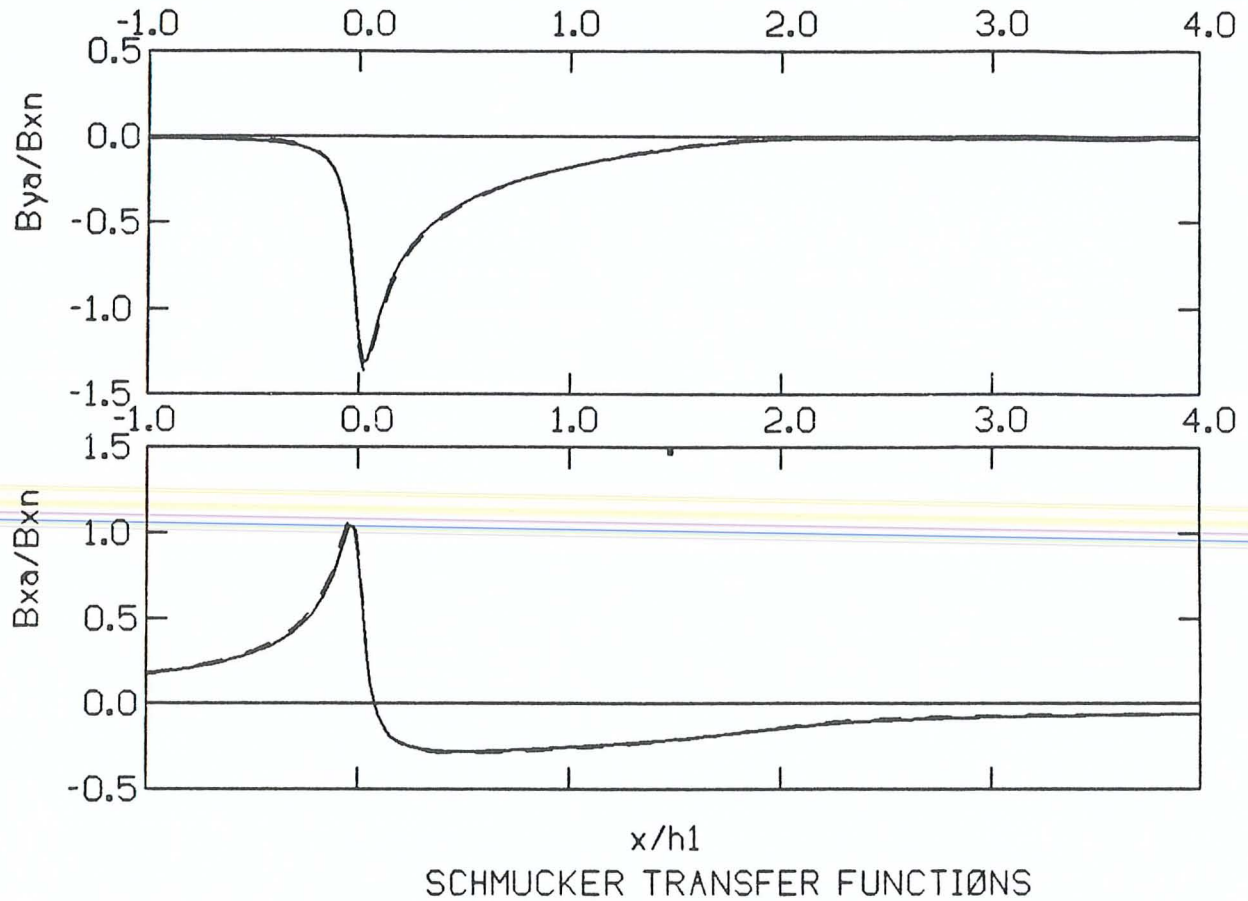

SCHMUCKER TRANSFER FUNCTIØNS

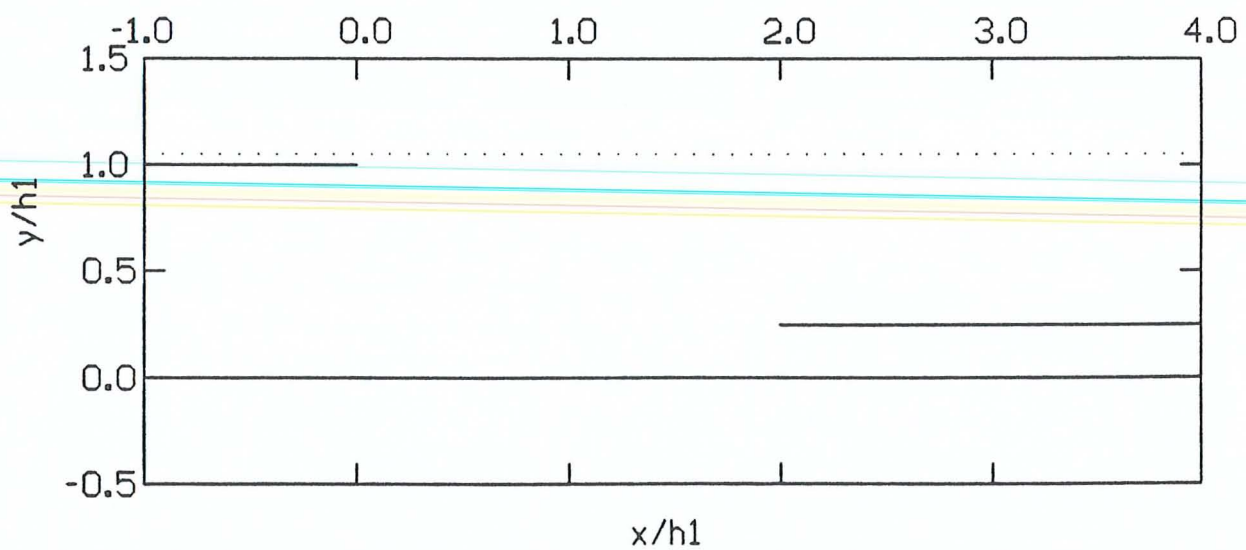

FIG. 6.4.3. L/h1 = 2.0 h2/h1 = 0.25

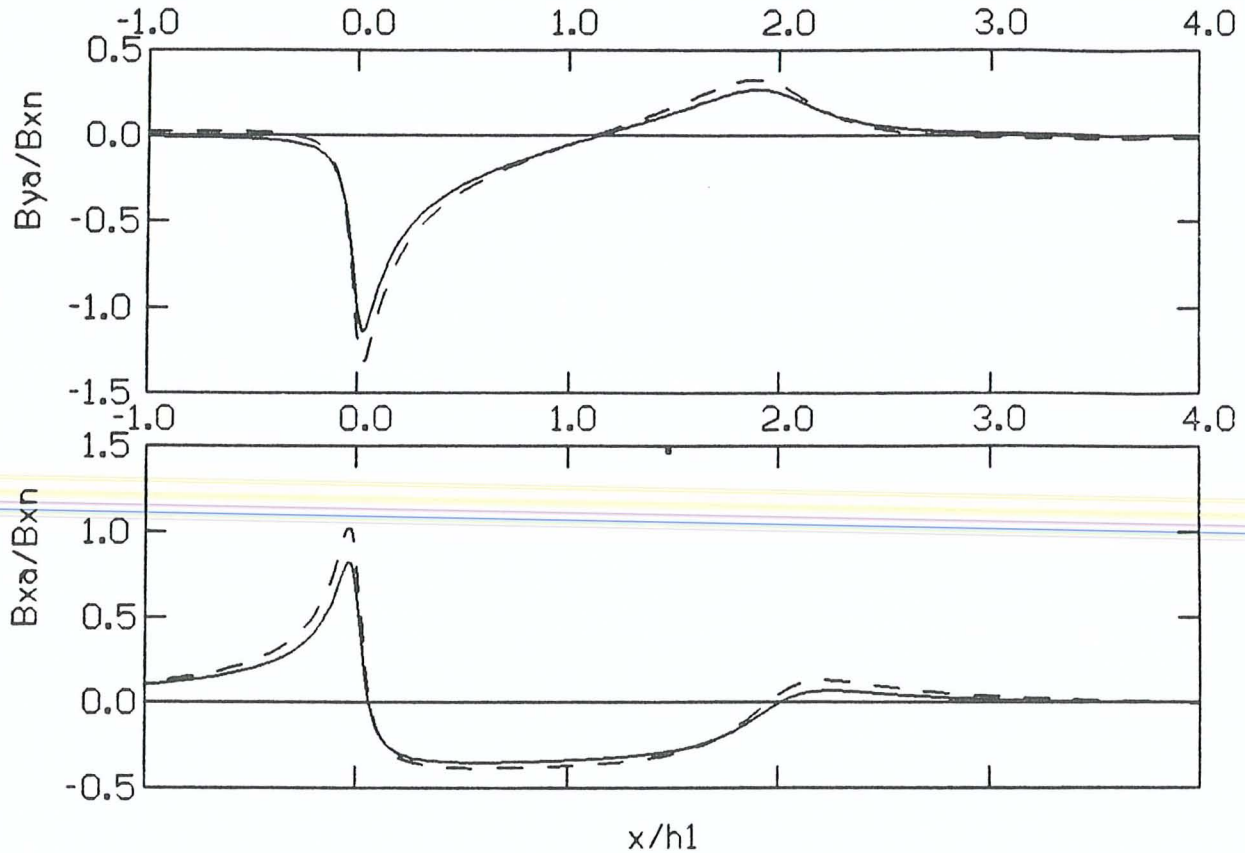

SCHMUCKER TRANSFER FUNCTIØNS

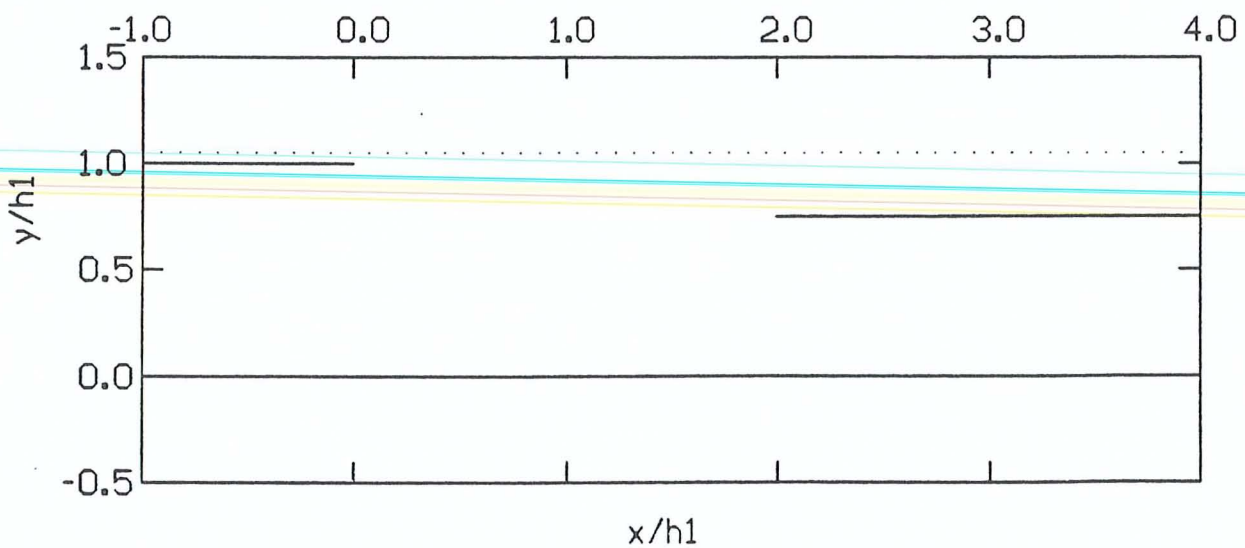

FIG. 6.4.4. L/h1 = 2.0 h2/h1 = 0.75

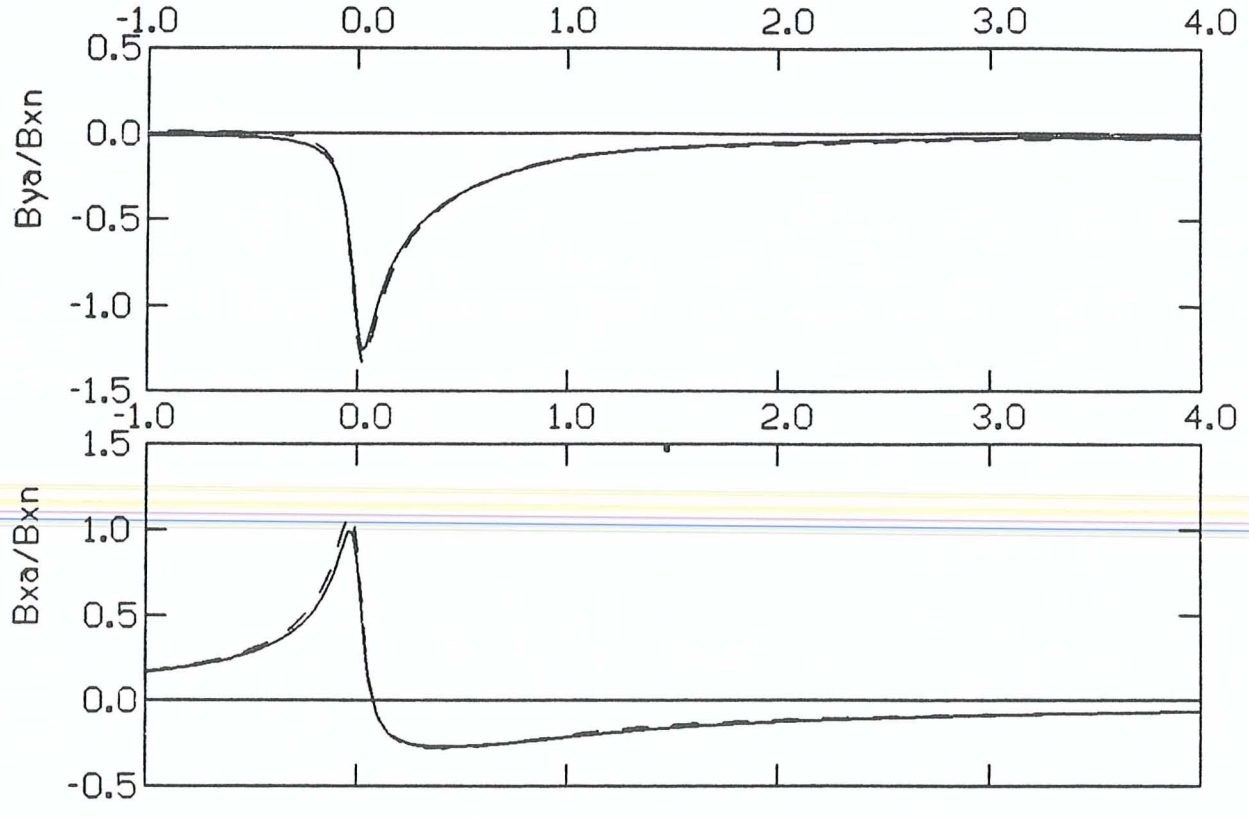

SCHMUCKER TRANSFER FUNCTIØNS

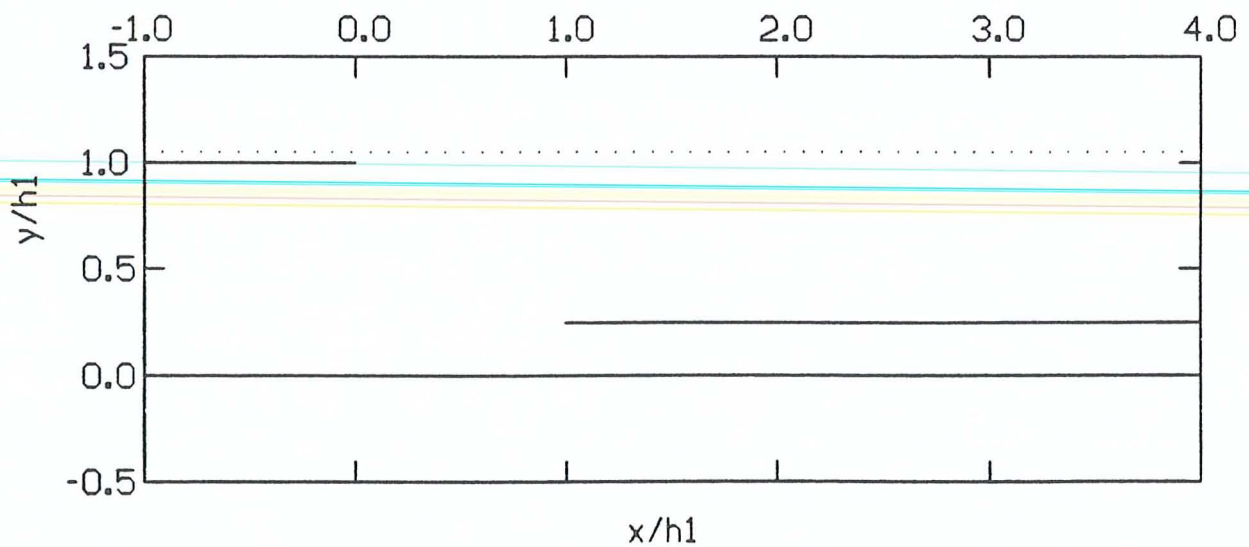

FIG. 6.4.5. L/h1 = 1.0 h2/h1 = 0.25

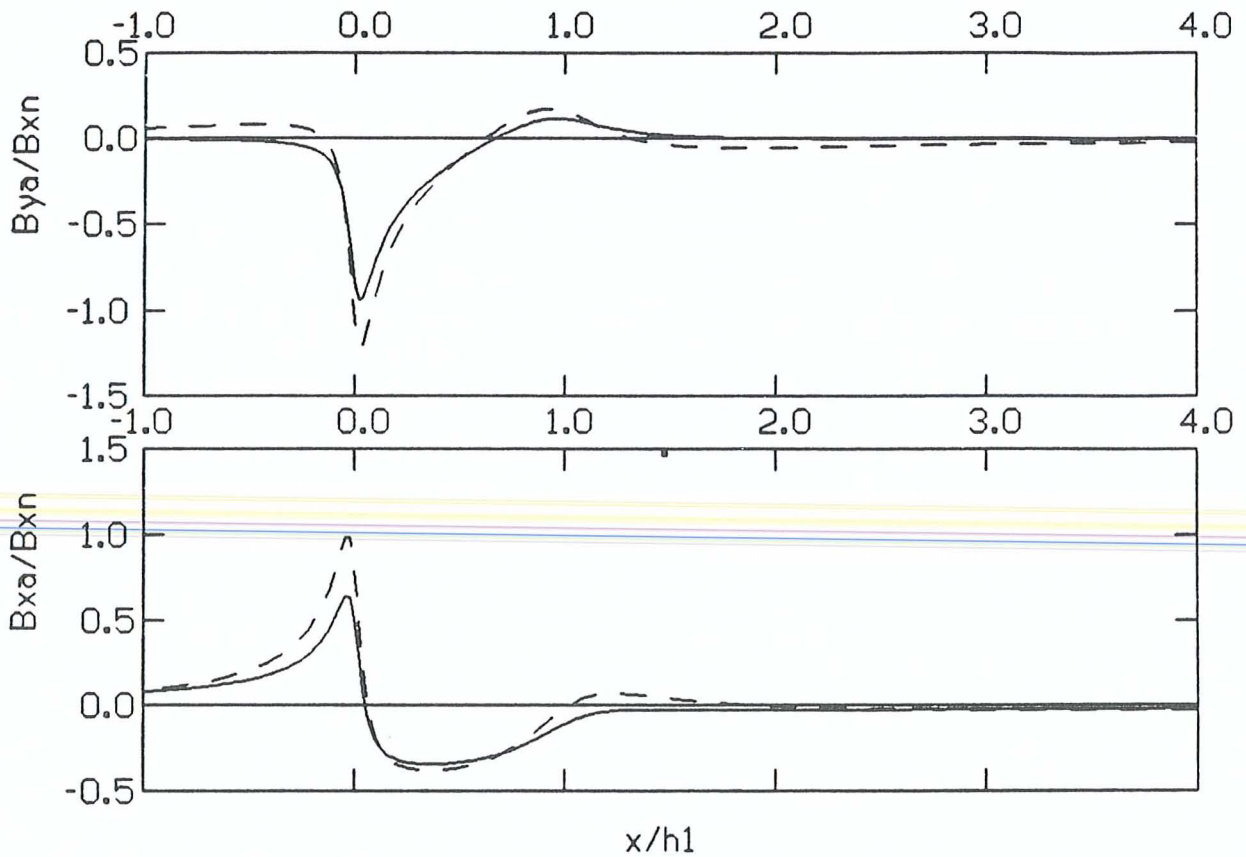

SCHMUCKER TRANSFER FUNCTIØNS

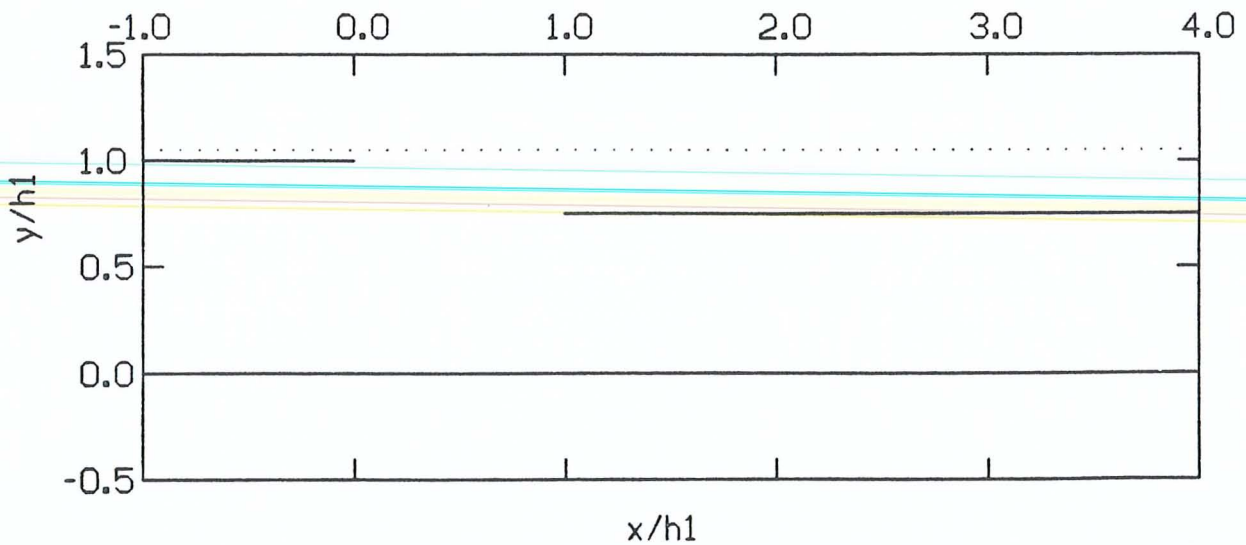

FIG. 6.4.6. L/h1 = 1.0 h2/h1 = 0.75

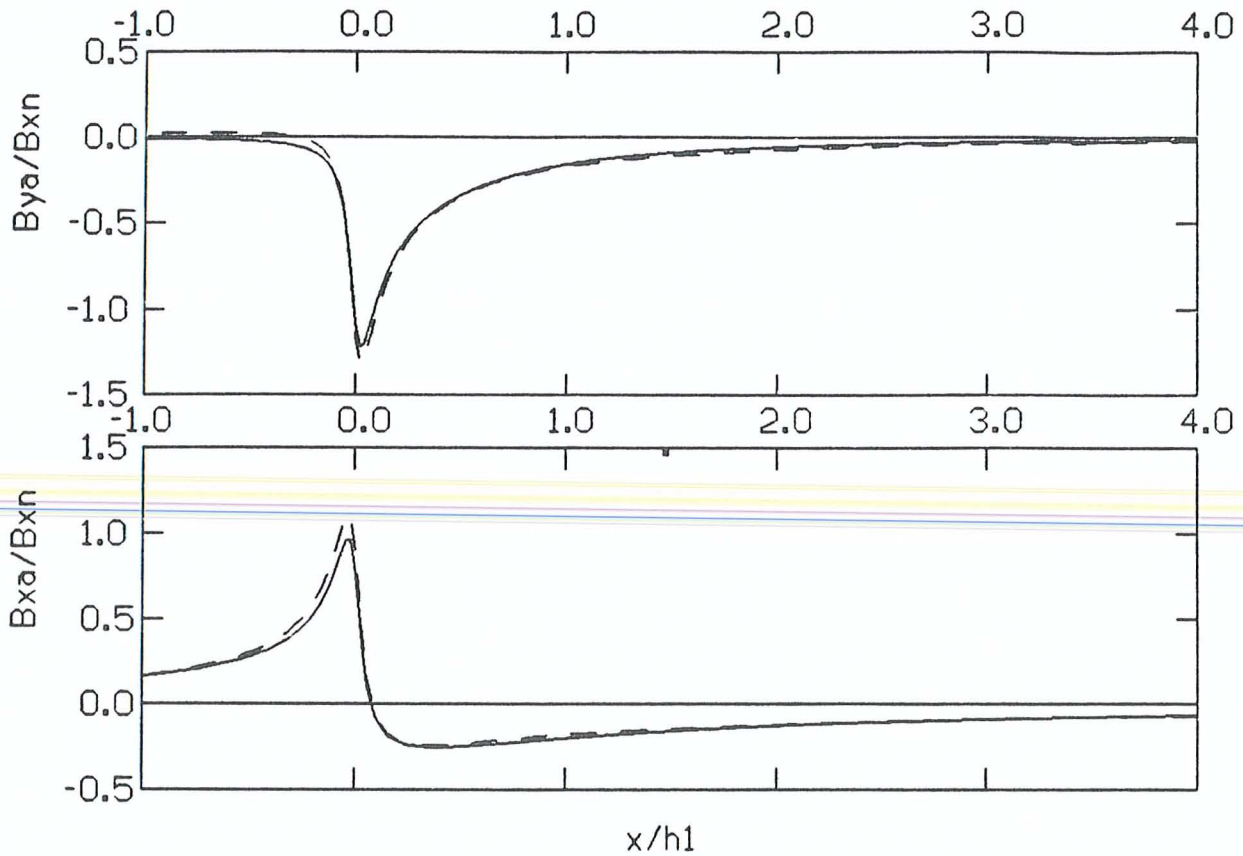

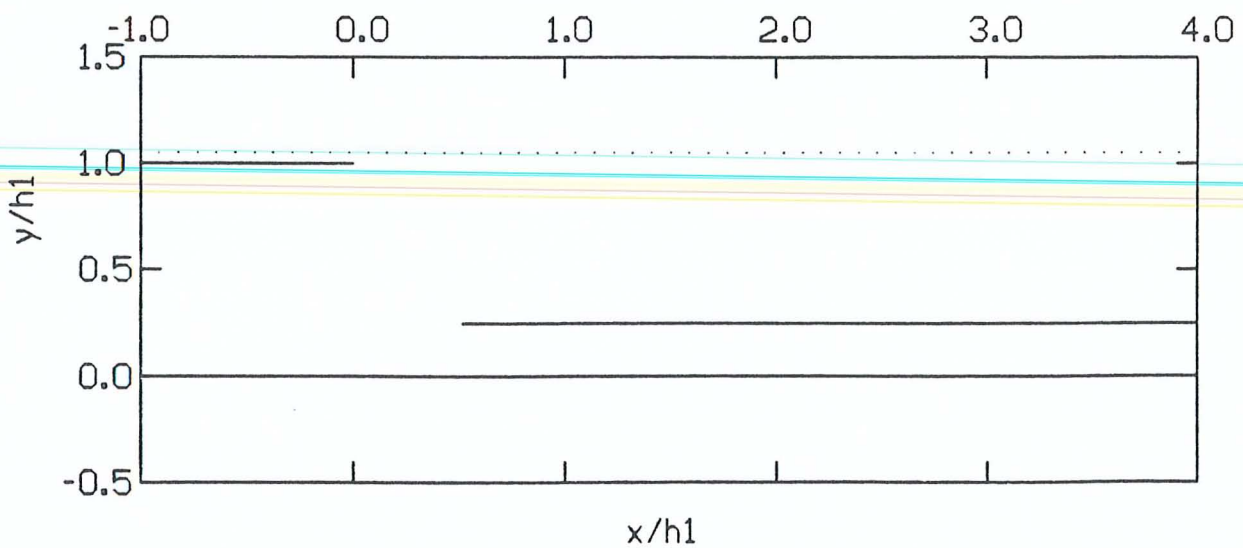

FIG. 6.4.7. L/h1 = 0.5 h2/h1 = 0.25

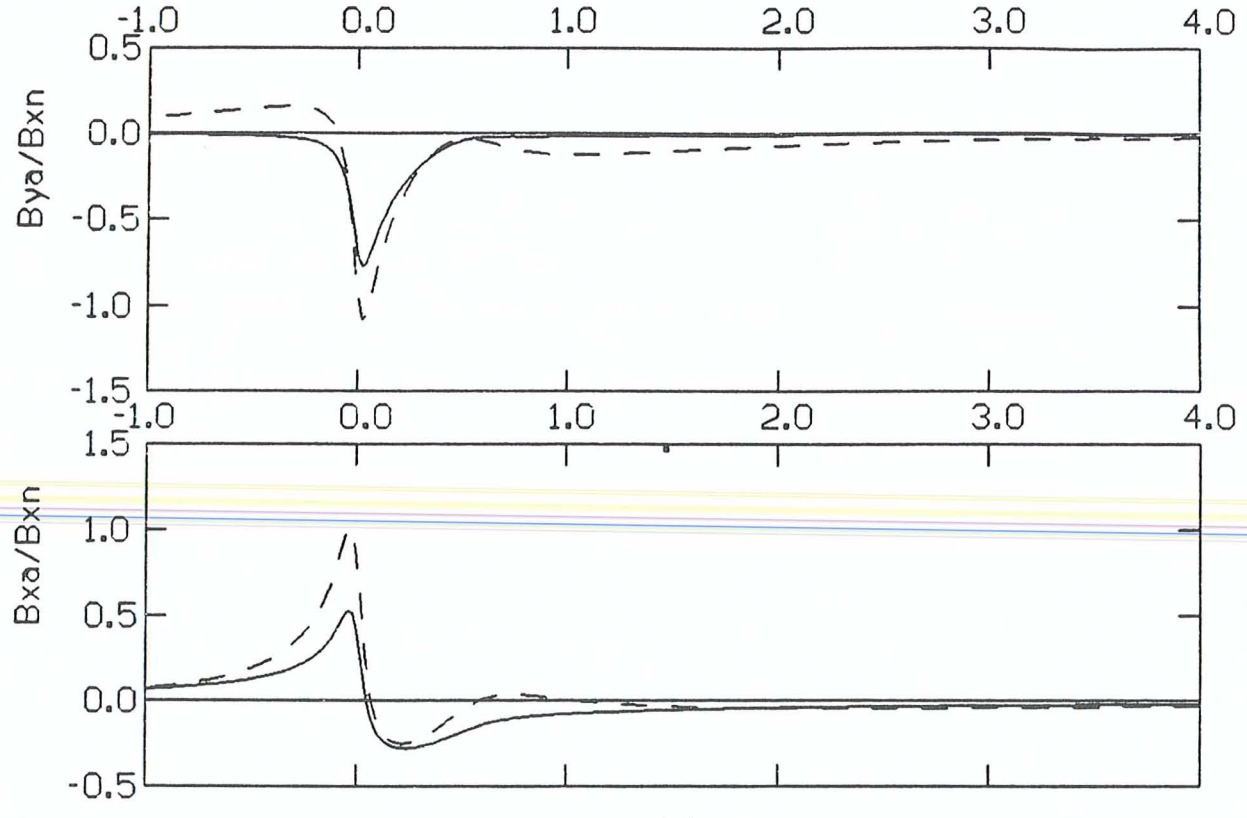

SCHMUCKER TRANSFER FUNCTIØNS

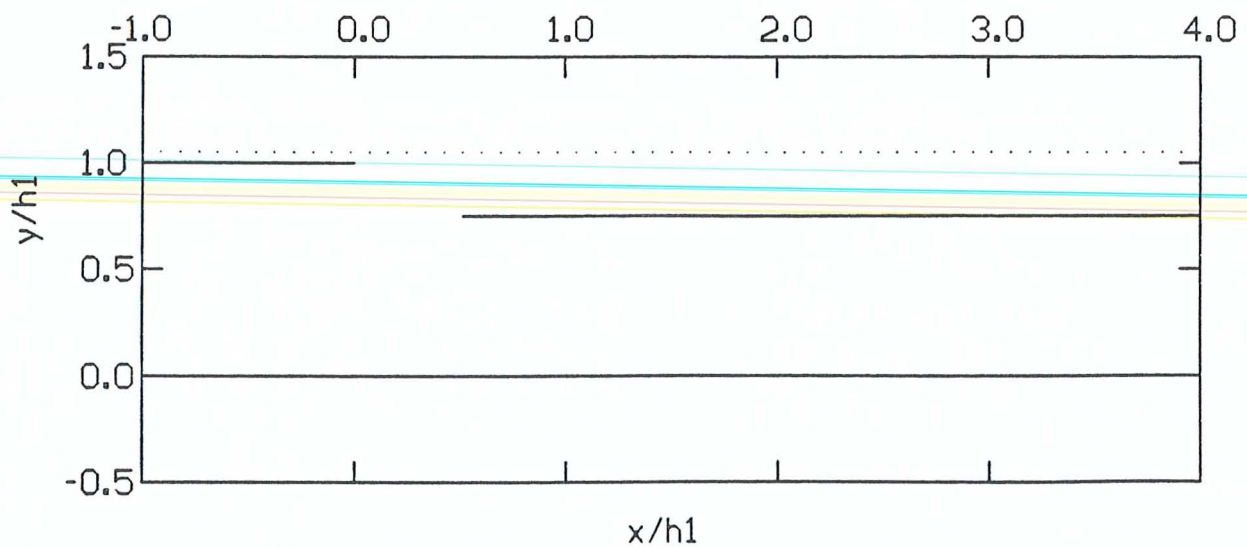

FIG. 6.4.8. L/h1 = 0.5 h2/h1 = 0.75

6.3. CASE B: NUMERICAL RESULTS AND DISCUSSION

Now the configurations are those of models B.L.1, B.L.2 or B.L.1/L.2. The earth conductor (half plane 2) extends from below the ocean (half plane 1) towards the land.

In interpreting the following model curves, we again concentrate on the perturbation of the inductive response of a laterally discontinuous earth conductor (model B.L.2) by an ocean (model B.L.1), which leads to the complete model B.L.1/L.2. A different interpretation is, as before, to consider the perturbation of the undisturbed ocean effect (model B.L.1) by an additional earth conductor (model B.L.2). This causes an attenuation of the ocean effect due to the decrease of the ocean's separation from the coupling surface below. It is again sufficient to limit the discussion to the following geometrical parameters: L/h_1 = 0.5, 1.0, 2.0, 3.0 and h_2/h_1 = 0.25, 0.75, which yields a total of eight configurations.

Vertical transfer functions are presented in the top panels of figs. 6.5.1 to 6.5.8. When interpreting the individual figures, the following points should be borne in mind. Both ocean and earth conductor cause a negative vertical transfer function. Thus, for linear superposition, the magnitude of the edge effect of the earth conductor

Figs. 6.5.1 to 6.5.8. Top and center: Transfer functions for model B.L.1 (dashed), model B.L.2 (dot-dashed) and model B.L.1/L.2 (solid). Bottom: Corresponding conductor configurations (solid) and position of measuring profile (dotted). For further explanations see text

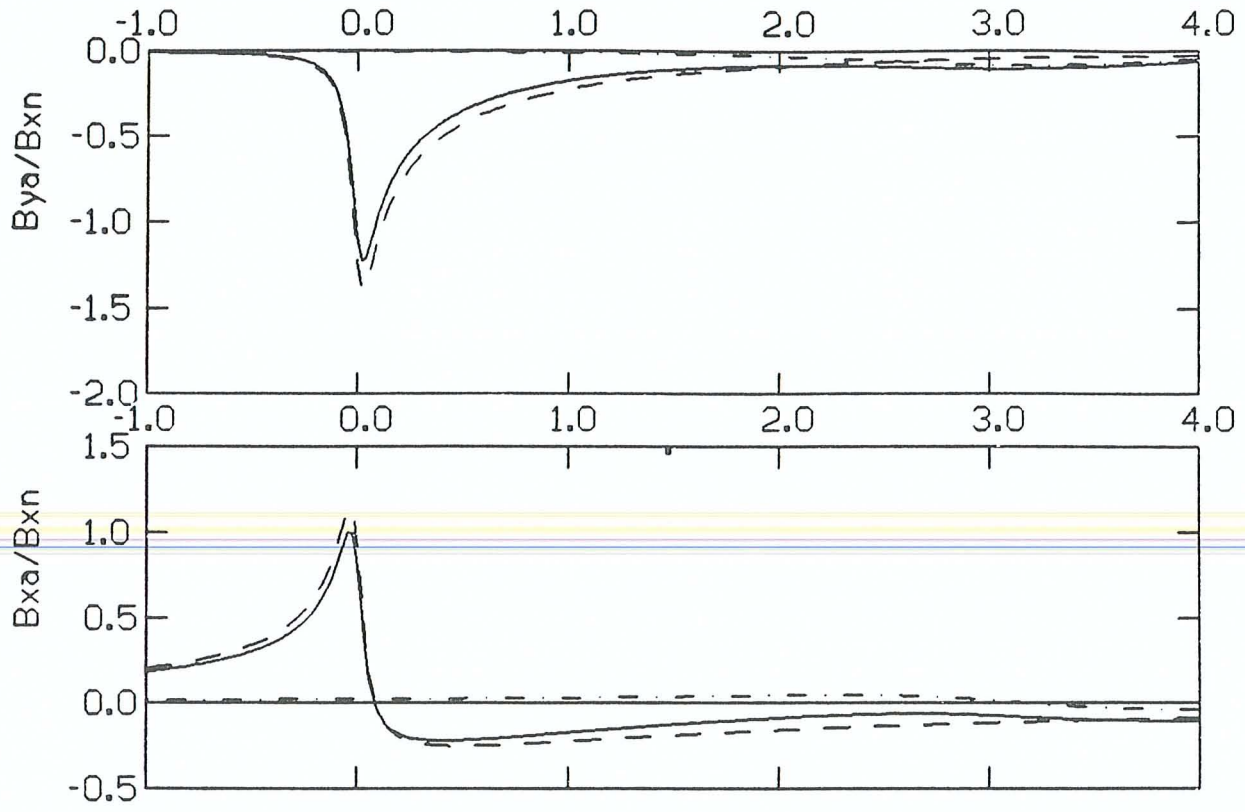

SCHMUCKER TRANSFER FUNCTIØNS

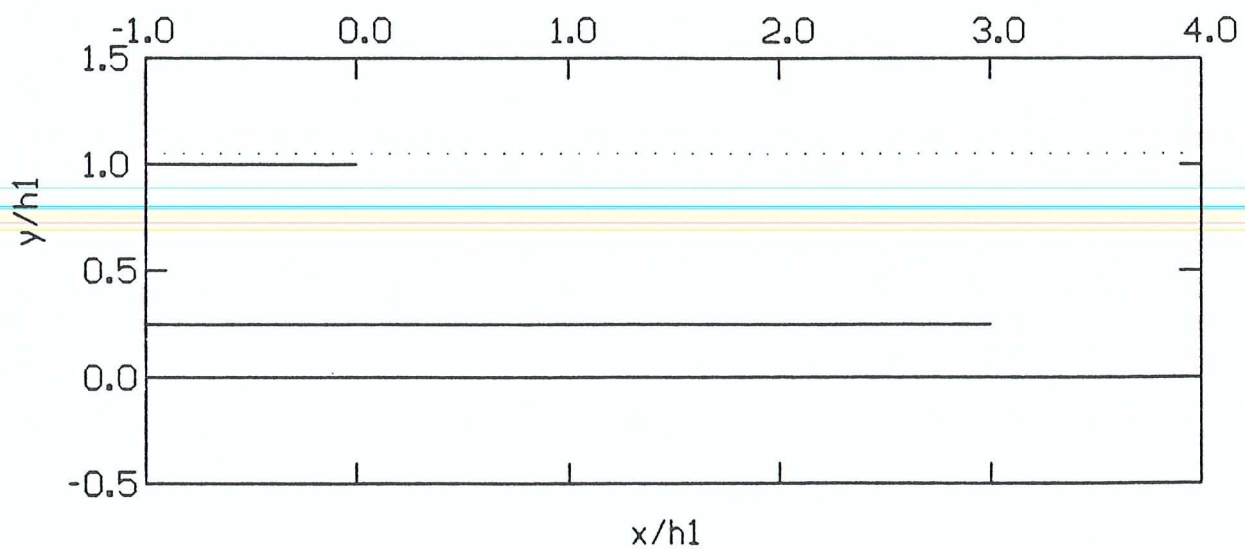

FIG. 6.5.1. L/h1 = 3.0 h2/h1 = 0.25

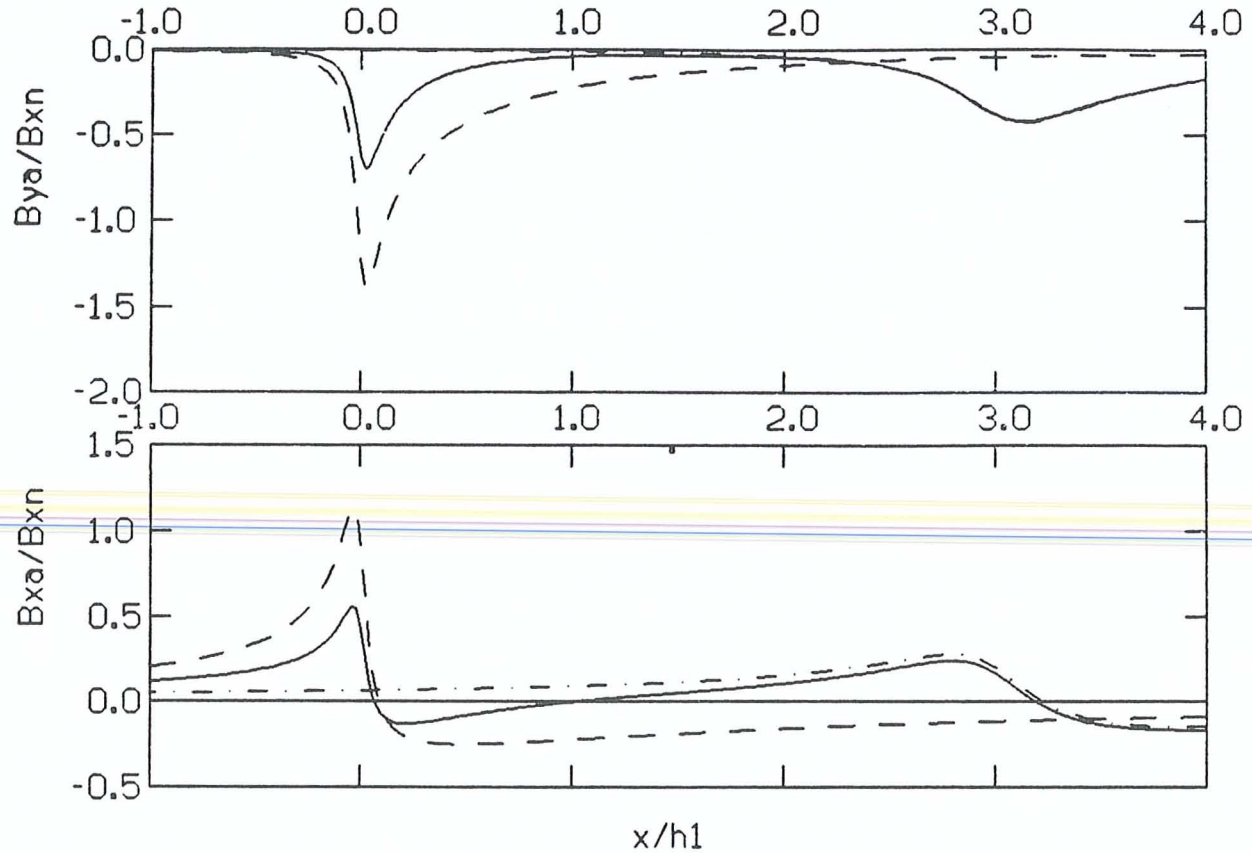

SCHMUCKER TRANSFER FUNCTIØNS

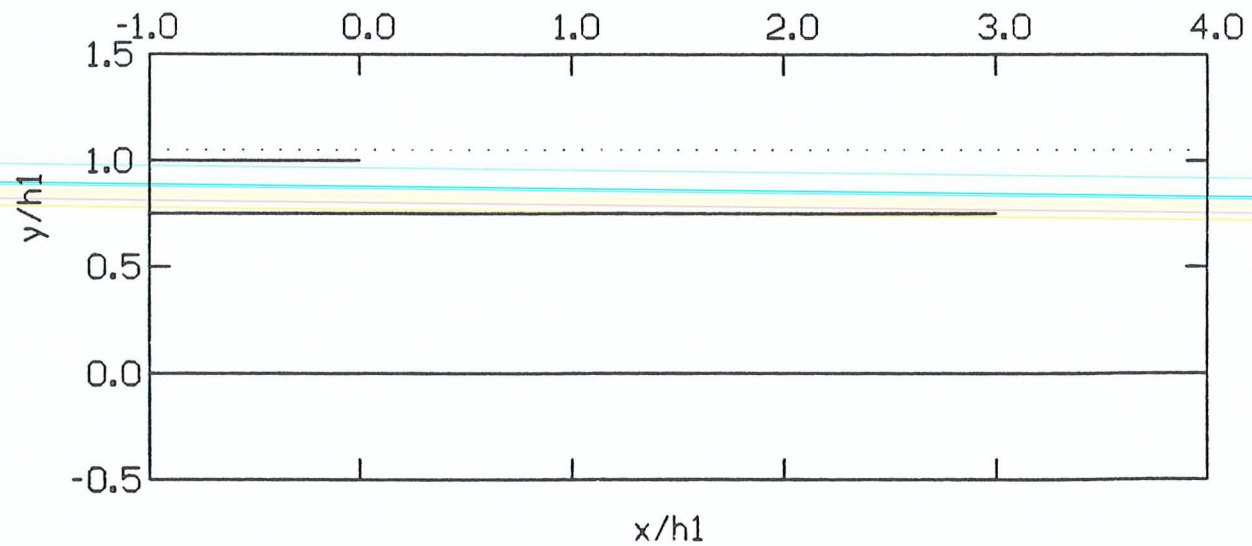

FIG. 6.5.2. L/h1 = 3.0 h2/h1 = 0.75

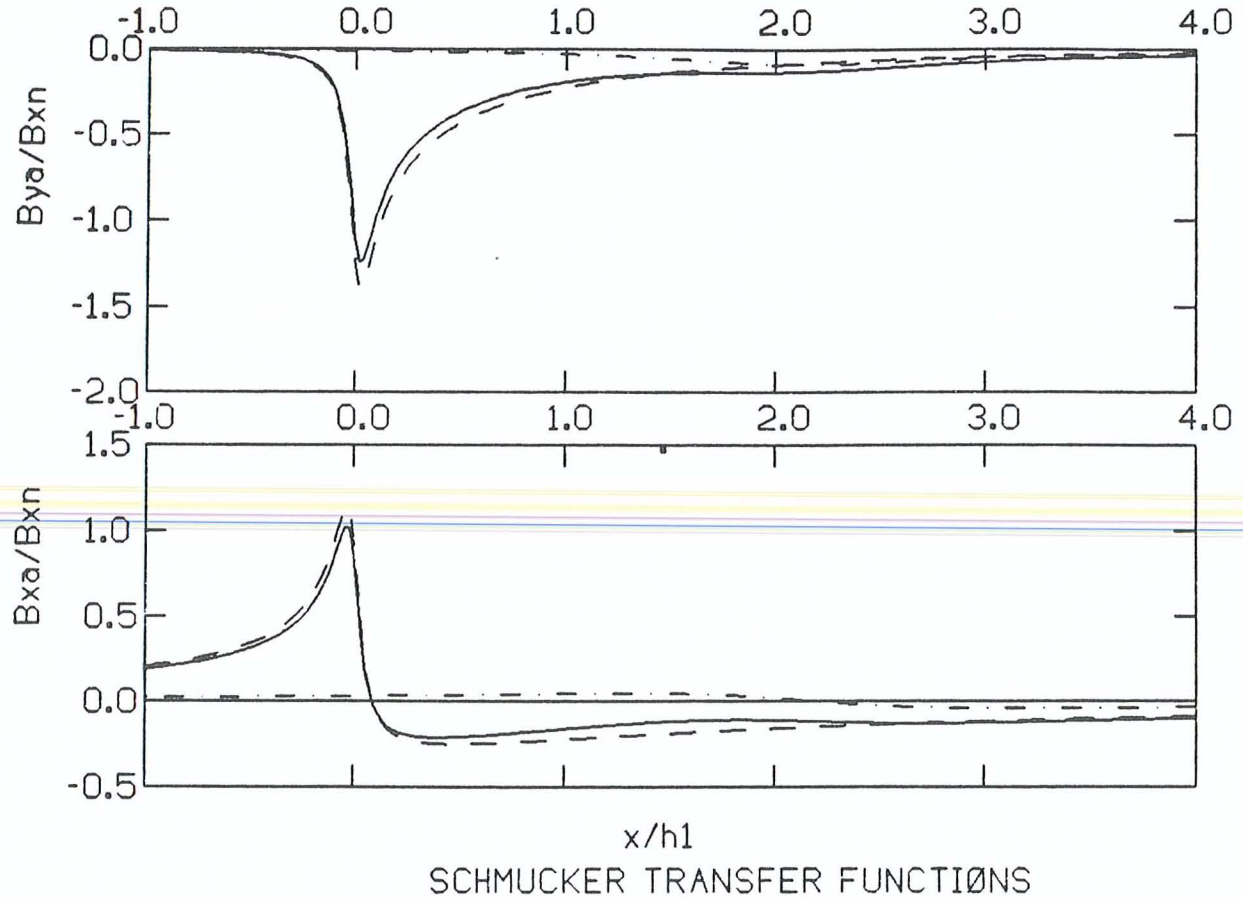

SCHMUCKER TRANSFER FUNCTIØNS

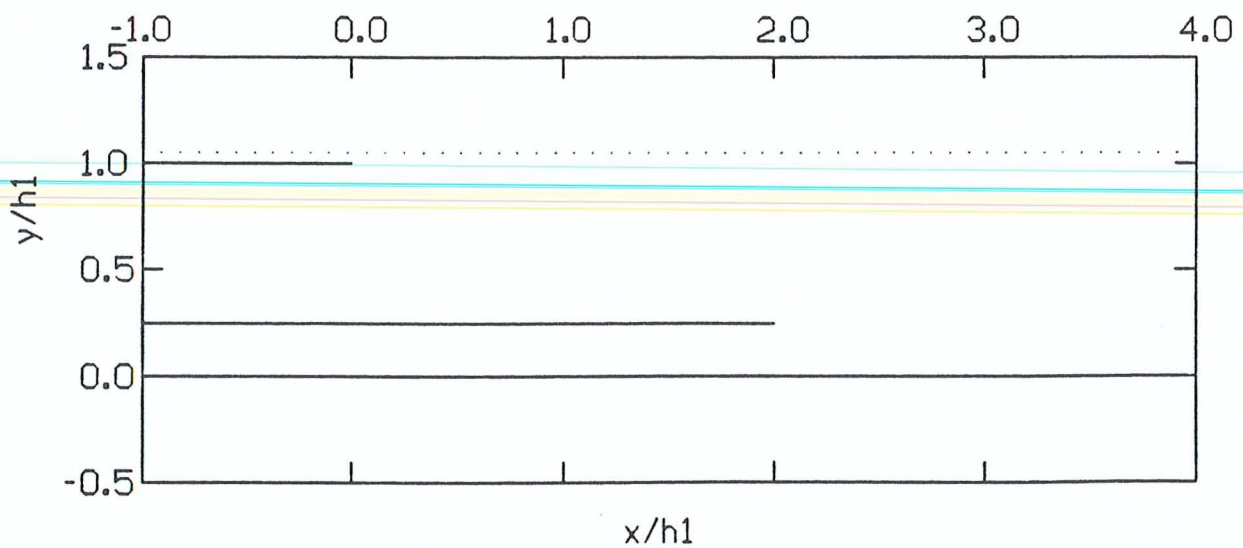

FIG. 6.5.3. L/h1 = 2.0 h2/h1 = 0.25

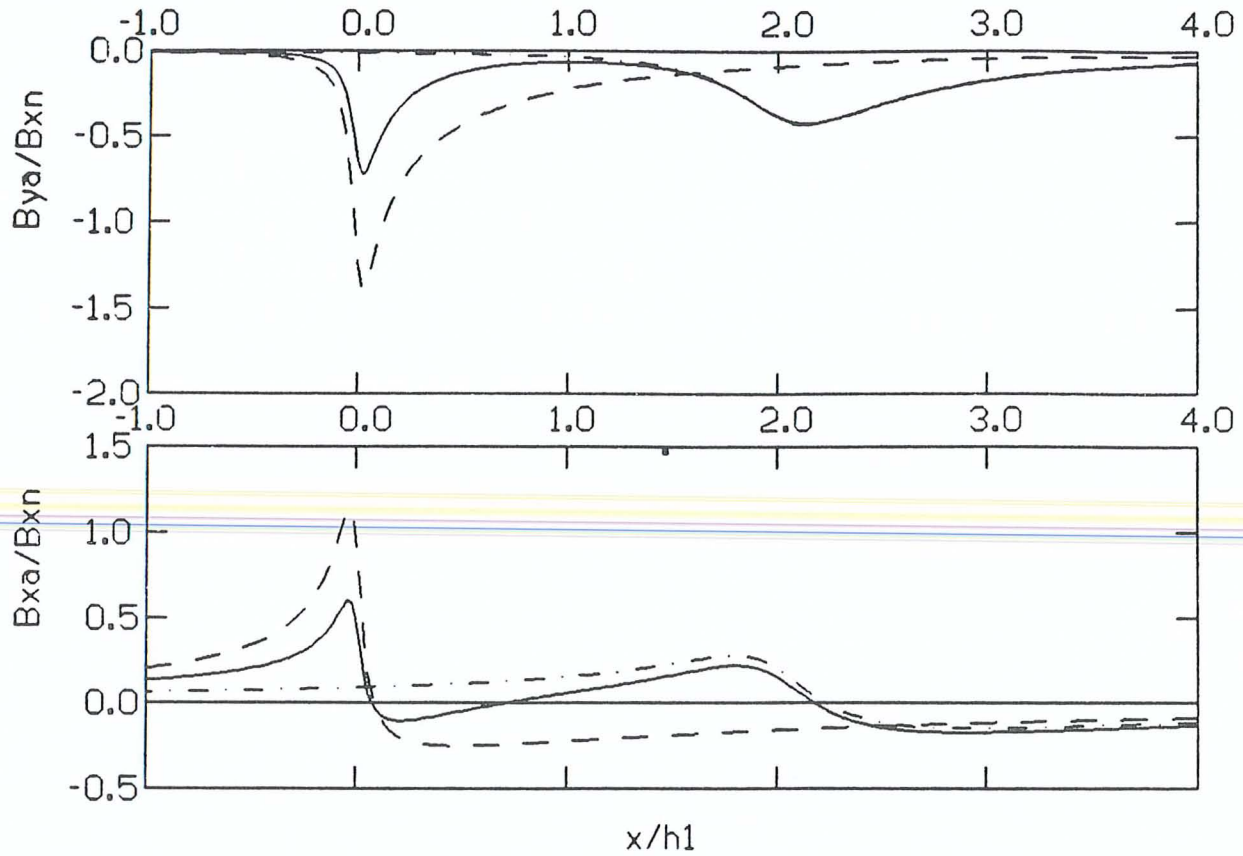

SCHMUCKER TRANSFER FUNCTIØNS

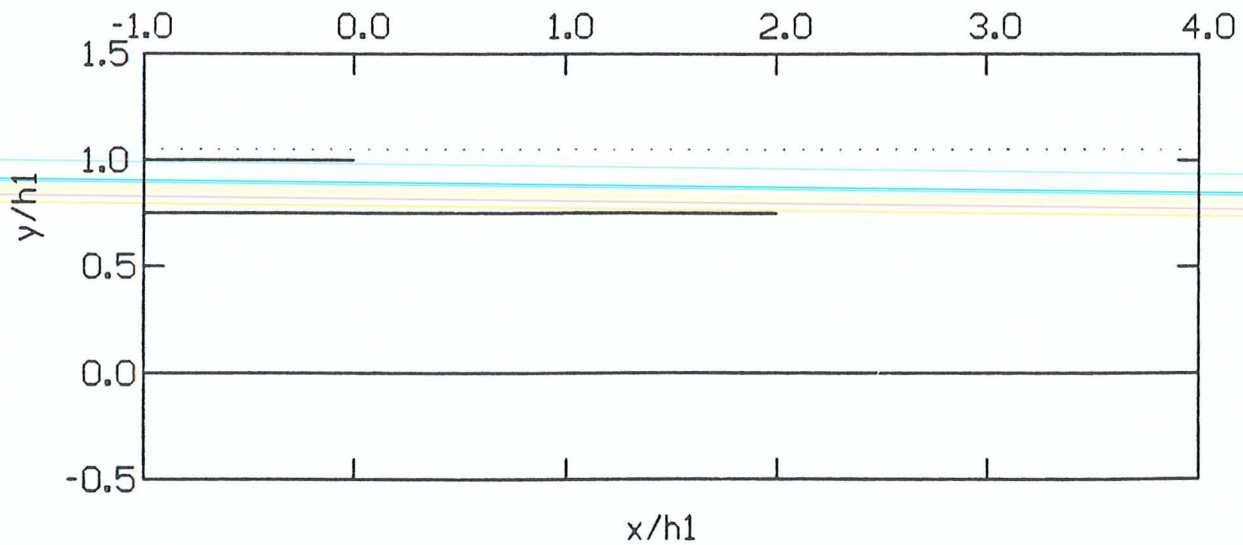

FIG. 6.5.4. L/h1 = 2.0 h2/h1 = 0.75

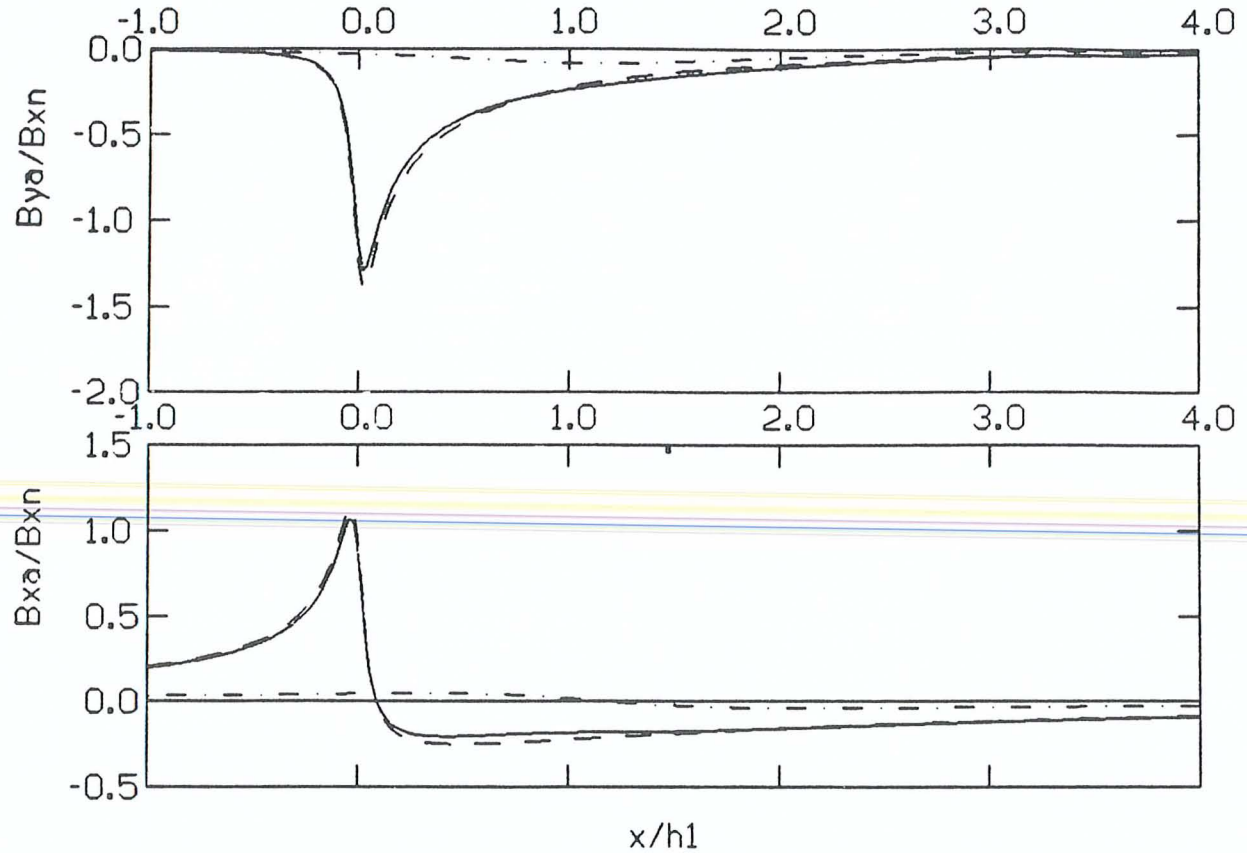

SCHMUCKER TRANSFER FUNCTIØNS

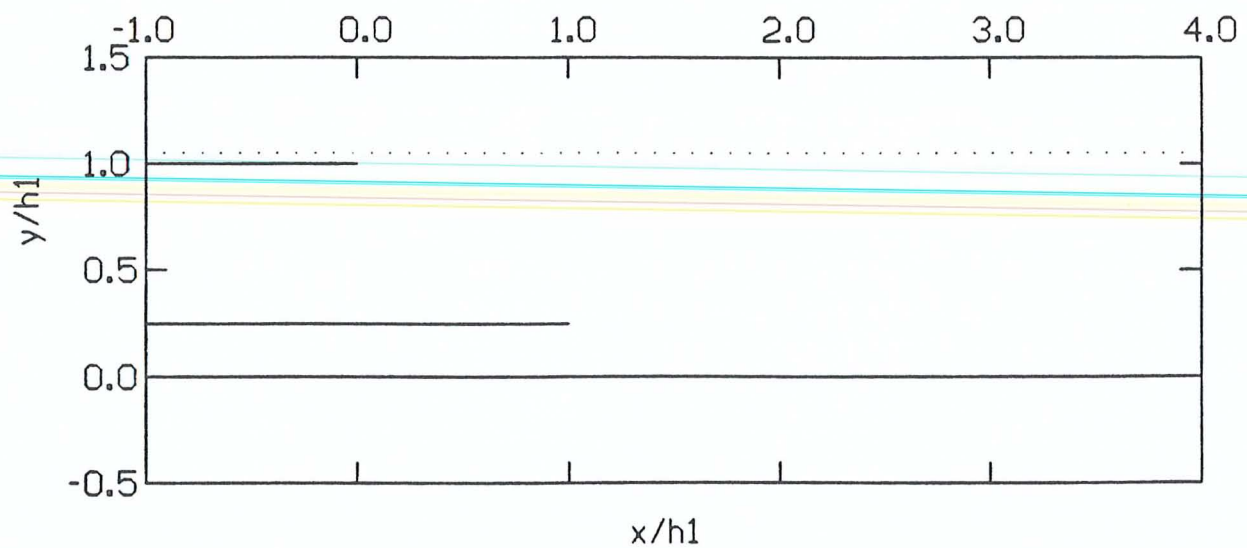

FIG. 6.5.5. L/h1 = 1.0 h2/h1 = 0.25

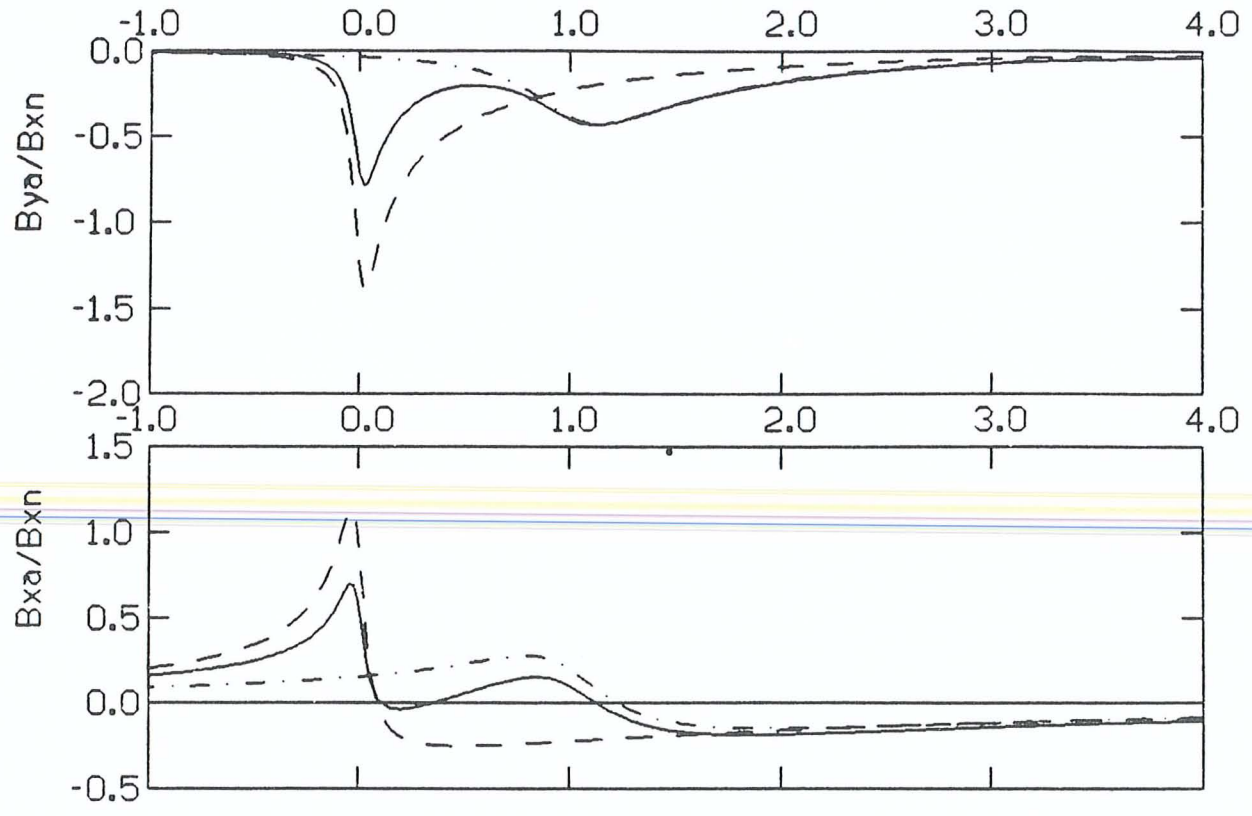

SCHMUCKER TRANSFER FUNCTIØNS

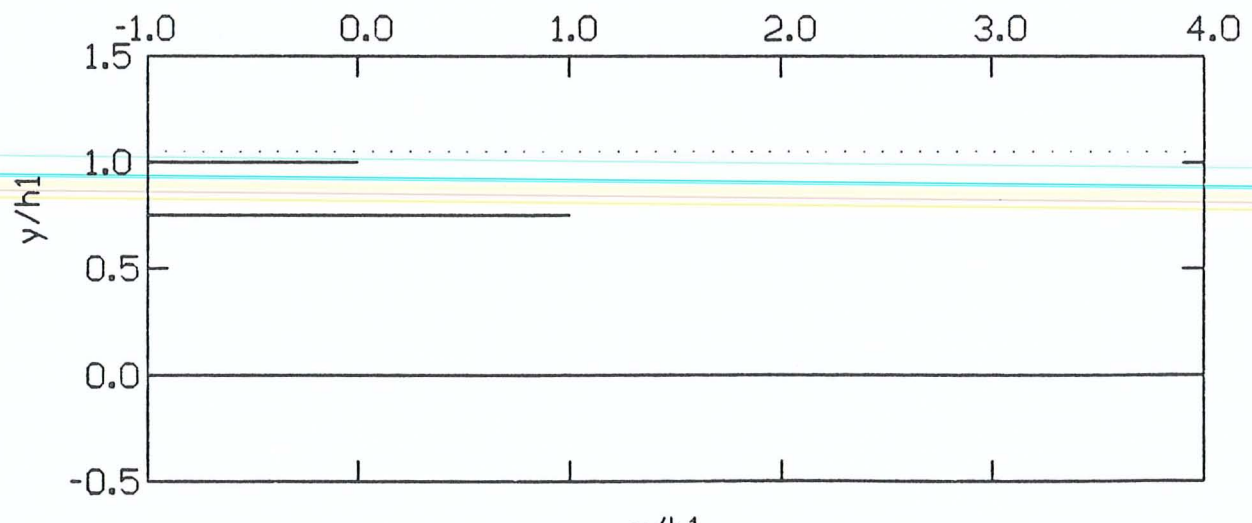

FIG. 6.5.6. L/h1 = 1.0 h2/h1 = 0.75

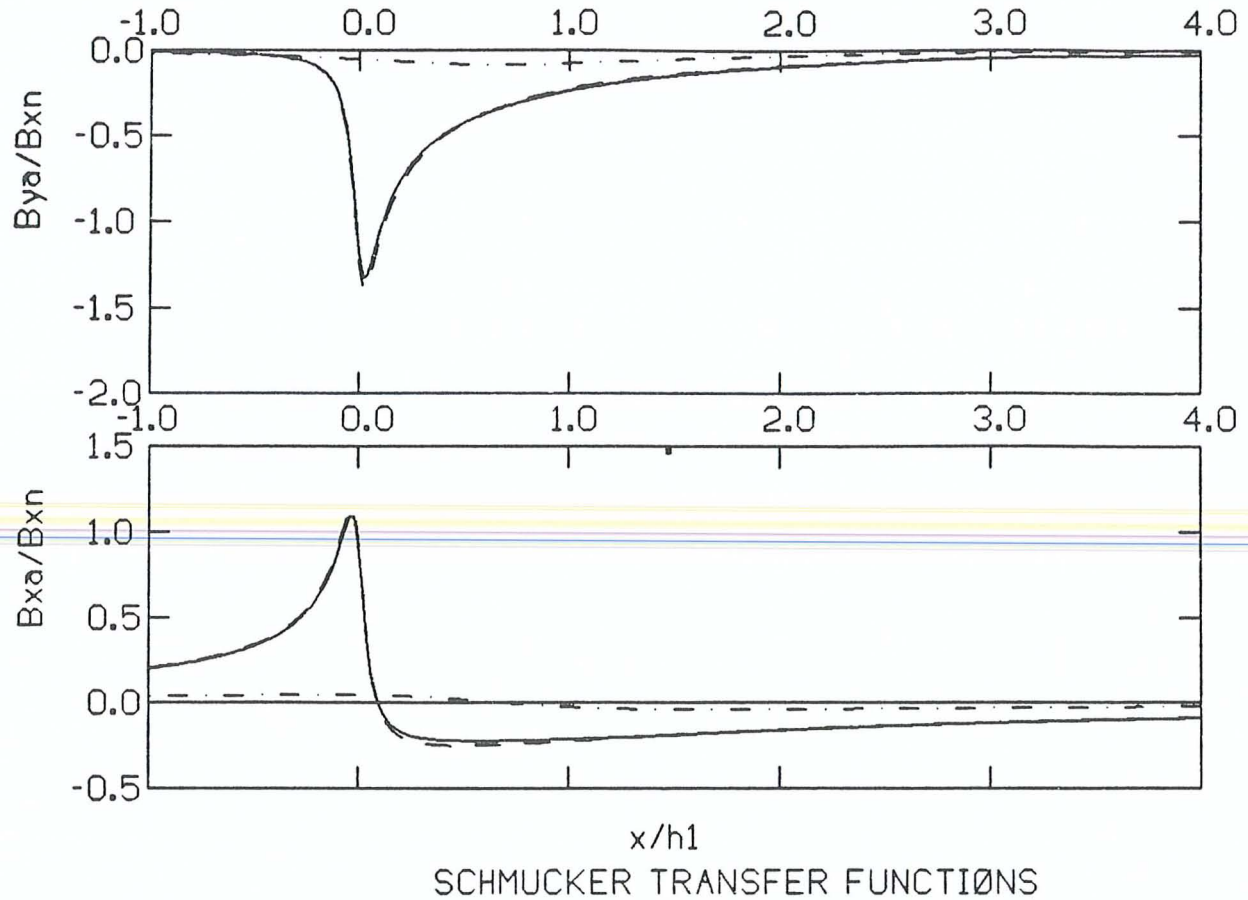

SCHMUCKER TRANSFER FUNCTIØNS

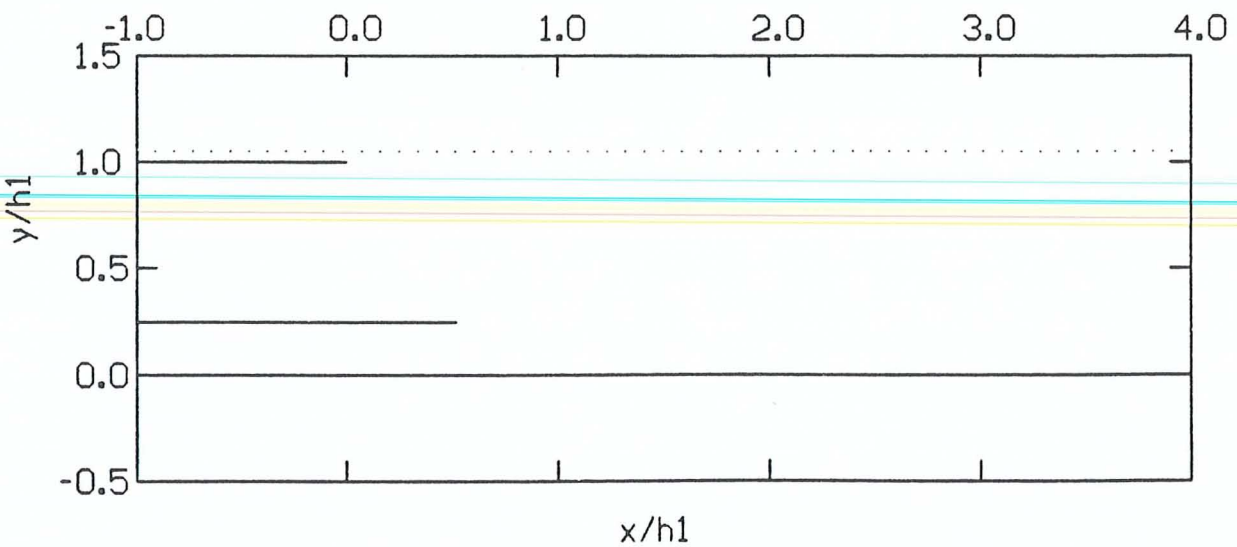

FIG. 6.5.7. L/h1 = 0.5 h2/h1 = 0.25

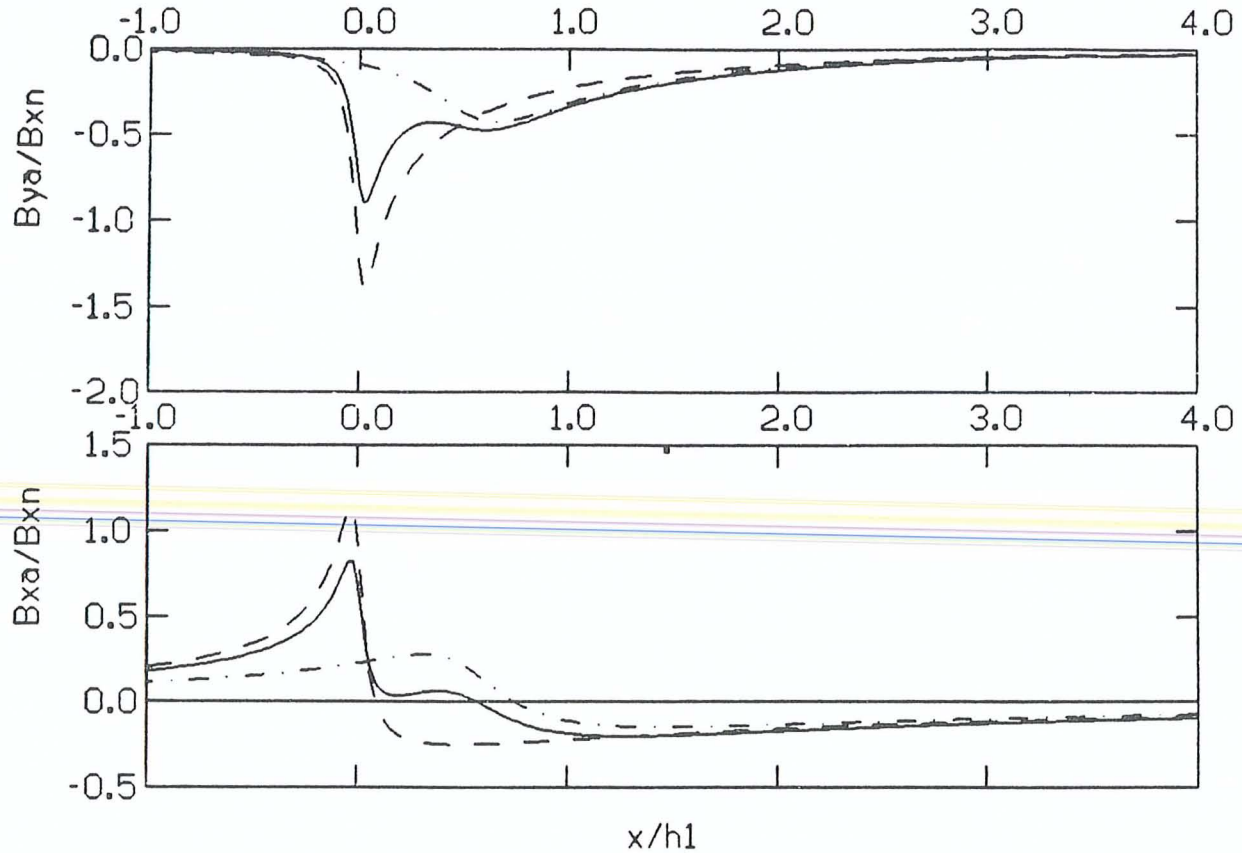

SCHMUCKER TRANSFER FUNCTIØNS

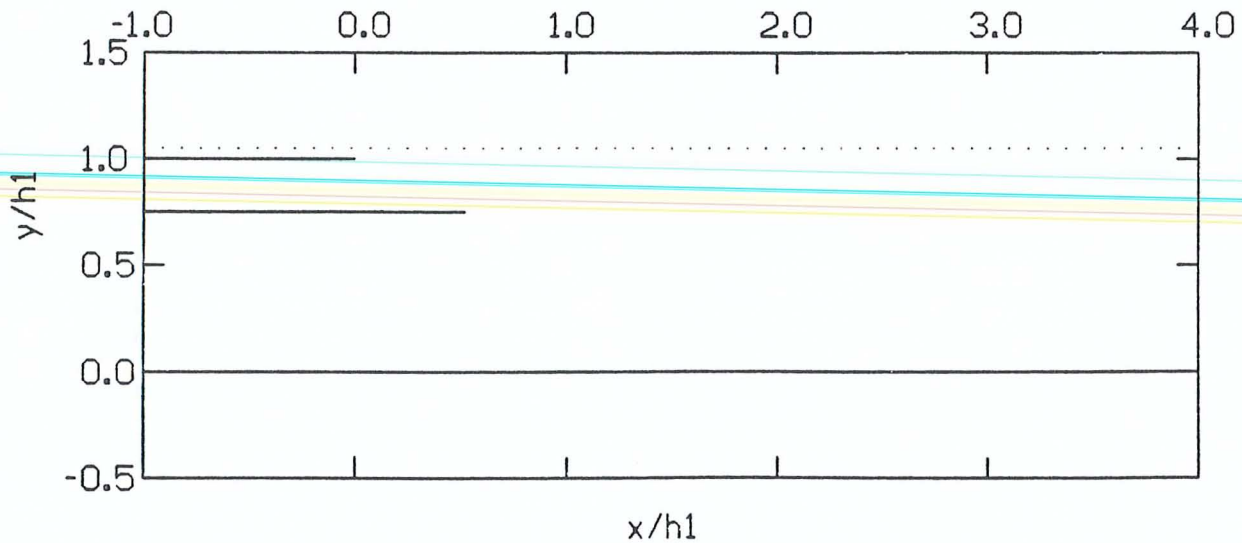

FIG. 6.5.8. L/h1 = 0.5 h2/h1 = 0.75

increases by the magnitude of the ocean effect. We can, near the edge of the earth conductor, compare the complete response (model B.L.1/L.2, solid line) with the anomaly of the corresponding configuration without an ocean (model B.L.2, dot-dashed line). Then we realize that linear superposition does not hold as accurately as for case A, particularly, if the earth conductor is shallow (h_2/h_1 = 0.75). Here, its "pure" edge effect according to model B.L.2 remains virtually unchanged after the ocean has been included into the solution (model B.L.1/L.2). This is to be expected, because the inductive coupling between half plane 1 and the whole plane corresponding to model B.L.1 has now been replaced by the stronger coupling between half planes 1 and 2. This in turn leads to a pronounced attenuation of the anomaly associated with the ocean, such that it has almost faded away near the edge of the earth conductor (see particularly figs. 6.5.2, 6.5.4 and 6.5.6). If the distance between the edges of half planes 1 and 2 becomes small ($L/h_1 < 1.0$), additional interaction between the edges of the two half planes arises.

The Schmucker horizontal transfer functions are displayed in the centre panels of figs. 6.5. If linear superposition holds, the anomaly of the ocean causes a downward shift of the edge effect of the earth conductor by the magnitude of the ocean effect. The calculated shift is

Figs. 6.6.1 to 6.6.8. Top and center: Sum of transfer functions for models B.L.1 and B.L.2 (dashed) and transfer function for model B.L.1/L.2 (solid). Bottom: Corresponding conductor configurations (solid) and position of measuring profile (dotted). For further explanations see text

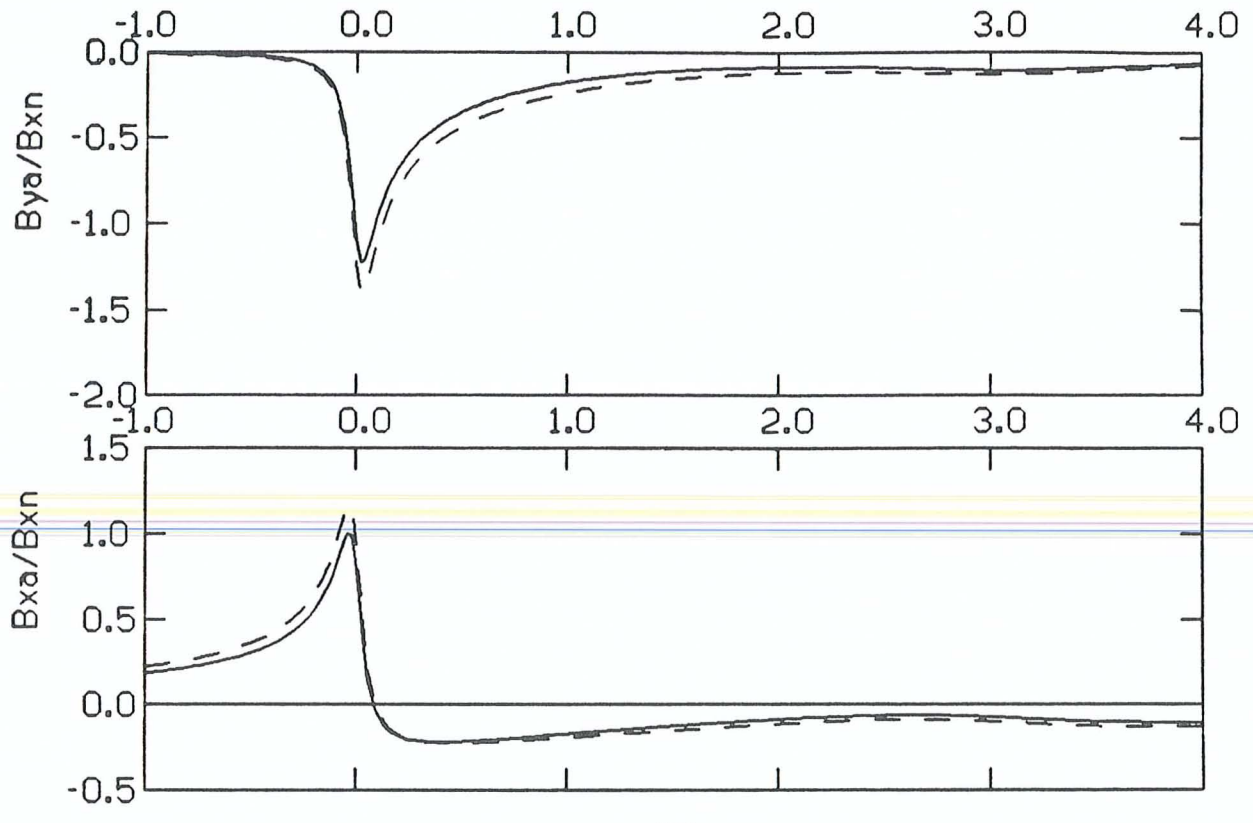

SCHMUCKER TRANSFER FUNCTIØNS

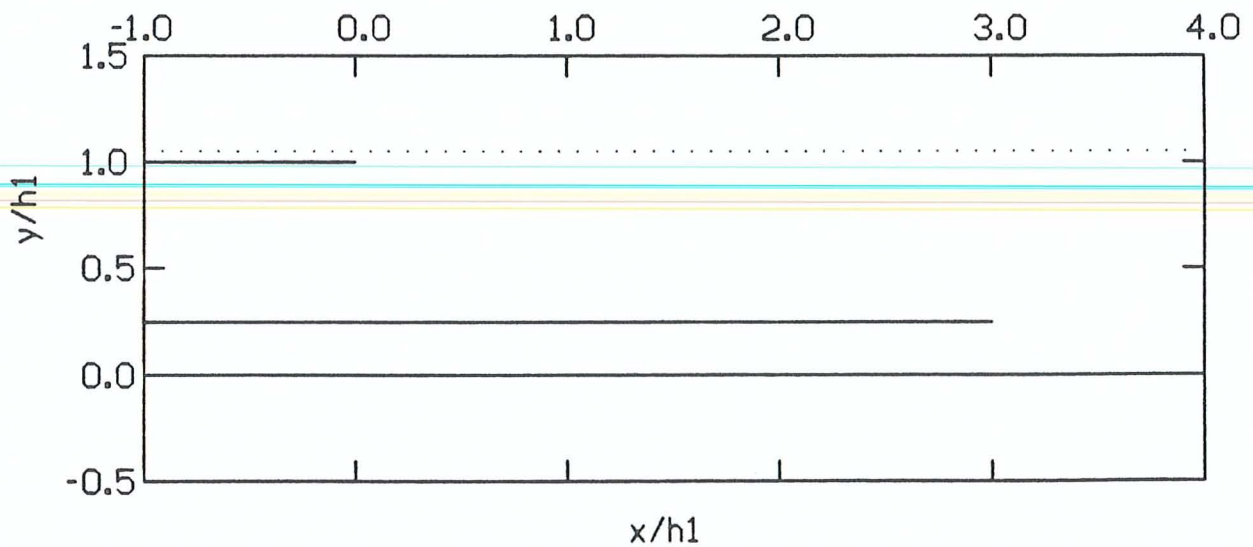

FIG. 6.6.1. L/h1 = 3.0 h2/h1 = 0.25

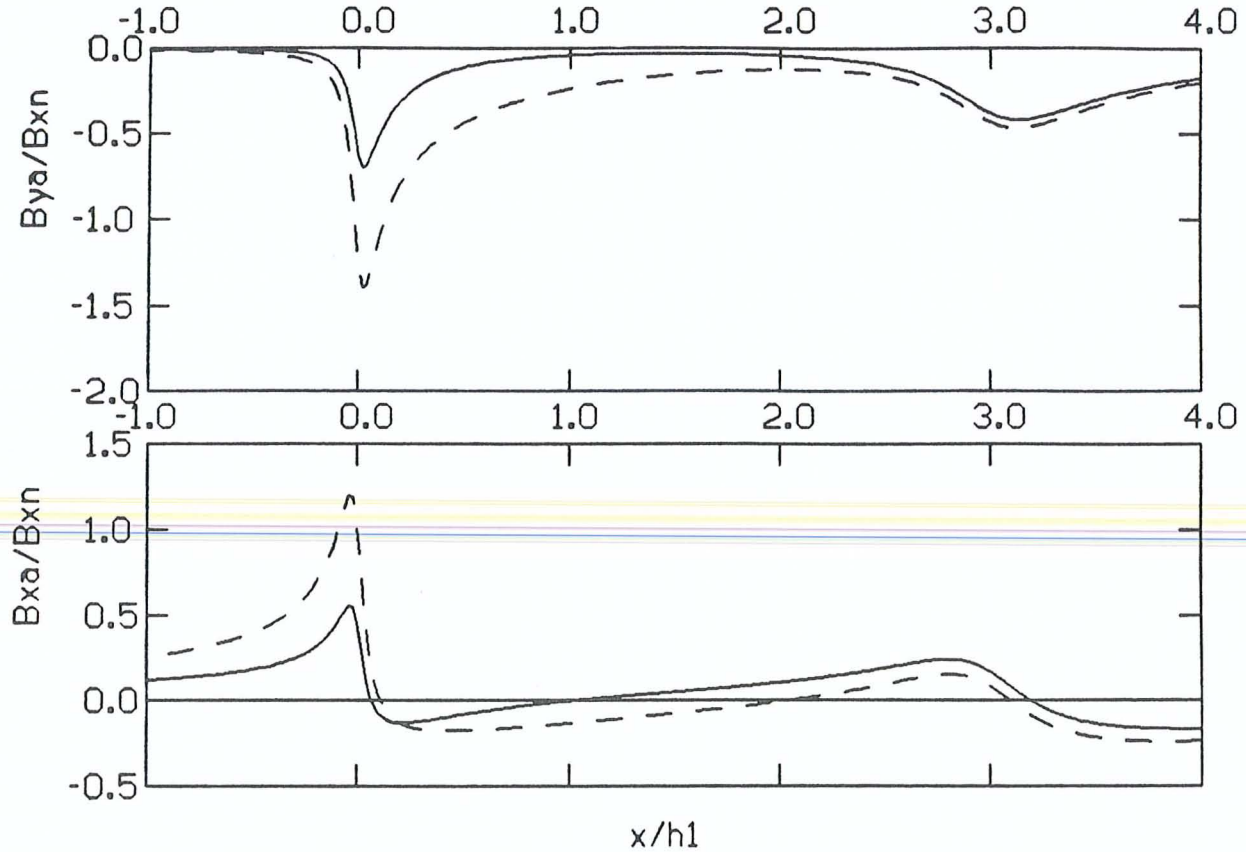

SCHMUCKER TRANSFER FUNCTIØNS

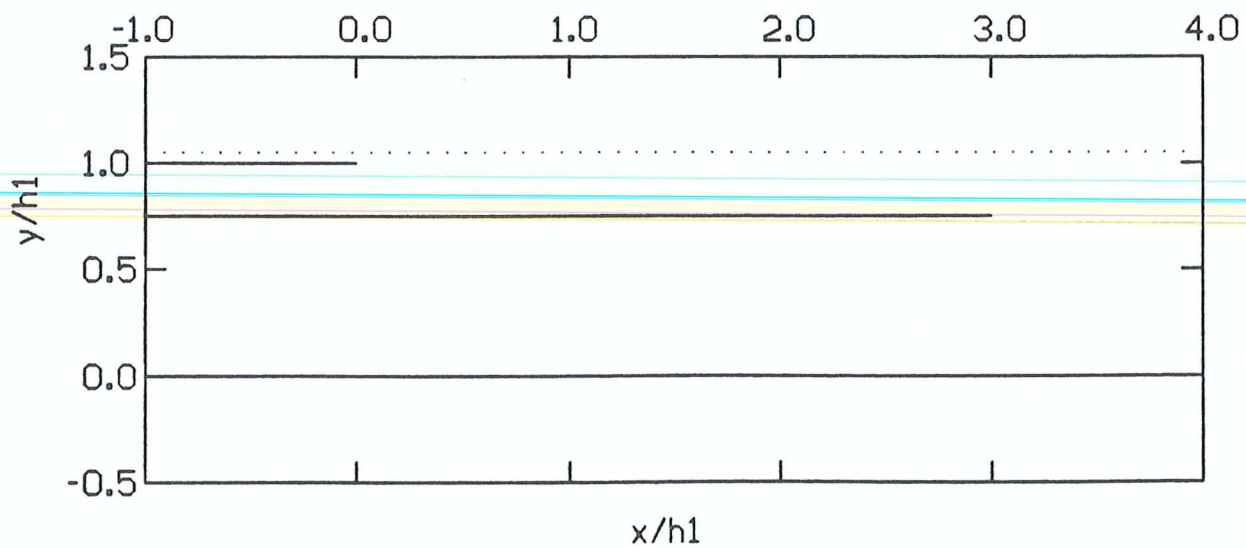

FIG. 6.6.2. L/h1 = 3.0 h2/h1 = 0.75

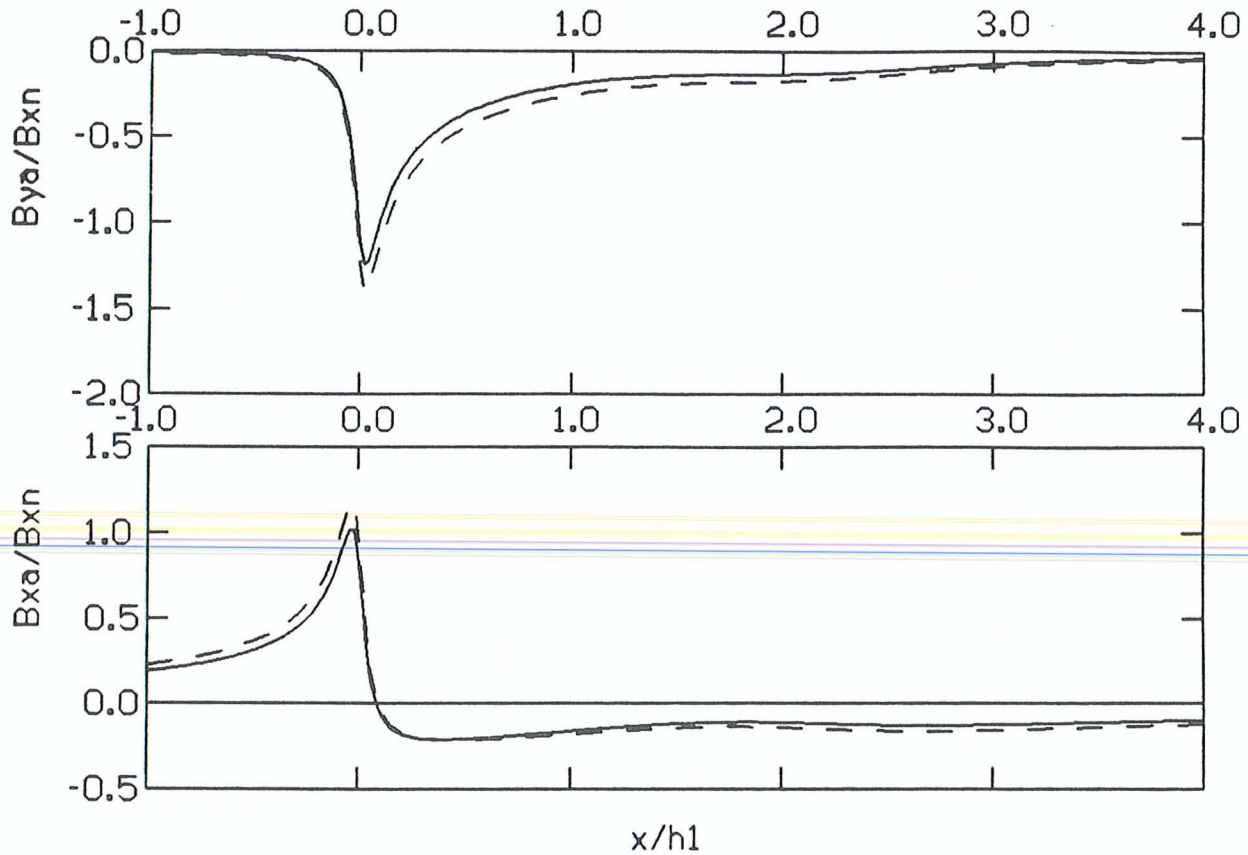

SCHMUCKER TRANSFER FUNCTIØNS

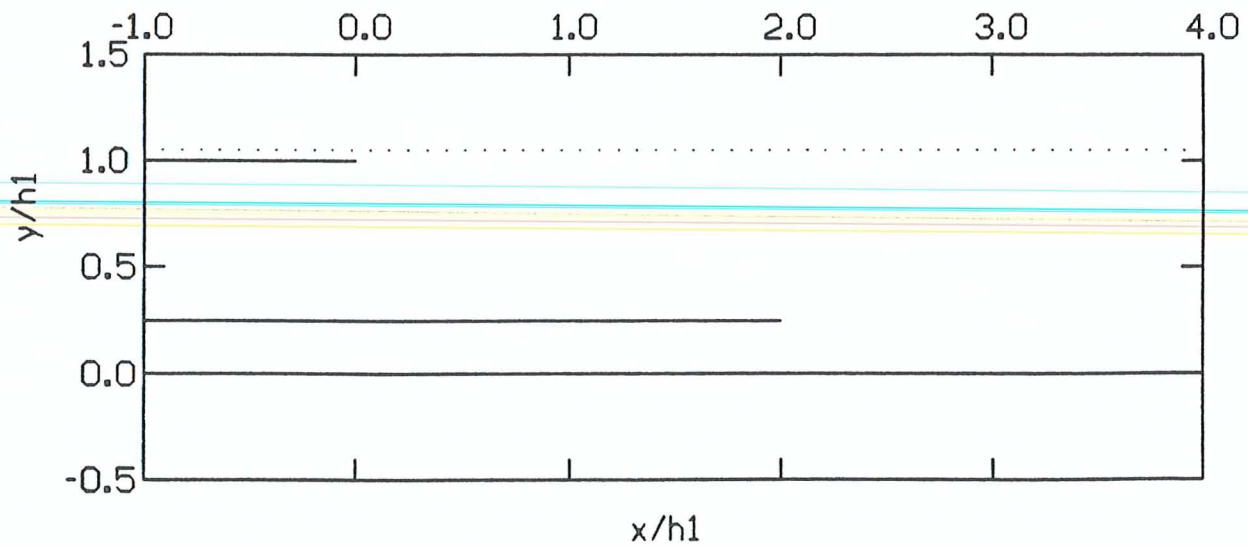

FIG. 6.6.3. L/h1 = 2.0 h2/h1 = 0.25

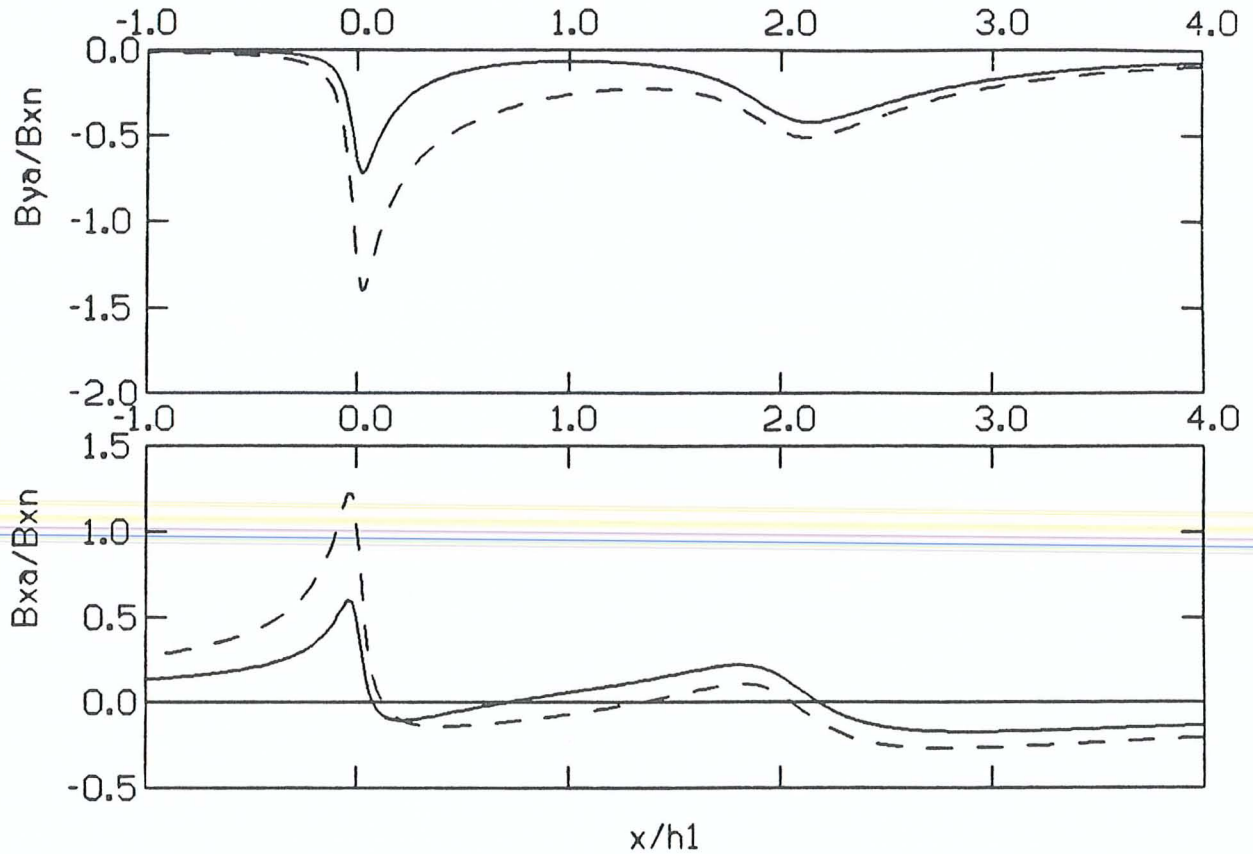

SCHMUCKER TRANSFER FUNCTIØNS

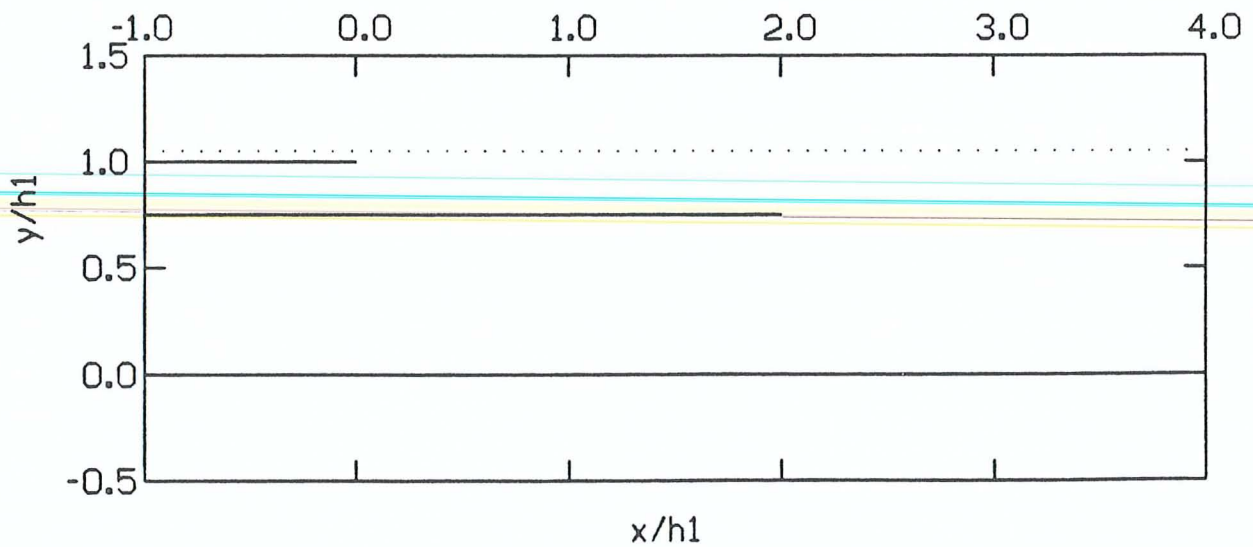

FIG. 6.6.4. L/h1 = 2.0 h2/h1 = 0.75

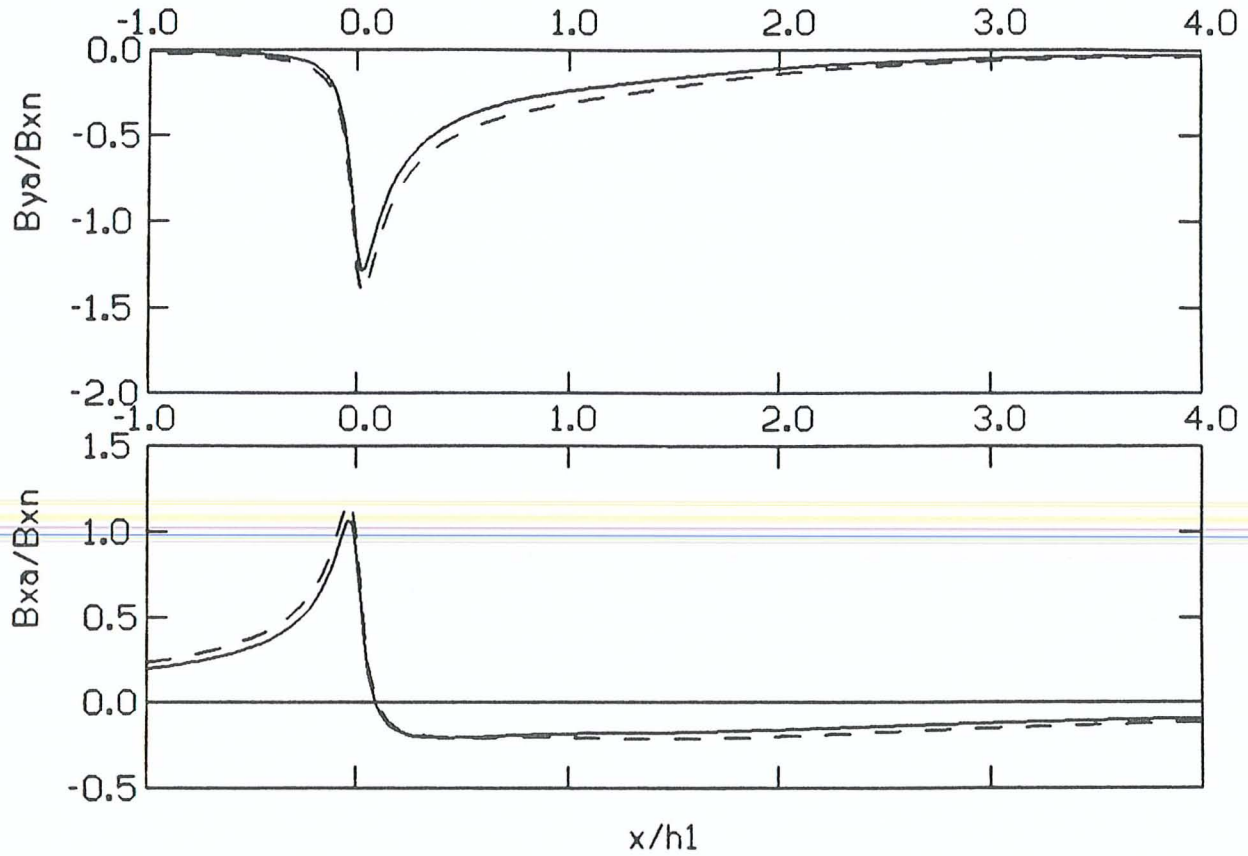

SCHMUCKER TRANSFER FUNCTIØNS

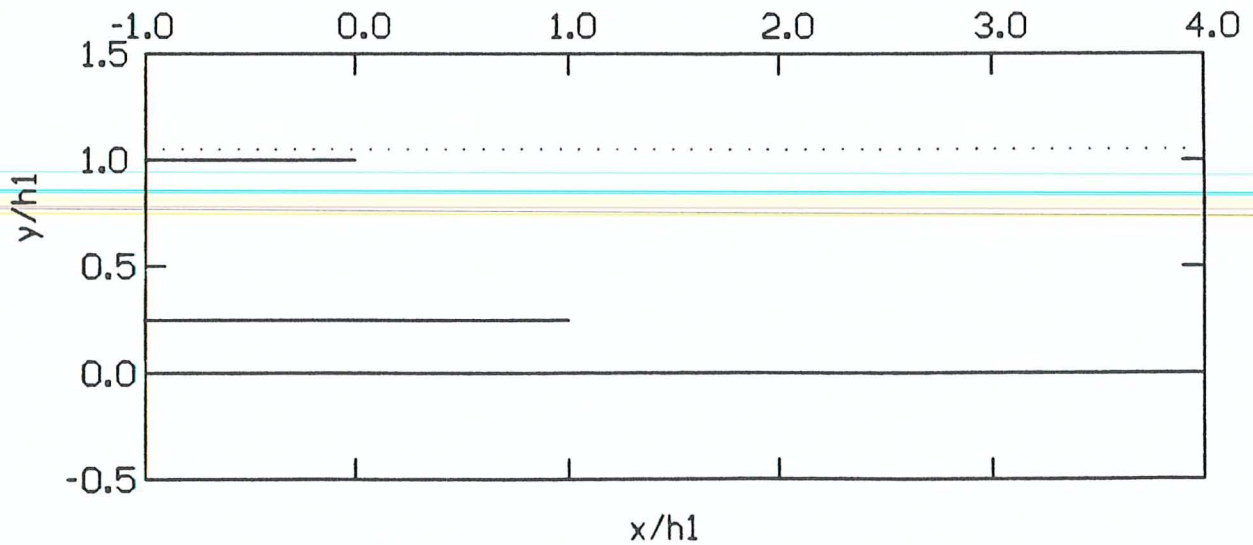

FIG. 6.6.5. L/h1 = 1.0 h2/h1 = 0.25

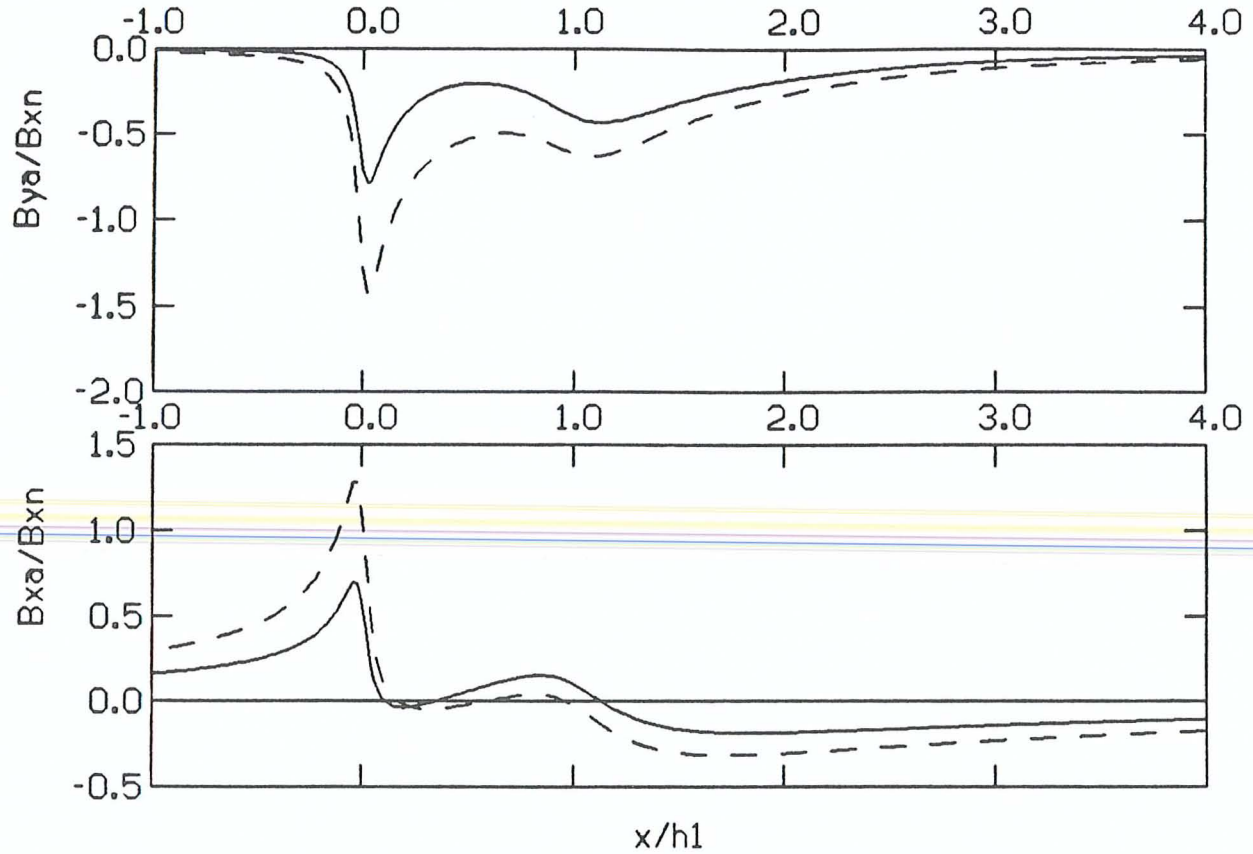

SCHMUCKER TRANSFER FUNCTIØNS

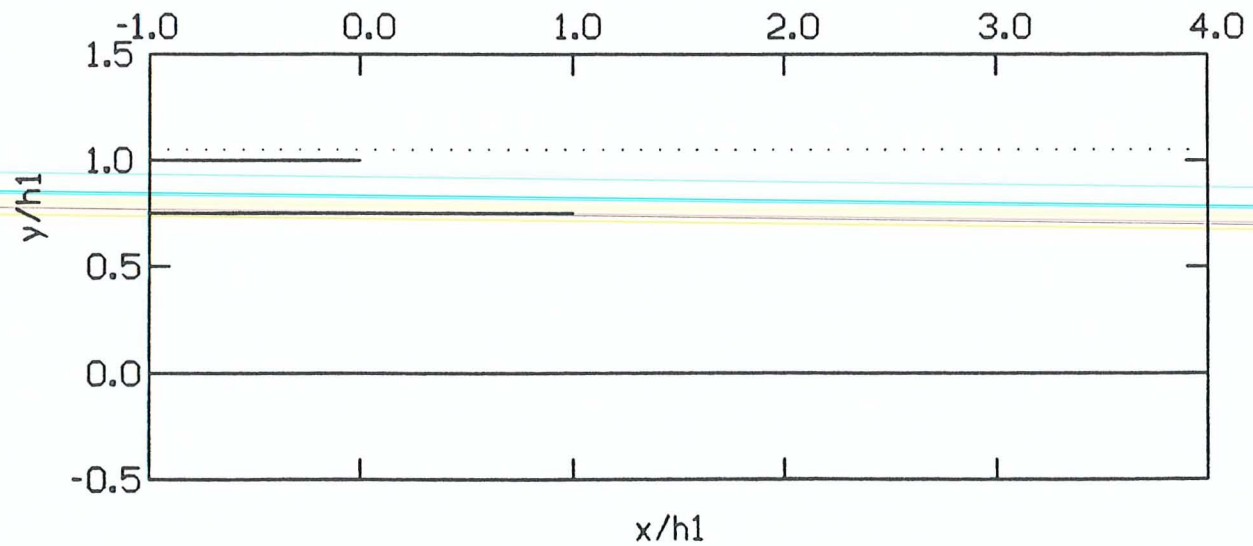

FIG. 6.6.6. L/h1 = 1.0 h2/h1 = 0.75

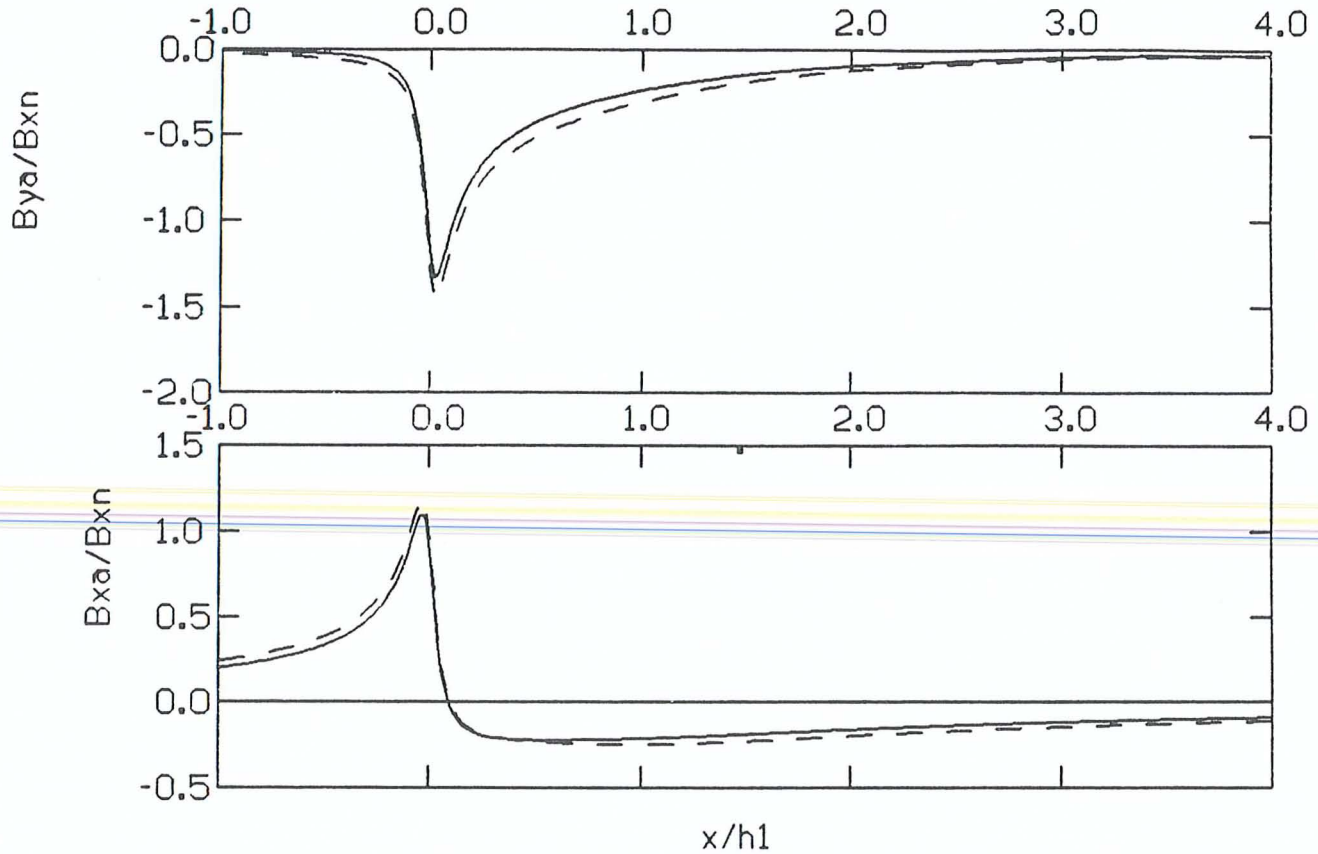

SCHMUCKER TRANSFER FUNCTIØNS

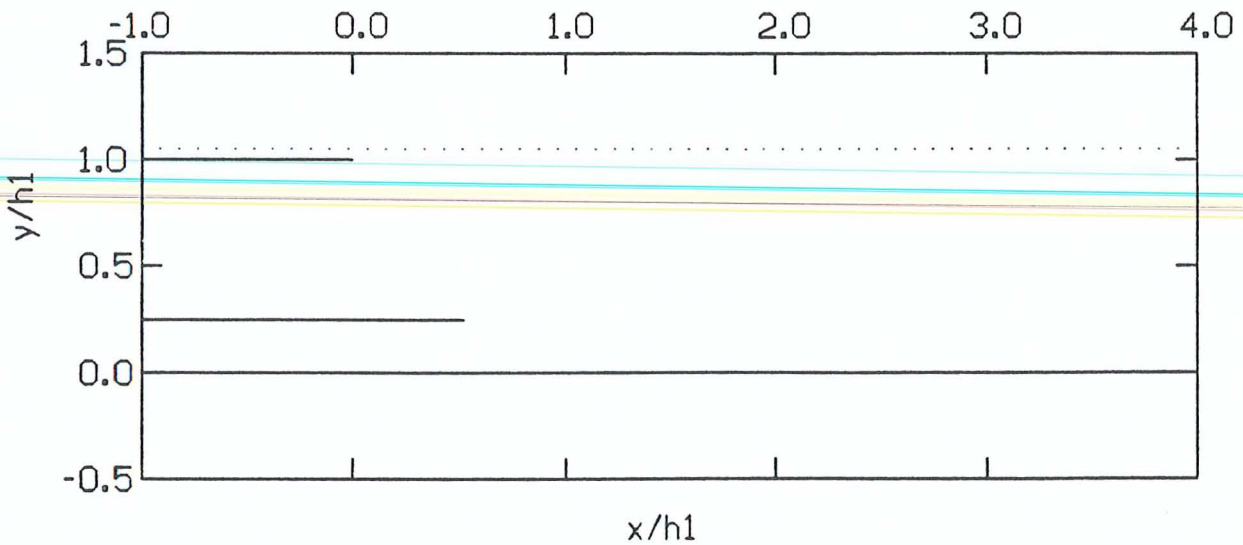

FIG. 6.6.7. L/h1 = 0.5 h2/h1 = 0.25

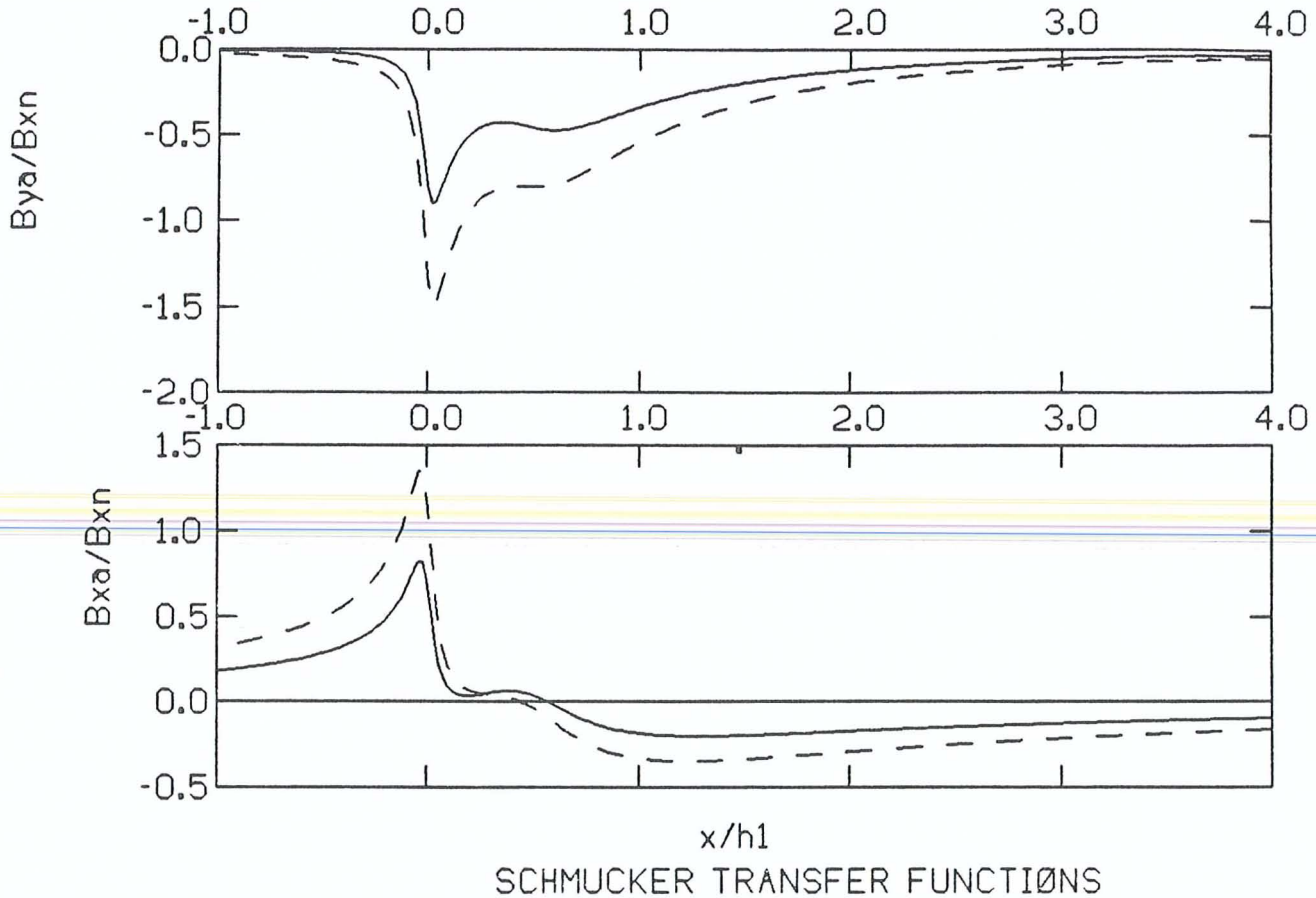

SCHMUCKER TRANSFER FUNCTIØNS

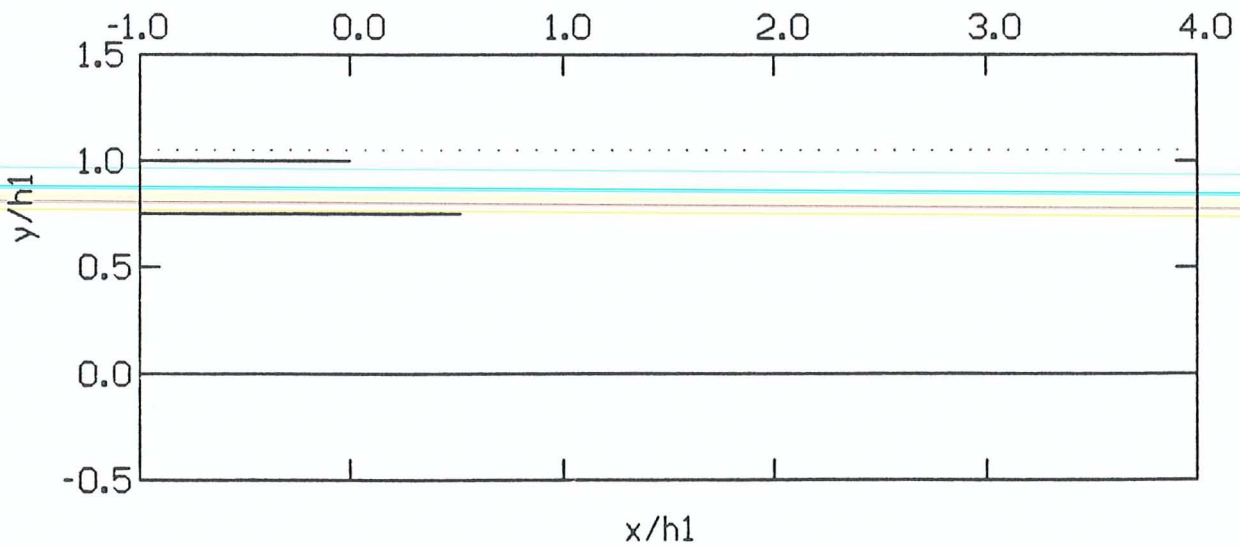

FIG. 6.6.8. L/h1 = 0.5 h2/h1 = 0.75

always less, and a closer inspection of figs. 6.5.2, 6.5.4 and 6.5.6 again shows that for shallow conductors (h_2/h_1 = 0.75) the superimposed ocean effect is largely cancelled because of the strongly attenuated anomaly of the ocean. Deep conductors (h_2/h_1 = 0.25) are also difficult to detect on the basis of their associated horizontal transfer functions, but linear superposition becomes a better approximation now.

These conclusions are also supported by figs. 6.6.1 to 6.6.8, which compare the sum of the responses of models B.L.1 and B.L.2 with the response of model B.L.1/L.2.

CHAPTER 7

RAPID MODELLING OF COAST EFFECTS

The theory outlined in chaps. 4 and 5 has primarily been developed to investigate the degree of inductive coupling between two conducting half planes and an underlying whole plane. However, it may also be used for the direct modelling of some measured magnetic variations, as long as the observed response is relatively close to the inductive limit. More general modelling techniques do exist (see chaps. 2 and 3), but the following two examples will demonstrate that our simple configurations consisting of two half planes and a whole plane often suffice for a representation of the fundamental character of the subsurface conductivity structure. As only three model parameters are involved, trial and error modelling is very rapid, and the final configuration can serve as a useful guide when considering more complicated models of the subsurface conductivity distribution.

7.1. COAST EFFECT IN SOUTH-WESTERN AUSTRALIA

As one example, real Parkinson transfer functions, as measured by Everett & Hyndman (1967) in south-western Australia, have been modelled. Strictly speaking, the authors regarded their transfer functions as vectors (pointing into the positive x direction, see eq. 3.1) and decomposed them into components perpendicular to two straight lines, which served as crude representations of the edges of the continental shelves west and south of the survey area. But this linear decomposition neglects any galvanic or inductive coupling between the two coastal anomalies. Siebert (1971) demonstrated that these extra effects would become small, if both anomalies were narrow and approximately orthogonal to each other. This seems to apply for south-western Australia and justifies Everett & Hyndman's (1967) approach.

Fig. 7.1 shows the modelling results for the observed transfer function components perpendicular to the west coast for one-hour periods, by a specific conductor configuration of model B.L.1/L.2. The edge of half plane 1 has been taken to coincide with the edge of the continental shelf. The exact height of the measuring profile above this half plane is only crucial for the behaviour of the model response very close to the singular edge of this half plane, where our

model becomes inappropriate and no field observations exist anyway. The most interesting aspect is that a second half plane is required to reconcile the observed attenuation of the coast effect close to the continental margin with the large depth of the conductosphere for one-hour periods far away from the ocean, as established by other work (see Lilley et al., 1981). Whether this second conductor actually extends below the real ocean, cannot be inferred from our results, because the model ocean has been assumed opaque.

To explain the subdued vertical variation at their westernmost station, Everett & Hyndman (1967) themselves speculated that the Australian shield might terminate along the Darling fault, which seperates the sedimentary Perth basin to the west from the shield area to the east. In our model, the non-shield region is represented by half plane 2 at a depth of 45 km below the surface, whereas the conductosphere is more than 200 km deep. This is similar to the configuration of fig. 6.5.6, which has been discussed in the previous chapter.

Fig. 7.1. Top: Measured (dashed) and calculated (solid) transfer functions as a function of the distance from the continental margin. Bottom: Model conductors (solid) and measuring profile (dotted). South-western Australia; T = 1 h (see also text)

Fig. 7.2. Top: Measured (dashed) and calculated (solid) transfer functions as a function of the distance from the continental margin. Bottom: Model conductors (solid) and measuring profile (dotted). Eastern United States; T = 1 h (see also text)

Fig. 7.3. Top: Measured (dashed) and calculated (solid) transfer functions as a function of the distance from the continental margin. Bottom: Model conductors (solid) and measuring profile (dotted). Eastern United States; T = 16 min (see also text)

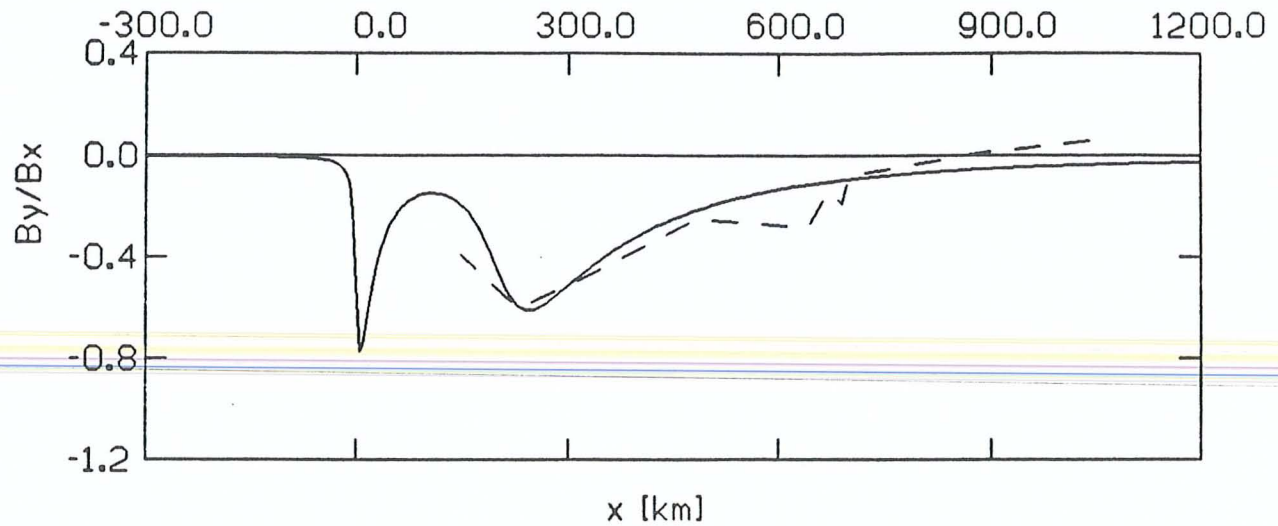

PARKINSØN TRANSFER FUNCTIØN

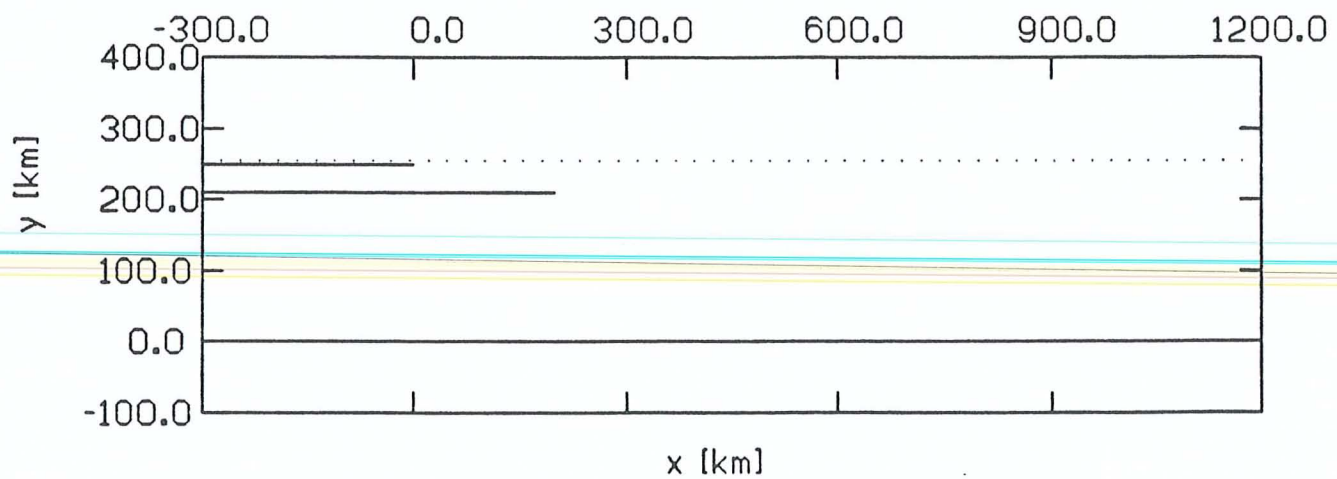

FIG. 7.1. h1=250 h2=210 h3=255 L=200 [km]

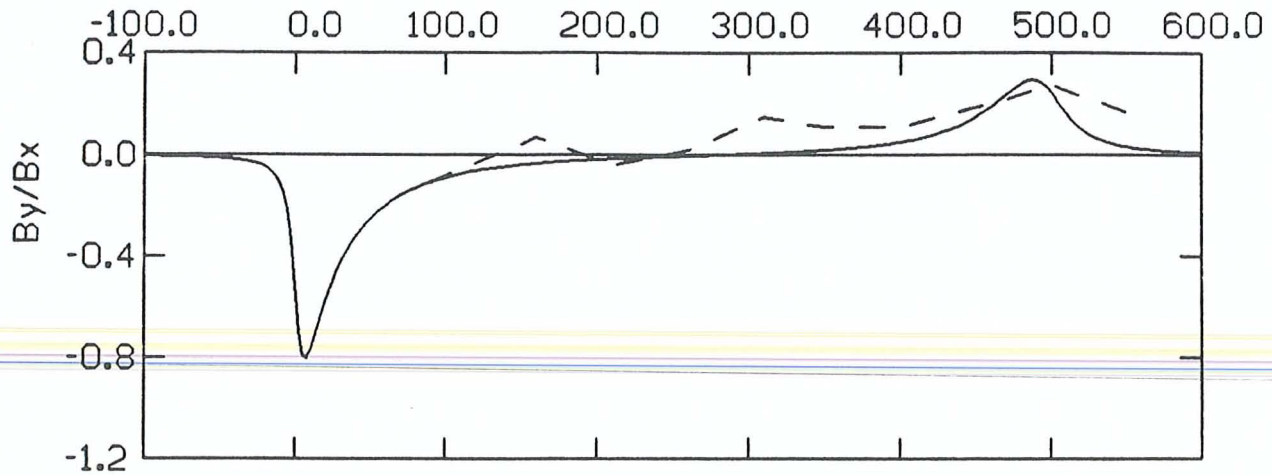

PARKINSØN TRANSFER FUNCTIØN

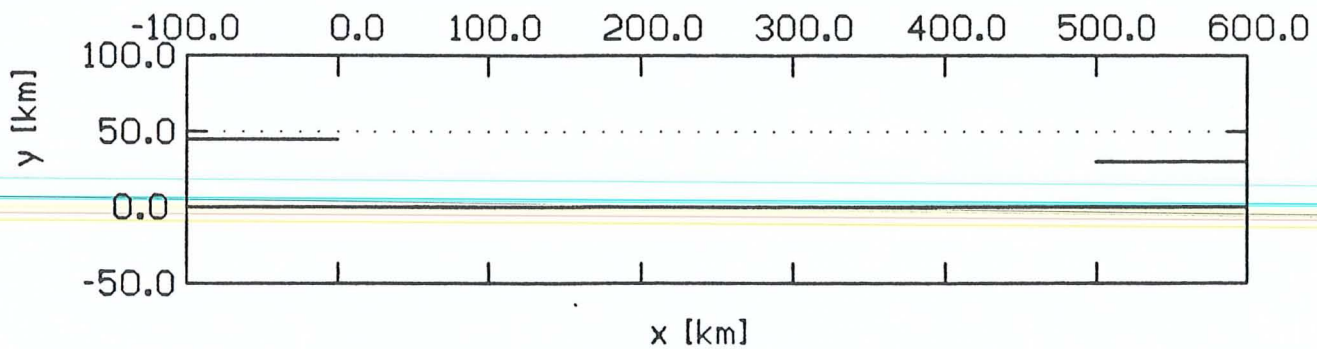

FIG. 7.2. h1=45 h2=30 h3=50 L=500 [km]

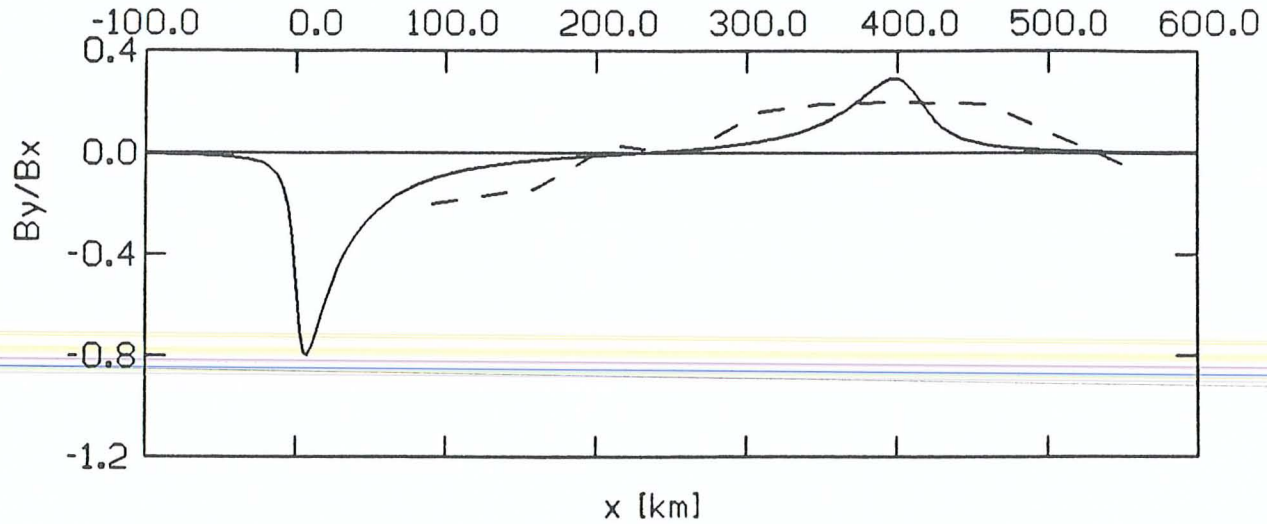

PARKINSØN TRANSFER FUNCTIØN

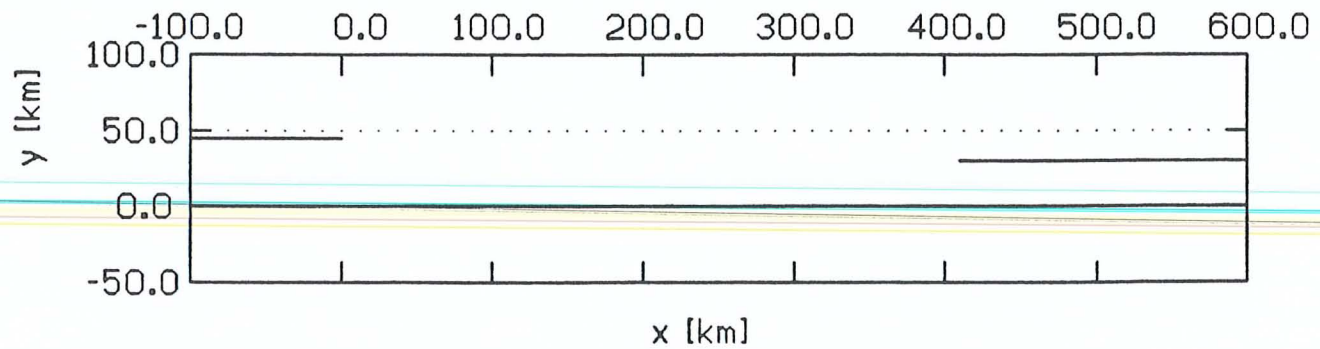

FIG. 7.3. h1=45 h2=30 h3=50 L=410 [km]

7.2. COAST EFFECT IN THE EASTERN UNITED STATES

As a second example, the coast effect observed by Edwards & Greenhouse (1975) in the eastern United States is considered. In contrast to Everett & Hyndman (1967), the former modelled their anomalies quantitatively and concluded that a region of enhanced conductivity lay in the lower crust or uppermost mantle at some distance from the ocean. This conductive zone shows an increase in conductivity with increasing distance from the coast.

The general character of their assumed conductivity distribution together with the smallness of the observed out-of-phase response suggests an explanation of the anomaly by model A.L.1/R.2. Since transfer function estimates for the periods of 16 min and 1 h are available, both data sets have been modelled. Again the edge of half plane 1 coincides with the edge of the continental shelf. Comparing fig. 7.2 (1 h) with fig. 7.3 (16 min), their main difference is that, for the shorter period, the earth conductor (half plane 2) extends closer to the ocean, whereas its depth is not affected at all. This is consistent with the model conductor proposed by Edwards & Greenhouse (1975), which has resistivities close to 1 Ωm at some distance from the coast, with a slight rise to about 20 Ωm towards the ocean. In contrast with the

Australian results, the conductosphere must now be assumed to begin at a shallow depth. In other words, the lower crust or upper mantle are highly conductive in the eastern United States.

Finer details in the observed response cannot be explained by our simple models. Furthermore, other anomalies may require models that are different from ours. The main aspect to be emphasized here is, however, that our fast modelling technique has the capability of furnishing basic quantitative information on the conductivity distribution in the ground.

CHAPTER 8

CONCLUSIONS AND SUGGESTIONS FOR FUTURE WORK

In chap. 6 it became obvious that our distinction between cases A and B was not only a matter of mathematical convenience. The conductor configurations corresponding to these two cases also had essentially different response characteristics. This is summarized here.

If we first recapitulate the behaviour of model A.L.1/R.2, we realize that its inductive response was nearly the sum of the responses of models A.L.1 and A.R.2. This approximation was particularly good if the earth conductor had a large depth ($h_2/h_1 = 0.25$). If it was shallow ($h_2/h_1 = 0.75$), the extent of inductive coupling still remained small and just started to become more significant for $L/h_1 = 0.50$. We therefore call case A the additive case.

For finitely conducting bodies, additivity should be a still better approximation, because the relative importance

of interaction between conductors decreases with decreasing conductivity. And even if the assumption of a two-dimensional conductivity configuration is violated, the basic behaviour ought to be very similar. A problem of current interest is the interpretation of the combined anomaly of a two-dimensional earth conductor extending away from a three-dimensional ocean. Here the anomaly of the ocean can simply be subtracted and the residual can be interpreted in terms of the earth conductor alone.

Case B was designed to simulate an earth conductor extending towards the ocean. The corresponding model B.L.1/L.2 incorporates two strongly coupled half planes. Therefore, essentially different response characteristics were to be expected, and the edge effect of the earth conductor was found to be nearly unaffected by the ocean. This behaviour was closely followed when the former conductor was shallow (h_2/h_1 = 0.75). It was interpreted as being due to the strong attenuation of the response of the ocean caused by its interaction with the earth conductor. Case B is therefore called the persistent case. This emphasizes the fact that the response of the earth conductor at large distances from the ocean was found to be very nearly identical with the anomaly that it causes in close proximity to this ocean.

If bodies of finite conductivity are considered, the interaction between ocean and earth conductor becomes weaker. But it can be expected that the in-phase portion of the anomaly of the earth conductor still displays this persistency to a high degree. On the other hand, the out-of-phase portion of the ocean anomaly ought not to be attenuated significantly and probably superimposes with the out-of-phase portion of the anomaly due to the earth conductor.

If the earth conductor of case B was deeper (h_2/h_1 = 0.25), its edge effect decreased, whereas the ocean effect increased. The latter was explained by the weaker interaction between both conductors and hence the ocean could not be disregarded. But the main problem is now the separation of the minute signature of the earth conductor from the much stronger ocean anomaly. Any further considerations, such as the question of interaction, are only of minor practical importance by comparison.

We may, however, wish to make explicit allowance for the finite conductivity of the ocean. The numerical method of Greenhouse et al. (1973) appears to be a useful way of doing so. It allows the calculation of the total response of a thin sheet of variable conductivity above a perfectly conducting undulating surface, where the whole configuration

is two-dimensional. Various shapes can be assumed for these undulations, e.g. combinations of half planes and steps, elliptical bulges or general distortions as considered at the end of sec. 5.5. Also, the response of (i) a finitely conducting sheet above a horizontal conductosphere or (ii) an undulated conductosphere alone, can be calculated separately and then be superimposed. This again allows the coupling of the thin sheet and the undulated perfect conductor to be investigated. But, the number of free parameters tends to become larger for such a model. This hinders the task of extracting useful general trends from the results.

Another possible extension of our work is to define a useful inverse problem, which is based on the anomalous response, as observed in the vicinity of a coastline. Weidelt (1978, 1980, 1981) considered configurations without an ocean and constructed extremal models that maximize the depth below the surface, of the top of a perfect conductor. In Weidelt's analysis, the measured response at one or two observation points had to be satisfied. The general approach is a problem of constrained maximization of a forward solution, which is based on the Cauchy integral formula (see sec. 5.5). The inclusion of an ocean into Weidelt's approach results in an additional constraint, because the observation points become fixed relative to the

edge of a perfectly conducting half plane. Nevertheless, if the response at only one observation point is to be satisfied, the solution is straightforward. It leads to a system of equations that must be solved numerically, and which provides an upper limit for the depth of the top of an earth conductor near an ocean.

REFERENCES

Ashour, A.A.: Theoretical models for electromagnetic induction in the oceans. Phys. Earth Planet. Inter., 7, 303-312, 1973.

Bailey, R.C.: Electromagnetic induction over the edge of a perfectly conducting ocean: the H-polarization case. Geophys. J. R. Astron. Soc., 48, 385-392, 1977.

Bailey, R.C., Edwards, R.N., Garland, G.D.: Geomagnetic depth sounding and magnetotelluric results from a seismically active region northeast of Quebec City: discussion. Can. J. Earth Sci., 14, 2426-2427, 1977.

Bailey, R.C., Edwards, R.N., Garland, G.D., Kurtz, R., Pitcher, D.: Electrical conductivity studies over a tectonically active area in eastern Canada. J. Geomagn. Geolelectr., 26, 125-146, 1974.

Bartels, J.: Erdmagnetisch erschliessbare lokale Inhomogenitaeten der elektrischen Leitfaehigkeit im Untergrund. Nachr. Akad. Wiss. Goettingen, Math.-Phys. Kl. IIa, no. 5, 95-100, 1954.

Bartels, J.: Erdmagnetische Tiefen-Sondierungen. Geol. Rundsch., 46, 99-101, 1957.

Bullard, E.C.: Electromagnetic induction in the earth. Q. J. R. Astron. Soc., 8, 143-160, 1967.

Bullard, E.C., Parker, R.L.: Electromagnetic induction in the oceans. In: The sea, vol. 4, A. Maxwell, ed.: pp. 695-730. New York: Wiley, 1970.

Cagniard, L.: Basic theory of the magneto-telluric method of geophysical prospecting. Geophysics, 18, 605-635, 1953.

Coode, A.M., Tozer, D.C.: Low-velocity layer as a source of the anomalous vertical component of geomagnetic variations near the coast. Nature, 205, 164-165, 1965.

Dawson, T.W., Weaver, J.T.: Three-dimensional induction in a non-uniform thin sheet at the surface of a uniformly conducting earth. Geophys. J. R. Astron. Soc., 59, 445-462, 1979.

Dosso, H.W.: A review of analogue model studies of the coast effect. Phys. Earth Planet. Inter., 7, 294-302, 1973.

Dosso, H.W., Nienaber, W., Wright, J.A., Greenhouse, J.P., Bailey, R.C.: An analogue model study of electromagnetic induction in the eastern coastal region of North America. Phys. Earth Planet. Inter., 23, 13-30, 1980.

Edwards, R.N., Greenhouse, J.P.: Geomagnetic variations in the eastern United States: evidence for a highly conducting lower crust? Science, 188, 726-728, 1975.

Edwards, R.N., Law, L.K., White, A.: Geomagnetic variations in the British Isles and their relation to electrical currents in the ocean and shallow seas. Philos. Trans. R. Soc. London Ser. A, 270, 289-323, 1971.

Everett, J.E., Hyndman, R.D.: Geomagnetic variations and electrical conductivity structure in south-western Australia. Phys. Earth Planet. Inter., 1, 24-34, 1967.

Fischer, G.: Electromagnetic induction effects at an ocean coast. Proc. IEEE, 67, 1050-1060, 1979.

Garland, G.D.: Electrical conductivity anomalies - mantle or crust? Comm. Earth Sci., Geophysics, 1, 167-172, 1971.

Garland, G.D.: Correlation between electrical conductivity and other geophysical parameters. Phys. Earth Planet. Inter., 10, 220-230, 1975.

Garland, G.D.: The significance of terrestrial conductivity variations. Annu. Rev. Earth Planet. Sci., 9, 147-174, 1981.

Gough, D.I.: The geophysical significance of geomagnetic variation anomalies. Phys. Earth Planet. Inter., 7, 379-388, 1973.

Grant, F.S., West, G.F.: Interpretation theory in applied geophysics. New York: McGraw-Hill, 1965.

Greenhouse, J.P.: Geomagnetic time variations on the sea floor off southern California. Ph.D. thesis, Univ. California, 1972.

Greenhouse, J.P., Bailey, R.C.: A review of geomagnetic variation measurements in the eastern United States: implications for continental tectonics. Can. J. Earth Sci., 18, 1268-1289, 1981.

Greenhouse, J.P., Parker, R.L., White, A.: Modelling geomagnetic variations in or near an ocean using a generalized image technique. Geophys. J. R. Astron. Soc., 32, 325-338, 1973.

Gregori, G.P., Lanzerotti, L.J.: The effect of coastlines on geomagnetic measurements: a commentary. Riv. Ital. Geofis. Sci. Affini, 5, 81-86, 1978/79.

Haak, V.: Interpretations-Verfahren fuer die Magnetotellurik unter besonderer Beruecksichtigung lateral variierender elektrischer Leitfaehigkeit im Erdinnern und eines raeumlich inhomogenen induzierenden Magnetfelds. Bayer. Akad. Wiss., Math.-Naturwiss. Kl., Abh., Neue Folge, 158, 1-105, 1978.

Haak, V.: Relations between electrical conductivity and petrological parameters of the crust and upper mantle. Geophys. Surv., 4, 57-69, 1980.

Hermance, J.F.: Model studies of the coast effect on geomagnetic variations. Can. J. Earth Sci., 5, 515-522, 1968.

Honkura, Y.: Electrical conductivity anomalies in the earth. Geophys. Surv., 3, 225-253, 1978.

Hutton, R.: Induction studies in rifts and other active regions. Acta Geod. Geophys. Montanist., Acad. Sci. Hung., 11, 347-376, 1976a.

Hutton, V.R.S.: The electrical conductivity of the earth and planets. Rep. Progr. Phys., 39, 487-572, 1976b.

Hyndman, R.D., Hyndman, D.W.: Water saturation and high electrical conductivity in the lower continental crust. Earth Planet. Sci. Lett., 4, 427-432, 1968.

Jacobs, J.A.: Continental drift. Nature, 185, 231-232, 1960.

Jones, A.G.: Geomagnetic induction studies in Scandinavia - II. Geomagnetic depth sounding, induction vectors and the coast effect. J. Geophys., 50, 23-36, 1981.

Jones, F.W., Lokken, J.E.: Irregular coastline and channeling effects in three-dimensional geomagnetic perturbation models. Phys. Earth Planet. Inter., 10, 140-150, 1975.

Jones, F.W., Pascoe, L.J.: A general computer program to determine the perturbation of alternating electric currents in a two-dimensional model of a region of uniform conductivity with an embedded inhomogeneity. Geophys. J. R. Astron. Soc., 24, 3-30, 1971.

Jones, F.W., Price, A.T.: The perturbations of alternating geomagnetic fields by conductivity anomalies. Geophys. J. R. Astron. Soc., 20, 317-334, 1970.

Jones, F.W., Price, A.T.: Geomagnetic effects of sloping and shelving discontinuities of earth conductivity. Geophysics, 36, 58-66, 1971.

Jones, F.W., Pascoe, L.J., Ramaswamy, V., Sydora, L.J.: The relationship between temperature distribution and the perturbation of time-varying electromagnetic fields for a two-dimensional model of a subducting lithospheric slab. J. Geophys. Res., 86, 10870-10874, 1981.

Kertz, W.: The conductivity anomaly in the upper mantle found in Europe. J. Geomagn. Geoelectr., 15, 185-192, 1964.

Koppenfels, W.v., Stallmann, F.: Praxis der konformen Abbildung. Grundlehren Math. Wiss., vol. 100. Berlin: Springer, 1959.

Kuckes, A.F.: Relations between electrical conductivity of a mantle and fluctuating magnetic fields. Geophys. J. R. Astron. Soc., 32, 119-131, 1973a.

Kuckes, A.F.: Correspondence between the magnetotelluric and field penetration depth analyses for measuring electrical conductivity. Geophys. J. R. Astron. Soc., 32, 381-385, 1973b.

Law, L.K., Riddihough, R.P.: A geographical relation between geomagnetic variation anomalies and tectonics. Can. J. Earth Sci., 8, 1094-1106, 1971.

Lilley, F.E.M., Woods, D.V., Sloane, M.N.: Electrical conductivity from Australian magnetometer arrays using spatial gradient data. Phys. Earth Planet. Inter., 25, 202-209, 1981.

Lines, L.R., Ainslie, B.A., Jones, F.W.: Investigation of the coastal effect by three numerical models. J. Geomagn. Geoelectr., 25, 63-73, 1973.

Madden, T.R., Swift, C.M., jr.: Magnetotelluric studies of the electrical conductivity structure of the crust and upper mantle. In: The earth's crust and upper mantle, D.J. Hart, ed.: pp. 469-479. Washington: American Geophysical Union, 1969.

Morse, P.M., Feshbach, H.: Methods of theoretical physics, 2 vols. New York: McGraw-Hill, 1953.

Parker, R.L.: Electromagnetic induction in a thin strip. Geophys. J. R. Astron. Soc., 14, 487-495, 1968.

Parkinson, W.D.: Directions of rapid geomagnetic fluctuations. Geophys. J. R. Astron. Soc., 2, 1-14, 1959.

Parkinson, W.D.: The influence of continents and oceans on geomagnetic variations. Geophys. J. R. Astron. Soc., 6, 441-449, 1962.

Parkinson, W.D.: Conductivity anomalies in Australia and the ocean effect. J. Geomagn. Geoelectr., 15, 222-226, 1964.

Parkinson, W.D., Jones, F.W.: The geomagnetic coast effect. Rev. Geophys. Space Phys., 17, 1999-2015, 1979.

Pascoe, L.J., Jones, F.W.: Boundary conditions and calculation of surface values for the general two-dimensional electromagnetic induction problem. Geophys. J. R. Astron. Soc., 27, 179-193, 1972.

Price, A.T.: The induction of electric currents in non-uniform thin sheets and shells. Q. J. Mech. Appl. Math., 2, 283-310, 1949.

Price, A.T.: A note on the interpretation of magnetic variations and magnetotelluric data. J. Geomagn. Geoelectr., 15, 241-248, 1964.

Price, A.T.: Electromagnetic induction within the earth. In: Physics of geomagnetic phenomena, 2 vols., S. Matsushita, W.H. Campbell, eds.: pp. 235-298. New York: Academic Press, 1967.

Rikitake, T.: Outline of the anomaly of geomagnetic variations in Japan. J. Geomagn. Geoelectr., 15, 181-184, 1964.

Rikitake, T.: Electromagnetism and the earth's interior. Amsterdam: Elsevier, 1966.

Rikitake, T., Yokoyama, I.: Anomalous relations between H and Z components of transient geomagnetic variations. J. Geomagn. Geoelectr., 5, 59-65, 1953.

Schmucker, U.: Erdmagnetische Tiefensondierung in Deutschland 1957/59: Magnetogramme und erste Auswertung. Abh. Akad. Wiss. Goettingen, Math.-Phys. Kl. IIa, Beitr. IGJ, no. 5, 1-51, 1959.

Schmucker, U.: Anomalies of geomagnetic variations in the southwestern United States. J. Geomagn. Geoelectr., 15, 193-221, 1964.

Schmucker, U.: Conductivity anomalies, with special reference to the Andes. In: The application of modern physics to the earth and planetary interiors, S.K. Runcorn, ed.: pp. 125-138. London: Wiley, 1969a.

Schmucker, U.: Zwei neue Verfahren zur Bestimmung des elektrischen Widerstandes als Funktion der Tiefe aus erdmagnetischen und erdelektrischen Beobachtungen. In: Prot. Koll. "Erdmagnetische Tiefensondierung", Reinhausen, J. Meyer, ed.: pp. 134-147. Univ. Goettingen, 1969b.

Schmucker, U.: Anomalies of geomagnetic variations in the southwestern United States. Bull. Scripps. Inst. Oceanogr., 13, 1-165, 1970a.

Schmucker, U.: An introduction to induction anomalies. J. Geomagn. Geoelectr., 22, 9-33, 1970b.

Schmucker, U.: Interpretation of induction anomalies above nonuniform surface layers. Geophysics, 36, 156-165, 1971.

Schmucker, U., Weidelt, P.: Electromagnetic induction in the earth. Lect. Notes, Univ. Aarhus, 1975.

Schmucker, U., Forbush, S.E., Hartmann, O., Giesecke, A.A., jr., Casaverde, M., Castillo, J., Salgueiro, R., del Pozo, S.: Electrical conductivity anomaly under the Andes. Carnegie Inst. Washington Yearbook, 65, 11-28, 1966.

Siebert, M.: Bemerkungen zur Untersuchung der Norddeutschen Leitfaehigkeitsanomalie. In: Prot. Symp. "Erdmagnetische Tiefensondierung", Goslar: pp. 108-129. Univ. Braunschweig, 1965.

Siebert, M.: Zur Deutung von Induktionspfeilen bei schmalen, langgestreckten orthogonalen Leitfaehigkeitsanomalien. In: Prot. Koll. "Erdmagnetische Tiefensondierung", Rothenberge, P. Weidelt, ed.: pp. 53-62. Univ. Goettingen, 1971.

Siebert, M.: Analytische Behandlung der elektromagnetischen Induktion in einer eindimensional beliebig verformten Grenzflaeche idealer Leitfaehigkeit. In: Prot. Koll. "Erdmagnetische Tiefensondierung", Grafrath, A. Berkthold, ed.: pp. 343-365. Univ. Muenchen, 1974.

Untiedt, J.: Ueber den linearen Zusammenhang zwischen den Komponenten erdmagnetischer Variationen und seine Bedeutung fuer die erdmagnetische Tiefensondierung. Nachr. Akad. Wiss. Goettingen, Math.-Phys. Kl. IIa, no. 1, 1-24, 1964.

Untiedt, J.: Conductivity anomalies in central and southern Europe. J. Geomagn. Geoelectr., 22, 131-149, 1970.

Uyeda, S., Rikitake, T.: Electrical conductivity anomaly and terrestrial heat flow. J. Geomagn. Geoelectr., 22, 75-90, 1970.

Vasseur, G., Weidelt, P.: Bimodal electromagnetic induction in non-uniform thin sheets with an application to the northern Pyrenean induction anomaly. Geophys. J. R. Astron. Soc., 51, 669-690, 1977.

Weaver, J.T.: The electromagnetic field within a discontinuous conductor with reference to geomagnetic micropulsations near a coastline. Can. J. Phys., 41, 484-495, 1963.

Weidelt, P.: The inverse problem of geomagnetic induction. Z. Geophys., 38, 257-289, 1972.

Weidelt, P.: Entwicklung und Erprobung eines Verfahrens zur Inversion zweidimensionaler Leitfaehigkeitsstrukturen in E-Polarisation. Habilitiation thesis, Univ. Goettingen, 1978.

Weidelt, P.: Die Maximaltiefe einer Leitfaehigkeitsanomalie fuer ideale Leiter. In: Prot. Koll. "Elektromagnetische Tiefenforschung", Berlin, V. Haak, J. Homilius, eds.: pp. 243-250. Univ. Berlin, 1980.

Weidelt, P.: Extremal models for electromagnetic induction in two-dimensional perfect conductors. J. Geophys., 49, 217-225, 1981.

Wiese, H.: Geomagnetische Tiefentellurik. Abh. Deutsche Akad. Wiss. Berlin, Geomagn. Inst. Potsdam, 36, 1-146, 1965.